



universität
wien

DIPLOMARBEIT

Titel der Diplomarbeit

The position of the RPL3 gene
in a gene network relevant to diabetic microangiopathy

angestrebter akademischer Grad

Magistra der Naturwissenschaften (Mag.rer.nat.)

Verfasserin:	Hannelore Lechtermann
Matrikel-Nummer:	9503432
Studienrichtung /Studienzweig (lt. Studienblatt):	A441
Betreuer:	Dr. Nikolaus Wick (Medizinische Universität Wien) Uni.-Prof. Dr. Thomas Decker (Universität Wien)

Wien, im November 2009

1. ABSTRACT	- 5 -
2. ZUSAMMENFASSUNG	- 6 -
3. INTRODUCTION.....	- 7 -
3.1. The disease of interest: diabetes mellitus.....	- 7 -
3.2 Diabetic microangiopathy	- 8 -
3.2.1. Increased polyol pathway flux	- 10 -
3.2.2. Intracellular production of advanced glycation end products	- 10 -
3.2.3. PKC activation	- 10 -
3.2.4. Increased hexosamine pathway activity.....	- 11 -
3.3. Translation.....	- 13 -
3.4. Ribosomes.....	- 17 -
3.4.1. Structural analysis of the large ribosomal subunit.....	- 17 -
3.4.2. The ribosomal protein of the large subunit 3	- 19 -
3.5. BTF3	- 24 -
3.6. Genetic Networks.....	- 25 -
3.6.1. Network identification by multiple regression	- 26 -
4. MATERIALS AND METHODS	- 29 -
4.1 Buffers and Solutions.....	- 29 -
4.2. Molecular Biology	- 33 -
4.3. Cell Culture	- 43 -
4.3.1. Immunofluorescence staining.....	- 43 -
4.3.2. Flow cytometry	- 44 -
4.3.3. Transfection.....	- 45 -
4.4. Biochemistry	- 46 -
4.4.1. Western blotting.....	- 46 -
4.4.2. Immunohistochemical staining	- 48 -
5 RESULTS	- 49 -
5.1 Gene selection.....	- 49 -
5.2. Endothelial RPL3 under diabetic conditions in situ	- 54 -
5.3. Endothelial RPL3 under diabetic conditions in vitro.....	- 55 -
5.3.1. Endogenous RPL3 protein	- 55 -
5.3.2. Exogenous RPL3 protein.....	- 57 -
5.4. Position of RPL3 in the genetic network	- 59 -
5.5. Verification of RPL3 interactions in a genetic network.....	- 65 -
5.6. The position of BTF3 in the final gene network	- 67 -
6. DISCUSSION.....	- 70 -
7. REFERENCES.....	- 77 -
8. APPENDIX.....	- 84 -

9. ABBREVIATIONS..... - 99 -

1. Abstract

Diabetic microangiopathy is a severe complication of long term diabetes mellitus. It systemically affects the blood capillaries and is characterized by a thickening of their basal membrane as a surrogate marker for impaired microcirculation. Clinically, this disease can be classified into nephropathy, neuropathy and retinopathy. To get a closer insight into the genetic factors causing diabetic microangiopathy the expression profiles of a variety of genes contributing to diabetes were obtained by high throughput TaqMan quantitative PCR and used to generate a gene network *in silico*. The final network comprised 37 genes and displayed the regulatory interactions of these participants. The network algorithm also identified a high correlation in the expression profiles of two candidate genes, *Btf3* and *Rpl3*. Confirmation by immunoblotting revealed a unilateral pathway, in which ectopically overexpressed BTF3 protein stimulated the expression of RPL3 protein. Thus, *Btf3* connected *Rpl3* to four out of those five genes having a vast number of regulatory interactions. Therefore, we propose that the Btf3/Rpl3 protein pair can be considered potential molecular players of diabetic microangiopathy.

2. Zusammenfassung

Diabetische Mikroangiopathie bezeichnet eine durch Hyperglykämie induzierte, krankhafte Veränderung der kleinen Blutgefäße. Die charakteristische Verdickung der kapillaren Basalmembran gilt als typisches Anzeichen der in Folge dieser Krankheit auftretenden, gestörten Mikrozirkulation dieser Gefäße. Diabetische Mikroangiopathie wird klinisch in Nephropathie, Retinopathie und Neuropathie klassifiziert.

Zur Ursachenforschung dieser Krankheit auf molekularer, genetischer Ebene wurden Gene, welche mit diabetischen Mikroangiopathie in Verbindung gebracht werden, hinsichtlich ihres Expressionsprofils verglichen. Diese Profile wurden mittels High Throughput TaqMan Quantitative PCR ermittelt und zum Design eines genetischen Netzwerkes *in silicio* verwendet. Das so entwickelte Netzwerk umfasste schlussendlich 37 Gene und spiegelte die funktionellen Verbindungen zwischen den einzelnen Netzwerkpartnern wider. Mit Hilfe der hierfür verwendeten Algorithmen konnten auch unterschiedliche Expressionsprofile der am Netzwerkdesign beteiligten Gene analysiert und eine hohe Korrelation im Expressionsmuster zwischen den zwei Kandidatengenen, *Btf3* und *Rpl3*, identifiziert werden. Diese Verbindung wurde auf Proteinebene durch Immunoblotting nachgewiesen, wodurch ein unilateraler Pathway identifiziert wurde, in welchem überexprimiertes BTF3 Protein die Expression des RPL3 Proteins fördert. Zusätzlich wurde *Rpl3* durch *Btf3* zu vier der fünf identifizierten Schlüsselgenen des Netzwerkes verbunden, wodurch angenommen werden kann, dass die Btf3/Rpl3 Wechselbeziehung eine zentrale Rolle in der Entstehung und dem Fortschreiten von diabetischer Mikroangiopathie spielt.

3. Introduction

3.1. *The disease of interest: diabetes mellitus*

Diabetes mellitus refers to a metabolic disorder that is characterized by chronic hyperglycaemia with disorders of carbohydrate, fat and protein metabolism due to a lack of insulin or because of the presence of factors that oppose the action of insulin. Patients suffering from full blown diabetes show characteristic symptoms as thirst, polyuria and blurring of vision. In its most severe form a development of ketoacidosis is diagnosed, which can lead to stupor, coma and, in the absence of effective treatment, to death. In the much more common milder variants, however, chronic pathological and functional changes due to hyperglycemia may occur, which insidiously be present for a long time before clinical diabetes is diagnosed.

Pathophysiologically and clinically diabetes mellitus can be subdivided in two types:

Type 1 diabetes, also known as insulin dependent- or juvenile onset- diabetes, is an autoimmune disease affecting the insulin producing β -cells in the Langerhans' islands in the pancreas. This type accounts for 10 to 15 % of all diabetes cases, and although the peak incidence appears in childhood and adolescence, the onset may occur at any age. Although there is a genetic predisposition to autoimmune destruction of the β -cells, type I diabetes is also related to environmental risk factors like viruses, diet or chemicals in people that are genetically predisposed (Watkins, 2003; World Health Organization, 1999).

Type 2 diabetes mellitus, also termed non-insulin-dependent or adult-onset diabetes, is usually diagnosed in patients over 30, although it occurs in people much younger as well. Pathophysiologically, type II patients suffer from impaired insulin action, since the cells do not longer react properly to insulin, although it is present in the blood. This so-called insulin resistance can be due to various cellular abnormalities. According to the etiological classification type II diabetes patients suffer from deficient insulin action and deficient insulin secretion. The first can be due to intracellular defects of glucose disposal, defects of insulin receptor function, different insulin structure and because of rare genetic disorders. A deficiency in the insulin secretion is due to defects in signalling as well as to a partly destruction of beta cells. Additionally environmental factors play a large role, e.g. obesity, an inactive lifestyle as well as wearing out beta

cells due to aging, all of which are high risk factors for the development of diabetes type II (Lindsay and Bennett, 2001).

3.2 Diabetic microangiopathy

A severe complication in both types of diabetes mellitus is the development of diabetic microangiopathy, a dysfunction concerning the small blood vessels leading to a thickening of the basal membrane, leaking of intravascular protein and slowing of the flow of blood. Clinically, this disease can be classified into nephropathy, neuropathy and retinopathy, thereby affecting cells of the kidneys, the nerves and the eyes (Dahl-Jørgensen, 1998).

Diabetic retinopathy is a disease of the eye, thereby being the number one cause of acquired blindness in adults. Due to microvascular damage of the retina, swelling of the blood vessels and leaking of fluid happens. This leads to growing of new vessels and a subsequent detachment of the retina (Kowluru and Chan, 2007).

Diabetic nephropathy affects the kidneys and developed in 25 % - 30 % of all patients suffering from diabetes. Incipient nephropathy is characterized by a low level of albumin in the urine, which rises with the ongoing of the disease. Progression of nephropathy leads to kidney failure due to the gradual decrease in the glomerular filtration rate (Thorp, 2005).

Diabetic neuropathy can be divided in several types, whereby the most common form of this disease is the diffuse polyneuropathy with damages of the distal peripheral nerves and of the autonomic nervous system. In contrast to mononeuropathies and acute painful neuropathies, which start from a relatively acute onset and end in the almost complete recovery after six to 18 months, polyneuropathies are irreversible and progressing with the duration of the diabetes (Watkins, 2003).

Today reactive oxygen species (ROS) are proposed as the key factor that connects all the different pathogenic effects of diabetes on blood vessels (Du et al., 2000; Nishikawa et al., 2000). These ROS are produced by the mitochondrial electron transport chain as a result of intracellular hyperglycaemia (Figure 1).

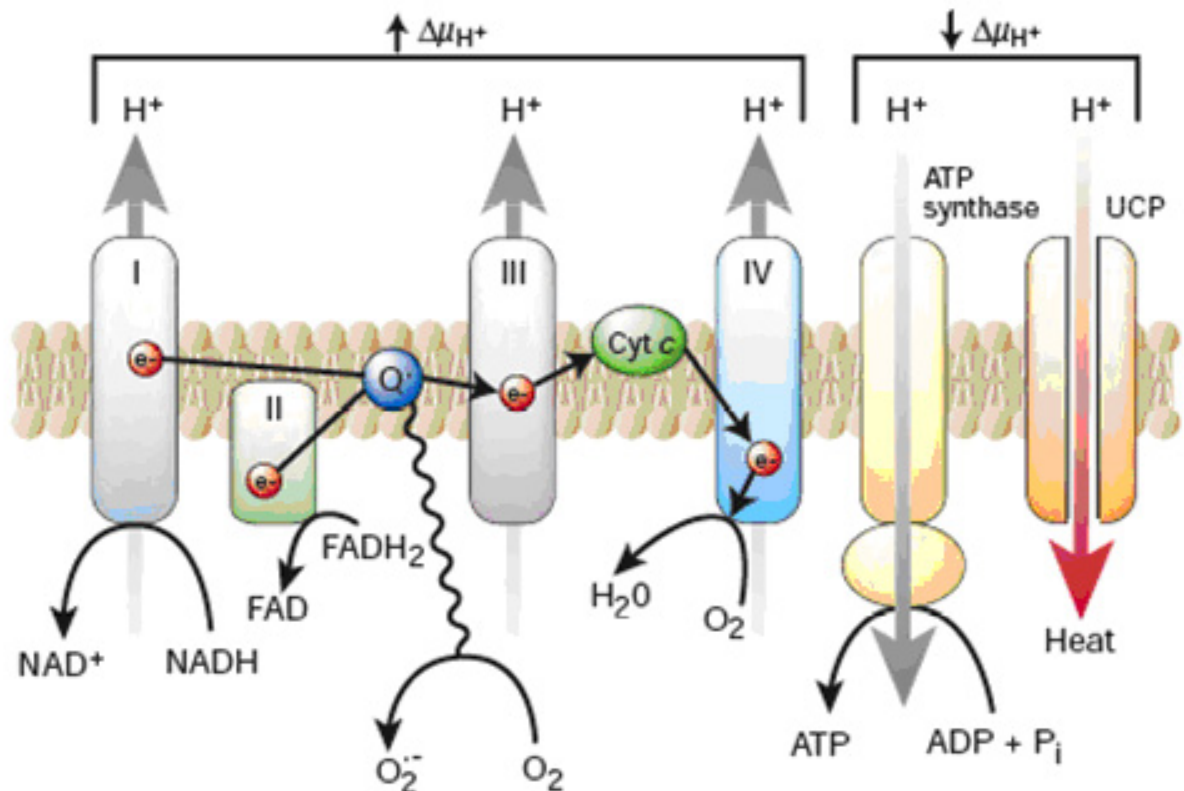


Figure 1. Production of reactive oxygen species by the mitochondrial electron transport chain in diabetic cells. Intracellular hyperglycaemia leads to a high membrane potential by increase of the electron donors NADH and FADH₂ (Brownlee, 2001).

The electron transport chain (Fig. 1) consist of four complexes built into the structure of the inner mitochondrial membrane, connected by the mobile carriers ubiquinone and cytochrome c. Complex I carries electrons from NADH, complex II from succinate via FADH₂ to ubiquinone, which then delivers them to complex III. There the electrons are transported by cytochrome c to complex IV and finally to molecular oxygen, which they reduce to water. Some of the energy of the electrons is used to pump protons across the mitochondrial membrane, thus generating a voltage to drive ATP synthesis by ATP synthase. Due to intracellular hyperglycaemia more electron donors (FADH₂, NADH) are pushed into the electron transport chain, resulting in an increase of the voltage gradient. By reaching a critical threshold value the electron transfer inside complex III is blocked, the electrons return to ubiquinone and are donated to molecular oxygen thus generating superoxide, a reactive oxygen species (ROS) (Korshunov et al., 1997). These molecules contribute to diabetic pathologies by inhibiting the activity of the key glycolytic enzyme glyceraldehyd-3 phosphate dehydrogenase (GADPH). This inhibition is achieved by a mechanism where ROS induce DNA strand breaks, thereby activating the DNA repair enzyme poly (ADP-ribose) polymerase (PARP) that splits

NAD⁺ into nicotinic acid and ADP-ribose. The latter is then converted to long polymers that accumulate on GAPDH, thereby inactivating this enzyme and leading to the activation of four major pathways of diabetic damage (Brownlee 2001; Brownlee 2005):

3.2.1. Increased polyol pathway flux

In the polyol pathway the enzyme aldose reductase catalyses the NADPH dependent reduction of carbonyl compounds like toxic aldehyds to inactive alcohols. Under diabetic conditions when glucose level gets too high, aldose reductase also reduces glucose to sorbitol, which then became oxidized to fructose by sorbitol dehydrogenase with NAD⁺ reduced to NADH.

During this process of the aldose reductase, the cofactor NADPH is converted to NADP⁺. This process reduces the amount of reduced glutathione, an important intracellular antioxidant, which leads to an increased susceptibility of the polyol pathway to intracellular oxidative stress (Lee and Chang, 1999).

3.2.2. Intracellular production of advanced glycation end products

AGEs precursor molecules alter cellular function in three different ways. First, it modifies intracellular proteins which results in an altered function, e.g. in transcription (Giardino et al., 1994; Shinohara et al., 1998). Second, AGEs modify the extra cellular matrix leading to cell dysfunction. This mechanism involves modifying of plasma proteins by AGE precursors, which then bind to AGE receptors e.g. on macrophages, resulting in production of inflammatory cytokines and growth factors as well as activation of the transcription factor NF- κ B, leading to changes in gene expression of growth factors and cytokines (Doi et al., 1992; Skolnik et al., 1991).

3.2.3. PKC activation

Protein kinase C, a cyclic nucleotide independent protein kinase, is primarily activated by the lipid second messenger diacylglycerol (DAG). The amount of DAG is increased by intracellular hyperglycaemia, thereby leading to activation of the PKC isoforms β and δ (Koya and King, 1998; Xia et al., 1994). This process activates NF- κ B and NAD(P)H oxidases (Yerneni et al., 1999) and alters the gene expression of endothelial

nitric oxide synthetase (eNOS), endothelin-1 (ET-1), vascular growth factor (VEGF), transforming growth factor β (TGF- β) and plasminogen activator inhibitor-1 (PAI-1), thereby contributing to blood flow abnormalities, vascular permeability, angiogenesis, capillary and vascular occlusion and pro-inflammatory gene expression (Kuboki et al., 2000) .

3.2.4. Increased hexosamine pathway activity

If intracellular glucose rises up to a high level it gets metabolized by glycolysis, resulting in the formation of pyruvate and NADH as well as ATP (Brownlee, 2001). Small amounts of the glycolytic intermediate fructose-6-phosphate do not enter the glycolytic pathway, but get sidetracked into the hexosamine signalling pathway, where fructose-6-phosphate is converted to uridine diphosphate N-acetylglucosamine (Wells and Hart, 2003). These products modify threonine and serine residues of transcription factors such as Sp1, resulting in altered gene expression of transforming growth factor- β 1 and plasminogen activator inhibitor-1, thus affecting diabetic blood vessels (Du et al., 2000).

Inhibition of GADPH leads to an increase of glycolytic intermediates like glyceraldehyde-3-phosphate, fructose-6-phosphate as well as glucose itself. The major intracellular AGE precursor methylglyoxal as well as diacylglycerol DAG are formed from glyceraldehyde-3 phosphate, thereby contributing to the AGE and the PKC pathway. Fructose-6 phosphate increases the flux through the hexosamine pathway and an increase of intracellular levels of glucose activates the polyol pathway (Brownlee 2001) (Fig.2).

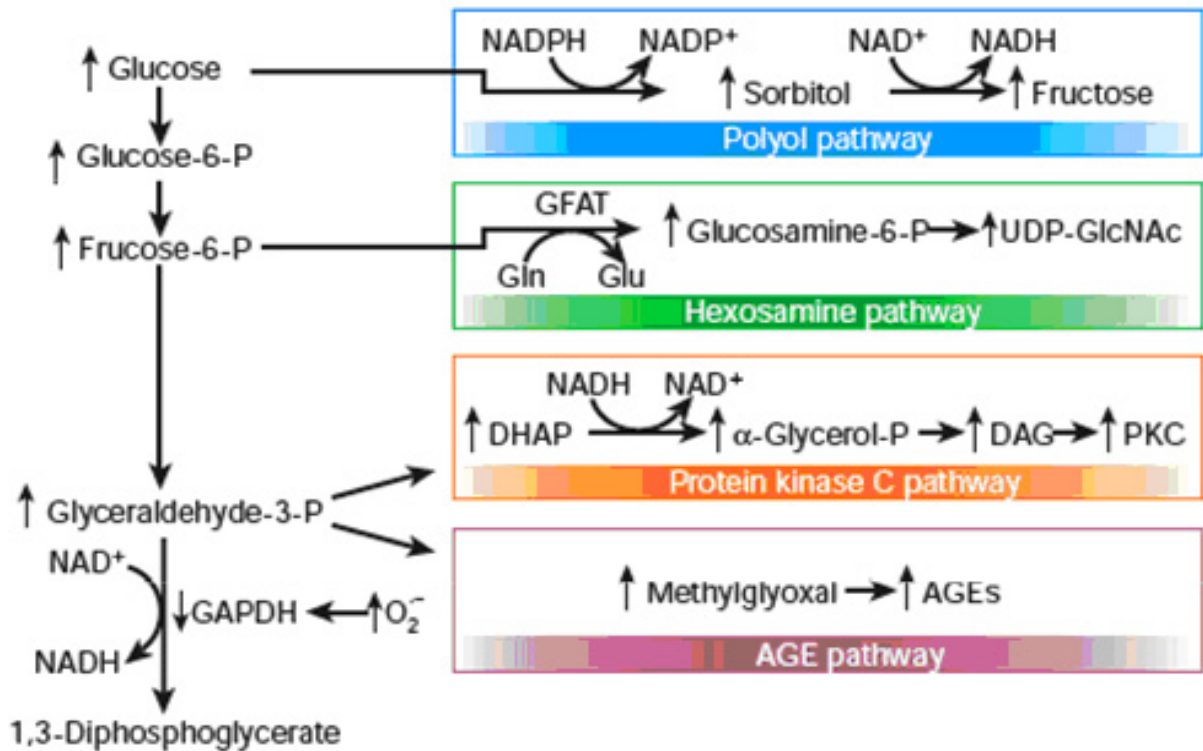


Figure 2. Inhibition of GAPDH by ROS overproduction leads to activation of four major pathways of diabetic pathologies. For detailed description see above (Brownlee 2001).

3.3. Translation

Translation is next to transcription one of cells most important processes. Ribosomes convert genetic information of mRNA into amino acids, thereby forming chains of polypeptides and proteins. These features reside in two ribosomal subunits. Of these, the smaller one performs the decoding function, thereby mediating interactions between tRNA and mRNA to determine the order of amino acids composing the synthesized protein. The large particle contains the peptidyl transferase centre (PTC), the active site of the ribosome where the formation of the peptide bonds occurs. Therefore the function of the large ribosome subunit is to catalyse the peptide bond formation. Both ribosome subunits contain three binding sites for tRNAs: Whereas the A site binds aminoacyl-tRNA that is going to be incorporated into the growing peptide chain, the P site binds peptidyl-tRNA, and at the E site deacylated-tRNAs are bound before they dissociate from the ribosome (Lafontaine and Tollervey, 2001). Translation itself can be subdivided into three main parts, initiation, elongation and termination. Initiation is one of the most extensively studied and rate limiting steps in the whole translation process. It starts with binding of a binary complex (eukaryotic translation initiation factor 2 (eIF2) and GTP) to methionyl-transfer RNA (Met-tRNA^{Met}), thereby forming a ternary complex that associates with the 40S ribosomal subunit. Binding of additional factors (eIF3, eIF1A) facilitates this interaction and creates a 43S preinitiation complex. Next the cap binding complex, consisting of eIF4E, eIF4G (a scaffold protein) and eIF4A (an RNA helix), binds to the 7-methyl-GTP cap structure of a mRNA, thereby bridging the 5' and 3' ends of the mRNA by simultaneously binding of eIF4G to the poly(A)-binding protein PABP. The 48S pre-initiation complex is formed by binding of the 43S pre-initiation complex to the mRNA. This process is promoted by the ATP-dependent helicase activity of eIF4A as well as by the circulation of the mRNA. Next the ribosome is scanned for the AUG start codon. The initiation factors that participate in translation are released after the formation of the 48S initiation complex and are recycled for another round of initiation. This release is assisted by eIF5, which facilitates the hydrolysis of GTP carried by eIF2 and, hence, the dissociation from of the 48S complex. Finally, the large 60S subunit is bound in a eIF5B- and GTP-dependent way, thereby forming the 80S initiation complex, which triggers elongation and protein synthesis (Holcik and Sonenberg, 2005; Klann and Dever, 2004).

During the elongation step peptide bond formation and mRNA decoding takes place. Nascent polypeptides are extended from the A to the P site of the ribosome by adding one amino acid at a time. This reaction is catalyzed by the elongation factor eEF1 and eEF2 and starts with an interaction between anticodon of tRNA with the analogous codon of the mRNA at the A-site. The correct codon-anticodon pairing activates the GTPase centre that is located in the large subunit and results in hydrolysis of the eEF1 GTP complex, release of eEF1 from the ribosome, accommodation of the aminoacyl end of the tRNA into the PTC and peptide bond formation. This reaction is catalyzed by the enzyme peptidyltransferase, a ribozyme that is located on the large ribosomal subunit. Subsequent translocation of the ribosome in 3'mRNA direction to decode the next mRNA codon is catalyzed by binding to eEF2, a GTPase that facilitates the shift of the deacylated tRNA from the P-site to the E-site and of the peptidyl-tRNA from the A site to the P-site upon GTP hydrolysis (Steitz 2008).

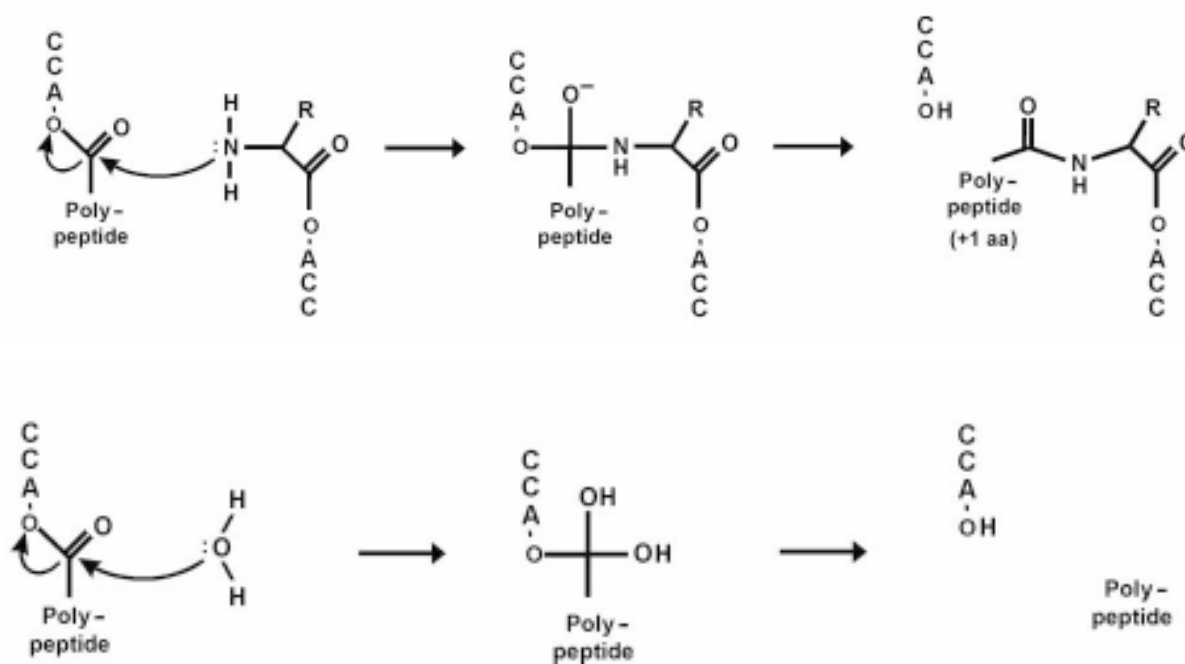


Figure 4. Peptid bond formation and peptidyl-tRNA hydrolysis. (A) In the first reaction, the α -amino group of aminoacyl tRNA in the A-site attacks the carbonyl carbon of the peptidyl tRNA in the P site, resulting in deacylated tRNA at the P-site and peptidyl-tRNA with an additional amino acid at the A-site. (B) Peptide release starts with a nucleophilic attack of the peptidyl-tRNA by activated water, leading to peptidyl-tRNA hydrolysis and polypeptide release (Polecek and Mankin, 2005).

Peptid bond formation itself starts with a nucleophilic attack on the carbonyl carbon on the peptidyl-tRNA by the α -amino group of the aminoacyl-tRNA, leading to the acetylation of the 3'-hydroxyl group of the peptidyl-tRNA and the formation of a tetrahedral intermediate at the carbonyl carbon (Fig. 4) (Polacek and Mankin, 2005).

Resolving of the intermediate results in a peptide, that is extended by one amino acid, esterifies to the A-site-bound tRNA and a deacylated tRNA in the P-site (Lafontaine and Tollervey, 2001). Besides peptide bond formation, the PTC carries out peptidyl-tRNA hydrolysis, which is required for termination of translation and subsequent release of the assembled polypeptide of the ribosome. This reaction starts with a nucleophilic attack of an activated water molecule on the carbonyl carbon of the peptidyl-tRNA ester, leading to peptidyl-tRNA hydrolysis and subsequent polypeptide release (Fig.3) (Polacek and Mankin, 2005).

After eEF2-GDP release, the ribosome is ready for a next round of elongation until a stop codon in the mRNA reaches the A site at the end of the elongation circle, thereby starting termination of translation. The activity of termination factor eRF-1 (eukaryotic release factor 1) is triggered by eRF-3, a GTP binding protein. eRF3 complexes with eRF-1, thereby permitting binding to the stop codon and leading to ester bond cleavage between peptide and peptidyl-tRNA, and the subsequent release of new protein. GTP hydrolysis enables releasing of the termination factors, thereby permitting the ribosome to start a new translation cycle (Steitz 2008).

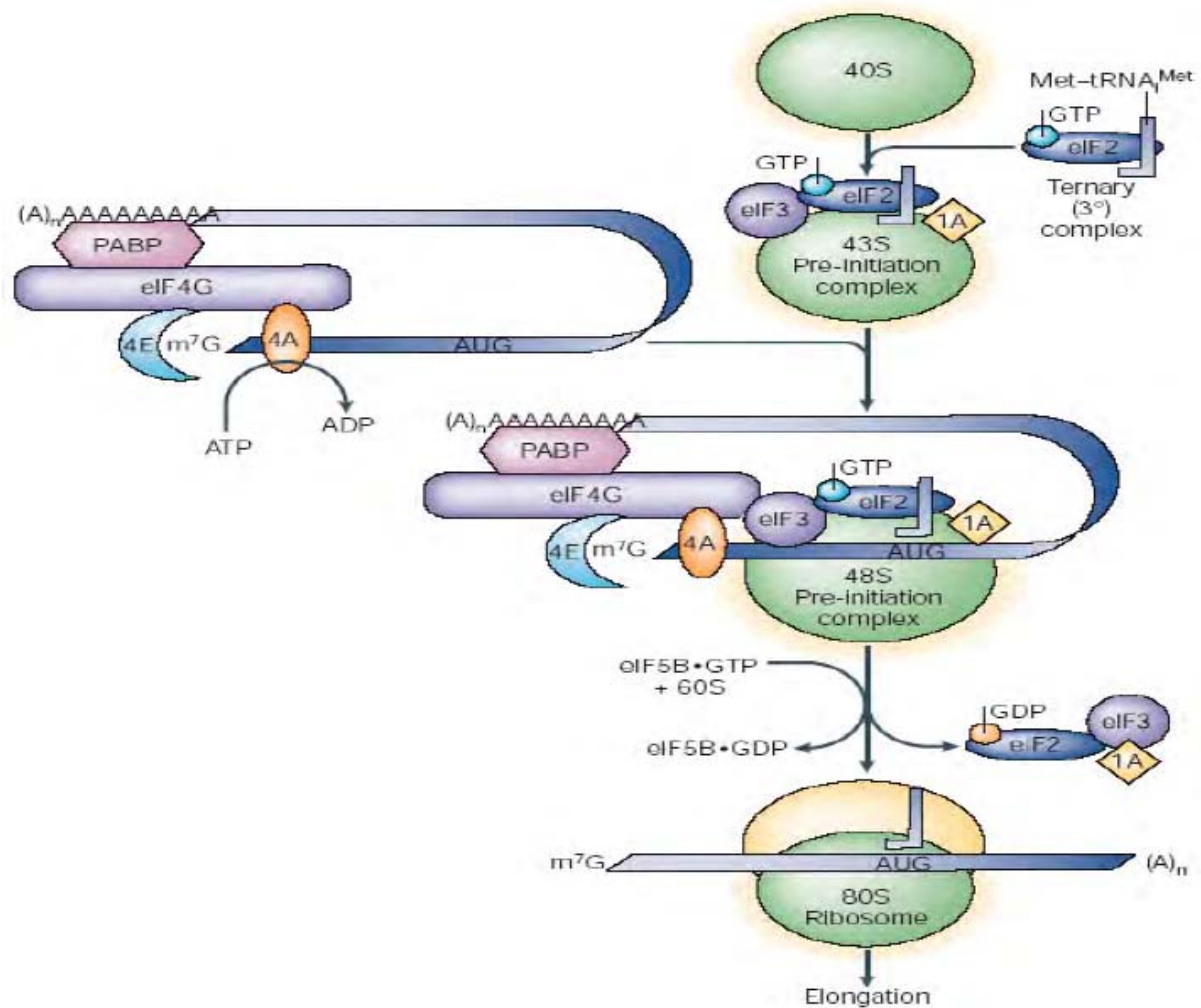


Figure 3. Eukaryotic translation initiation. Initiation of translation starts by forming the 43S pre-initiation complex. RNA circulation by association of the cap binding complex with Poly A binding protein leads together with the 43S protein complex to formation of the 48S pre-initiation complex. Initiation is finished by adding the 60S subunit to the growing particle, thereby forming the 80S initiation complex. (Klann and Dever, 2004).

3.4. Ribosomes

Ribosomes are highly conserved ribonucleoprotein particles that participate in protein synthesis and are made up of RNA and ribosomal proteins. Eukaryotic ribosomes sediment at 80S and as mentioned above are divided into a 60S, containing the 28S, 5.8S, 5S RNAs and 49 proteins, and a smaller 40S subunit which consists of the 18S RNA and 33 ribosomal proteins (Lafontaine and Tollervey, 2001)

3.4.1. Structural analysis of the large ribosomal subunit

Crystal structure analysis of ribosomal proteins of the halophilic archeon *Haloarcula marismortui* (Ban et al., 2000) and the eubacteria *Escherichia coli* (Vila-Sanjurjo et al., 2003) allows a deeper insight into ribosomal protein structure and their interactions with RNA (Fig. 5). Due to the universal conservation of ribosome features and the similarity between archaeal and bacterial subunit structures, these findings could be also applied on eukaryotic structures (Korostelev and Noller, 2007). The main functions of the large subunit comprise binding of tRNA, catalysing peptidyl transfer and performing translocation.

Before the complete subunit structures were published, it was not clear, if the multiple tasks of the ribosome were performed by RNA alone or if ribosomal proteins also contributed to these functions. Structure analysis identified the ribosome as a ribozyme, where RNA carries out the catalytic function. Nevertheless, some proteins are still connected with ribosomal features (Brodersen and Nissen, 2005).

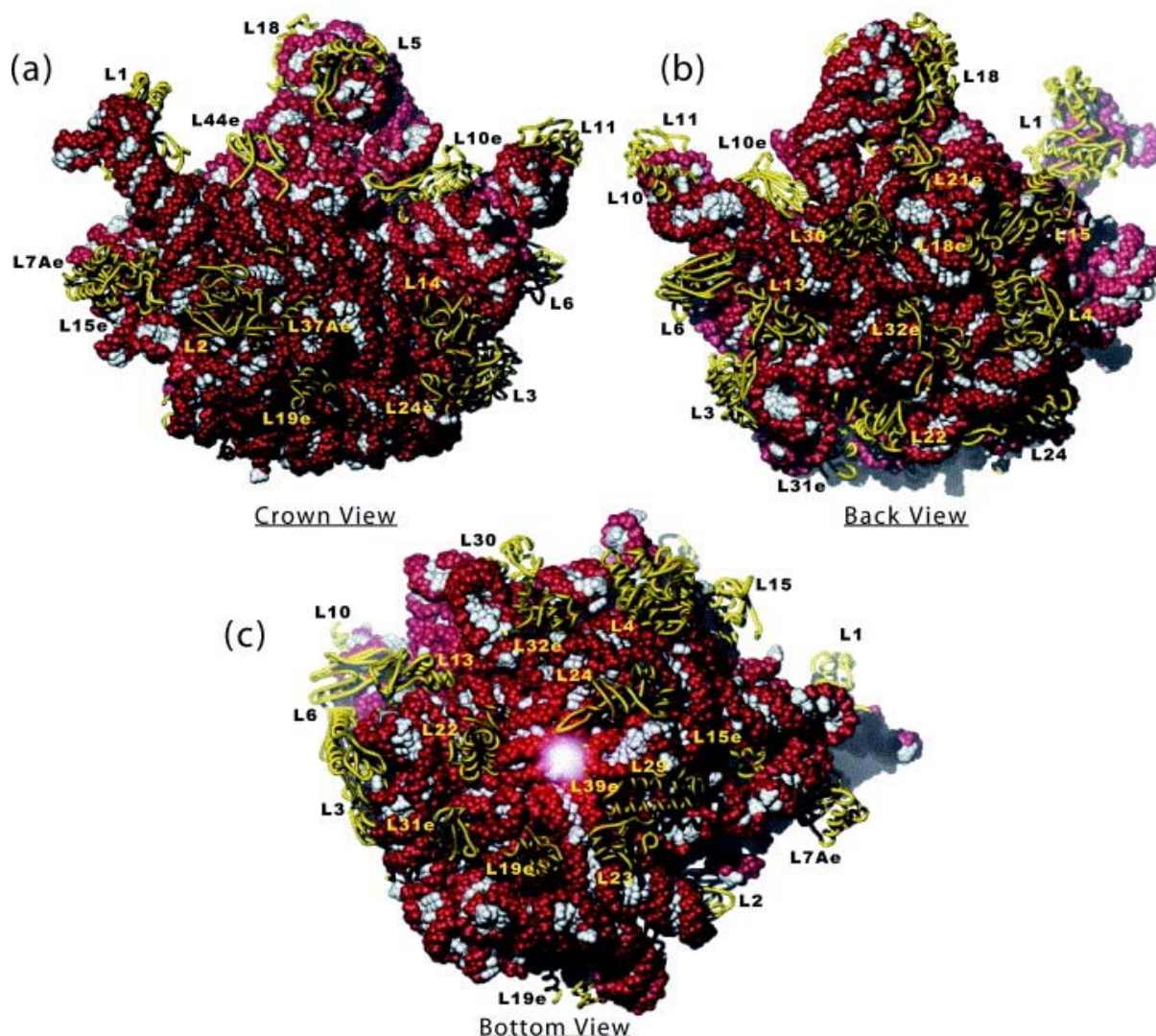


Figure 5. Structure of the 50 S ribosomal subunit of *Haloarcula marismortui* in (a) crown view, (b) back view and (c) bottom view. The sugar phosphate backbone of 23 S and 5 S RNAs are coloured in red, bases in grey. Ribosomal proteins are illustrated as yellow α -carbon ribbons (Klein et al., 2004).

The main function of ribosomal proteins is the stabilization of interdomain interactions of RNA, since most proteins bind several sites of the seven RNA domains of the large subunit, even if they are far separated in the sequence. Although the proteins of the large subunit seem to be regularly scattered, two regions with a denser distribution were identified: First, the upper right side of the particle that binds to translation factors and contains the ribosomal proteins L3, L6, L10, L11, L12, L13 and L14. The second region with higher protein concentration surrounds the distal end of the polypeptide exit tunnel and includes L19e, L22, L23, L24, L29, L31e, and L39e. Another important feature found in the large subunit is the widespread RNA surface area that is buried by r-

proteins, mostly due to the fact that these proteins contain extensions that reach deep into the RNA core of the ribosome. These idiosyncratically folded polypeptides form three dimensional structures with distinct amino acid composition, consisting mostly of glycine-, arginine-, and lysine residues. In contrast to the globular domains, the content of acid residues is rather low in the extensions, coming along with the fact that globular domains are found on the exterior, whereas the extensions reaches the interior of the ribosomal particle. The negatively charged RNA backbone of the core is therefore neutralized by basic residues of the extensions, allowing correct rRNA folding. Due to structural topology of the globular domain the ribosomal proteins were classified into the following six groups: The antiparallel $\alpha + \beta$ group (L5, L6, L10e, L15e, L22, L23), the β -barrel group (L2, L3, L14, L21e, L24), the zinc containing group (L24e, L37Ae, L37e, L44e), the α -helical group (L19e, L29, L39e), the L15 group (L15, L18e) and the mixed $\alpha + \beta$ group (L4, L7Ae, L13, L18, L30, L31e, L32) (Klein et al., 2004).

Since ribosomes are made up of protein and RNA, interactions between these two components were an important part of structure analysis. Hence four ways were found how these interactions in the large subunit were achieved: Hydrogen bonds with nucleotide bases via the minor groove and the major groove, protein recognition of the flipped out bases of bulged nucleotides and hydrophobic interactions of amino acid residues with crevices between the bases contributed to RNA stabilizing. Interactions between the various ribosomal proteins were also observed, although the average contact surface of protein interactions was much smaller than between proteins and RNA. Still, the proteins L37Ae, L24e and L7Ae participate in protein interactions that appear to be of greater importance than their RNA correlation (Klein et al., 2004).

3.4.2. The ribosomal protein of the large subunit 3

RPL3, a 44 kDa ribosomal protein of the large subunit, whose gene is located on the q13 of chromosome 22. Furthermore, it is one of the proteins that bury the largest RNA surface area due to their protein extensions. The archael and eukaryotic ribosomal protein L3 contains 2 extensions, one being positioned at the N terminus, the other reaching deep into the core of the large subunit. The latter is also referred as tryptophan- or W-finger, since this extension projects to the A site side of the PTC and a tryptophan at the tip of the finger approaches to the active site of the peptidyl transferase centre (PTC). Furthermore, two important rRNA helical structures were

anchored at this site, helix 95, that forms the sarcin-ricin loop, an important recognition site for translation elongation factors, and the structures formed by helices 90 – 92. The latter takes part in accommodation, the movement of aminoacyl tRNA from the partially bound “A/T” state to the fully bound “A/A” state, by forming together with helix 89 the corridor, through which 3'ends of aa-tRNAs slide. Beside the mentioned polypeptides finger, RPL3 includes 2 globular domains, whereas one harbours a β -barrel group structure that resembles domain II of the translational GTPases EF-Tu and EF-G. The second globular domain of RPL3 has an antiparallel $\alpha + \beta$ domain structure. The mentioned domains bind H95 and H96 and are positioned near helices 94 and 96, thereby flanking the sarcin/ricin loop (SRL), the site of ribosome interaction with the elongation factors eEF1 and eEF2. Interactions of these domains with RNA stabilize tertiary folding of the domain IV of the large subunit, therefore facilitating ribosome function. (Klein et al., 2004; Irvin and Uckun, 1992; Sanbonmatsu et al., 2005; Meskauskas et al., 2005)

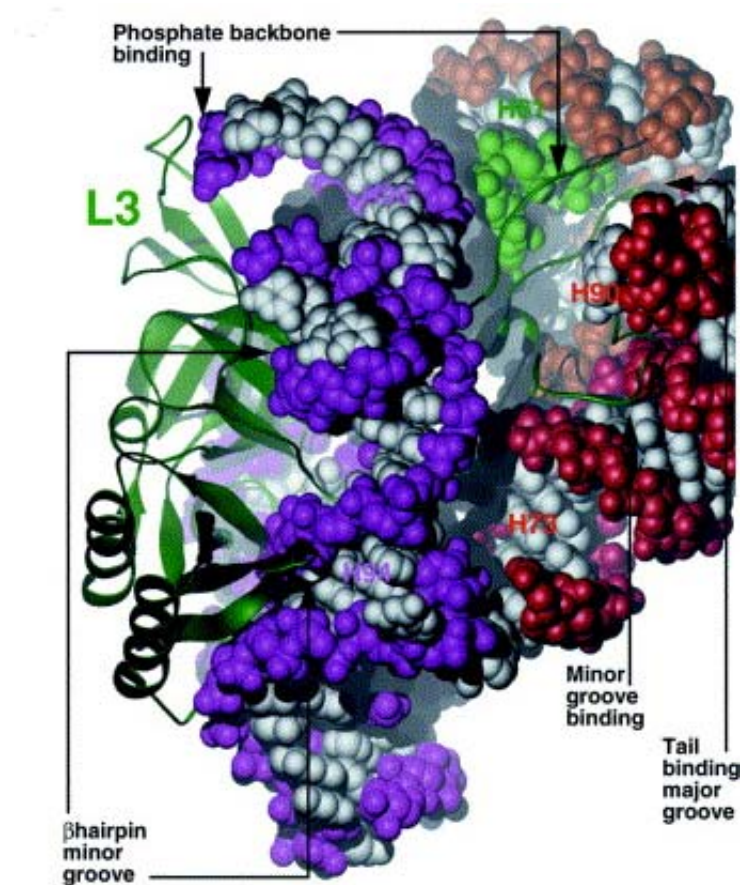


Figure 6. Ribosomal protein L3 and its interaction with RNA. The protein is displayed as green ribbons, the sugar phosphate backbone of RNA is illustrated in red and magenta, bases in grey. RPL3 interacts with RNA by major and minor groove special base recognition, specific protein binding pockets and amino acid residues. (Klein et al., 2004).

For RNA interactions of the RPL3 protein, specific base recognition through the major and minor groove, specific protein binding pockets as well as interactions due to insertion of amino acid residues into hydrophobic crevices between bases were observed (Fig. 6). Groove binding was mostly achieved by Watson Crick base pairing, although wobble base pairing and non canonical interactions were also detected. Additionally, RPL3 interacts with RPL13 and RPL14, thereby burying a total surface area of 7.3 %. (Klein et al., 2004)

Another important feature of RPL3 is its role in initiating subunit assembly. Next to L24, RPL3 is the only ribosomal protein that is able to initiate *in vitro* assembly of *E. coli*'s large subunit. Although the globular domain interacts only with domain VI, the extensions pass between the domains II, III, IV, V and VI, but not to domain I, that contains the entire RPL24 binding site, suggesting the roles of these two proteins in

subunit assembly being distinct and independently from each other (Spillmann et al., 1977; Nowotny and Nierhaus, 1982).

Given the fact that ribosomal proteins are too far away from the PTC to participate directly in its actions, RNA was identified as the main source of catalysing the PTC activity (Lafontaine and Tollervey, 2001; Steitz, T.A. 2008; Spirin A.S. 2004). Nevertheless, ribosomal proteins were still considered to contribute to ribosome associated functions (Meskauskas et al., 2005). Recently a new model was proposed, in which RPL3 acts as a “rocker switch” to organize translational elongation, thereby coordinating the functions of SRL and PTC. In the open conformation the helices 89, 90-92 and 95 are positioned, that they are able to form a binding site for the aa-tRNA•eEF1A•GTP ternary complex. In this state, the W-finger is in the “extended” conformation and occupies with its tip the A-site of the PTC. Interaction with the 25SrRNA stabilizes this status. At the same time, the N-terminal extension is in the retracted conformation, thereby opening the corridor. Accommodation of the aa-tRNA at the A-site triggers the opening of this site and retraction of the W-finger, followed by rotation of the globular domain of RPL3 and extension of the N-terminal domain towards helix 89. The displacement of helix 91 leads to the closure of the accommodation corridor and repositioning of the H90/H92 structure and from 25S rRNA in the A site permits interaction with aa-tRNA, thus activating peptidyltransfer. Finally, the movement of H91 away from H95 leads to formation of the eEF2-binding site (Meskauskas and Dinman, 2007; Meskauskas and Dinman, 2008) (Fig. 7). Taken together, these findings indicate a new role of RPL3 in translational elongation.

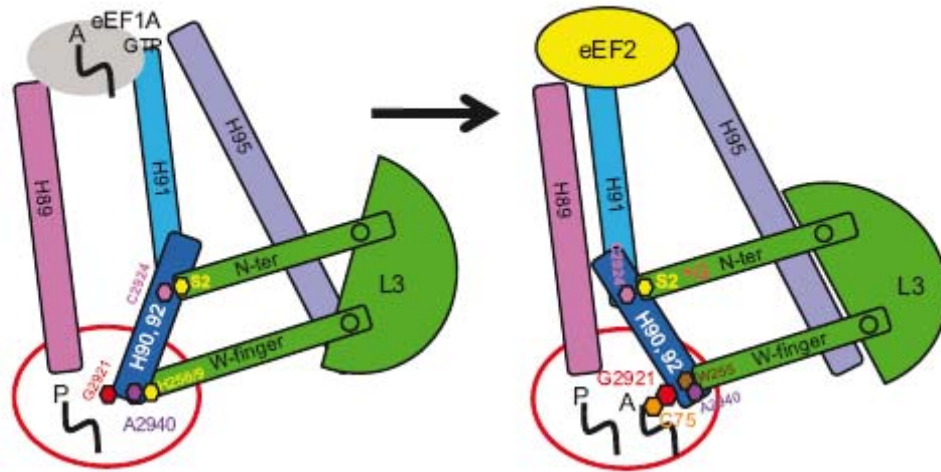


Figure 7. Model of RPL3 acting as a rocker switch in peptidyltransfer. In the ground state is the P site occupied by the peptidyl –tRNA, the W finger of RPL3 in the extended conformation, thereby maintaining the A site in the closed conformation. When the L3 N-terminal extension is in the retracted confirmation, the accommodation corridor opens, thereby leading to opening of the A site and retraction of the W finger, rotation of RPL3 globular domain, extension of the N-terminal domain toward Helix 89, displacement of Helix 91 and finally closure of the accommodation corridor. Peptidyltransfer is activated by reposition of H91/H92 structure and of G2921 in the A site, where an interaction with C75 of aa-tRNA could occur. The formation of the eEF2 binding site is achieved by movement of H91 away from H95 (Meskauskas and Dirnman, 2007).

3.5. BTF3

BTF3, the basic transcription factor 3, also known as RNA polymerase transcription factor 3 and nascent-polypeptide associated complex beta polypeptide, gives rise to the two splicing variants BTF3a and BTF3b, whereas the latter is an N-terminally truncated version that is shortened by 44 amino acids (Zheng et al., 1990; Kanno et al., 1992). Due to the fact that BTF3 binds to RNA polymerase II, this gene was believed to be essential for RNA polymerase II-dependent transcriptional initiation, although its role as transcription factor is still discussed (Zheng et al., 1987). Additionally, BTF3 protein was identified as part of the nascent-polypeptide-associated complex (NAC), a heterodimeric complex that can bind to eukaryotic ribosomes (Wiedmann et al., 1994). The NAC consist of a α subunit and a BTF3 encoded β -subunit, whereas both splicing variants of the beta subunit (BTF3a, BTF3b) form stable complexes with α NAC. Both subunits are located in close proximity to ribosome bound nascent polypeptide chains, and binding to nascent chains happens ubiquitously in a distance of 17 to 100 amino acids from the PTC, thereby taking part in cotranslational targeting of polypeptides to the endoplasmic reticulum (ER). Generally, protein translocation to the ER involves next to NAC, SRP, a cytosolic ribonucleoprotein complex that recognises a special signal sequence on the N-terminus of proteins. At the lipid bilayer, the signal sequence is additionally recognized by the Sec61 complex and leading to translocation of nascent polypeptides into the lumen of the ER (Rospert et al., 2002; Wickner, 1995).

Beside these described functions, BTF3 plays also a key role during initiation of protein synthesis. As already mentioned, translation initiation requires forming of the 43S pre-initiation complex (eIF2•GTP•Met-tRNA•40S ribosomal subunit) and binding it to the mRNA, a step that is promoted by the cap-binding complex eIF4F. This heterotrimeric complex is constituted of the cap-binding protein eIF4E, an RNA helicase and ATPase (eIF4A) and eIFG4, the scaffolding protein with binding site for PABP and ribosome associated factors. Two plant homologs of mammalian eIF4E interact with BTF3. The involved amino acid motif, RLQSTLKRIG, is part of the first 101 amino acids of BTF3 and interacts with a consensus motif that can be found on most of the 4E-binding proteins. This suggests a dual function of BTF3 in translation initiation as well as in elongation by acting on nascent polypeptide chains (Freire, 2005; Beatrix et al., 2000).

3.6. Genetic Networks

Most experimental understand cellular functions are based on a minimization, meaning that identification of certain structures and functions all the complex interactions of a living cell are put aside. Therefore all these attempts represent only a part of complex cellular processes, since distinct biological functions cannot be attributed to single molecules. Instead they come up from complex relations between all the cells components like proteins, DNA, RNA and small molecules. To understand these multipart interactions that contribute to cells function and structure is one of the major tasks in biology. Due to the development of high-throughput genomics it is now possible to determine when and how all these molecules interact with each other, thus generating regulatory networks instead of isolated linear pathways (Barabási and Oltvai, 2004). So the focus has switched from one particular process to a more global view. Generally, these molecular networks can be divided into three types:

A metabolic network is the complete set of metabolic and physical processes in a living cell that determine its physiological and biochemical properties. These networks comprise the chemical reactions of metabolism as well as the regulatory interactions that guide these reactions (Ma and Zeng, 2003). Transcriptional networks describe the relationship between pairs of genes, comparing the effect of the expression level of one gene on the expression level of the other one (Ronen et al., 2002; Evangelisti and Wagner, 2004). Protein interaction networks represent the relationship between different proteins such as forming complexes or modifications by signalling enzymes (Uetz et al., 2000; Maslov and Sneppen, 2002; Agraftoti et al., 2005) Even this classification is just a simplified version of the complex processes going on in the living cell since these networks are in reality highly connected: Gene expression always depends on the level of proteins as well as on metabolites, so there are some feedback loops between these systems demonstrating that regulation is a principle feature of biological systems (de Silva and Stumpf, 2005). Therefore these highly interconnected systems are referred as democratic, while hypothetical systems without feedback regulation are called dictatorial (D. Stokic, personal communication).

Networks themselves are complex systems, whose components communicate with each other through pairwise interactions, which can be reduced to a pair of nodes that are connected to each other by links. Links and nodes together form a network, or in mathematical terms, a graph. Complex networks can be charcaterised according to their

degree or connectivity k that defines the number of links between nodes. In contrast to undirected networks, in directed networks it can be distinguished between incoming and outgoing degrees. The first mentioned refers to the number of links that are directed to a node (k_{in}), whereas k_{out} refers to the number of links that start from a node. The degree distribution $P(k)$ refers to the probability, that selected nodes contain the connectivity k , and enables to characterize different networks. Furthermore, important information like the existence of highly connected nodes (hubs) in a network could be derived out of degree distribution. Another notable class of networks are scale-free ones, which have a power law degree distribution, $P(k) \sim k^{-\gamma}$, where γ is the degree exponent, that is inversely proportional to the importance of the role of the hubs in the network. Most processes within the cell contain a scale-free topology, like protein-protein-, and genetic regulatory networks, in which the nodes represent single genes and links are derived from perturbation experiments (Barabasi and Oltvai, 2004; Jeong et al., 2000; Wagner and Fell, 2001).

Shortest path and mean path lengths are important for network distances. The first refers to the number of links that have to be passed to travel between two nodes and the mean path length represents the average over the shortest paths between all pairs of nodes.

The last measure needed for network topology is the clustering coefficient, $C_I = 2n_I / k(k-1)$, which quantifies how close a node and its neighbours are to being a cluster. Otherwise put, if node A is connected to node B, and node B is connected to node C, then the clustering coefficient indicates the possible connection of node A to node C (Barabasi and Oltvai, Watts and Strogatz, 1998).

3.6.1. Network identification by multiple regression

In 2003, Gardner et al. developed algorithm that enables to represent complex biological connections in a gene regulatory network. Based only on steady-state expression measurement, a functional and predictive model of gene interactions could be constructed. Therefore a system identification method, called network identification by multiple regression (NIR) that comprises the response of genes and proteins to external perturbations, was applied. It was assumed, that such genetic networks can be described by nonlinear regression equations. Furthermore, near the steady-state, when gene expression does not change over time, a nonlinear system can be described by linear equations, where the rate of accumulation of RNA, protein or metabolite results

from a transcriptional perturbation. Out of these presumptions, the following formula was developed:

$$dx/dt = Ax + u$$

x ...concentrations of N RNA-species

dx/dt ...rate of accumulation of species x

u ...external perturbations

A ... $N \times N$ matrix, describing the regulatory interactions between the species in x

Under steady-state expression ($dx/dt = 0$), A can be solved by performing N distinct perturbations (u) and recovering N sets of RNA concentrations (x). Due to high levels of background noise, measurement of mRNA levels leads to wrong data. By applying a simplified model that rests on the fact that biological networks are not fully connected, the equation could be solved by assuming a maximum of k (where $k < N$) non-zero regulatory inputs to each gene, thus generating a robust system. Finally, multiple linear regression was used to select k in a way, that the final system is stable and the resulting coefficient of A is statistically significant (Gardner et al., 2003)

The NIR method was adapted on a subnetwork of the SOS pathway in *E.coli*, resulting in identification of most of the gene connections. Nevertheless, only nine transcriptional perturbations were applied, so that the effects and the applicability of larger networks on the identified algorithm were unknown. To overcome this limitation, the Complex System Research Group, Medical University of Vienna, developed further algorithm, which considers the features of larger networks with at least 30 transcriptional perturbations. Therefore the original equation $dx/dt = f(A, x)$ was expanded in following ways:

$$A = \ln(D+I)$$

Aadjacency matrix

Dinfluence matrix

Iidentity matrix

In order to describe the regulatory interactions in a network, the adjacency matrix has to be solved. Therefore, the influence matrix, $D_{ij} = \ln (x_{ij}/x_i^0)$ was determined. The term x_{ij}/x_i^0 refer to the gene expression of i^{th} gene, if the j^{th} gene is perturbed, whereas x_i^0 stands for gene expression of the i^{th} gene with the empty vector. Therefore, the influence matrix describes the effect of perturbation of one gene to the expression of another gene. The results of (x_{ij}/x_i^0) are always <1 , 0 , or >1 , indicating positiv-, negativ- or no interaction at all. The network consists of matrices for each possible path, and can finally be determined by summing up all matrices. Since D is also referred as function of all paths in a network, the adjacency matrix A can finally be calculated by the quoted equation. (D. Stokic, personal communication)

4. Materials and Methods

4.1 Buffers and Solutions

Luria Broth agar plates

7.00 g Bacto-tryptone (DIFCO, USA, Cat.No. 211705) 3.50 g Bacto-yeast extract (DIFCO, USA, Cat.No. 212750) } LB medium
7.00 g NaCl
10.5 g Agar (DIFCO, USA, Cat.No. 281230)
Distilled water was added to a volume of 700 ml, pH 7,5 (adjusted using 1N NaOH),
Medium was autoclaved, cooled down to 50°C
700 µl antibiotics were added (30µg/µl ampicillin, chloramphenicol or kanamycin).

50 x TAEBuffer

96.80 g TRIS
22.80 ml CH₃COOH
40.00 ml EDTA (0,5M)
Distilled water was added to a volume of 20 l.

Plasmid Preparation Lysis Buffer (TENS)

0.50 ml 1 M TRIS
100 µl 0.5 M EDTA
5.00 ml 1N NaOH
1.15 ml 20% SDS
Distilled water was added to a volume of 50 ml.

SOC Medium

5.0 g Bacto-yeast extract (DIFCO, USA, Cat.No. 212750)
20.0 g Bacto-tryptone (DIFCO, USA, Cat.No. 211705)
0.5 g NaCl,
10.0 ml 0.25 M KCL
5.0 ml 2 M MgCl₂
20.0 ml 1 M D-glucose
Distilled water was added to a volume of 1000 ml, pH adjusted to 7.0.

1 x Laemmli Buffer

6.25 ml 1M Tris-HCl pH 6,8
2.35 g SDS
1.54 g DTT
0.04 g EDTA
10 ml Glycerol
1 mg Bromphenol Blue
Distilled water was added to a volume of 100 ml

PBS (phosphate buffered saline)

0.20 g KCl
0.20 g KH₂PO₄
1.15 g Na₂HPO₄
8.00 g NaCl
Distilled water was added to a volume of 1000 ml and pH was adjusted to 7.4

1 x Cell Lysis Buffer

40 µl 1 M Tris-HCl pH 8.0
77 µl 4 M NaCl
10 µl 50 mM EDTA
10 µl 50 mM EGTA
20 µl Nonidet® P40 (Fluka, Cat.No. 94385)
20 µl 100 mM Na₃VO₄
2 µl 1 M Pefabloc [4-(2-Aminoethyl)benzenesulfonylfluoride.HCl] (Pentapharm Ltd., Germany, Cat.No.31682.01)
Distilled water was added to a volume of 2 ml

10 % SDS-Acrylamid Gel

4.0 ml Aqua dest.
3.3 ml 30 % Acrylamid BIS (29:1, BioRad)
2.5 ml Tris-HCl pH 8.8
ml 10 % SDS
0.1 ml 10 % APS
4 µl TEMED (N,N,N',N'-Tetramethylethylenediamine)

Stacking Gel

3.4 ml Aqua dest.
830 µl 30 % Acrylamid BIS (29:1)
630 µl Tris-HCl pH 6.8
50 µl 10 % SDS
50 µl 10 % APS
5 µl TEMED

Electrophoresis Buffer

72 g Glycin
15 g Tris
25 ml 20 % SDS
Distilled water was added to a volume of 2.5 l

Transfer Buffer

28.0 g Glycin
6.1 g Tris
500 ml Methanol
Distilled water was added to a volume of 2.5 l

Ponceau S Red

0.1 % Ponceau S Rot in Aqua dest.
5 % Acetic Acid

10 x TBS (Tris Buffered Saline)

24.5 g Tris
80.0 g NaCl
Distilled water was added to a volume of 1 l, pH was adjusted to 7.6

Washing Buffer

10 ml 10 x TBS
90 ml distilled water
1 ml Tween-20

Blocking Buffer

5 ml 10 x TBS
45 ml distilled water
2.5 g nonfat dry milk
50 µl Tween-20

Antibody Dilution Buffer

2 ml 10 x TBS
18 ml distilled water
1 g BSA
20 µl Tween-20

Citrate working solution

18 ml 0.1 M citric acid solution

(21 g citric acid, monohydrate, in 1000 ml H₂O)

82 ml 0.1 M sodium citrate solution

(29.4 g trisodium citrate dehydrate in 1000 ml H₂O)

Distilled water was added to a volume of 1 l, pH was adjusted to 6

4.2. Molecular Biology

Vectors containing the coding sequence of the gene of interest were purchased from the German Resource Centre for Genome Research RZPD, www.rzpd.de (Fig. 7).

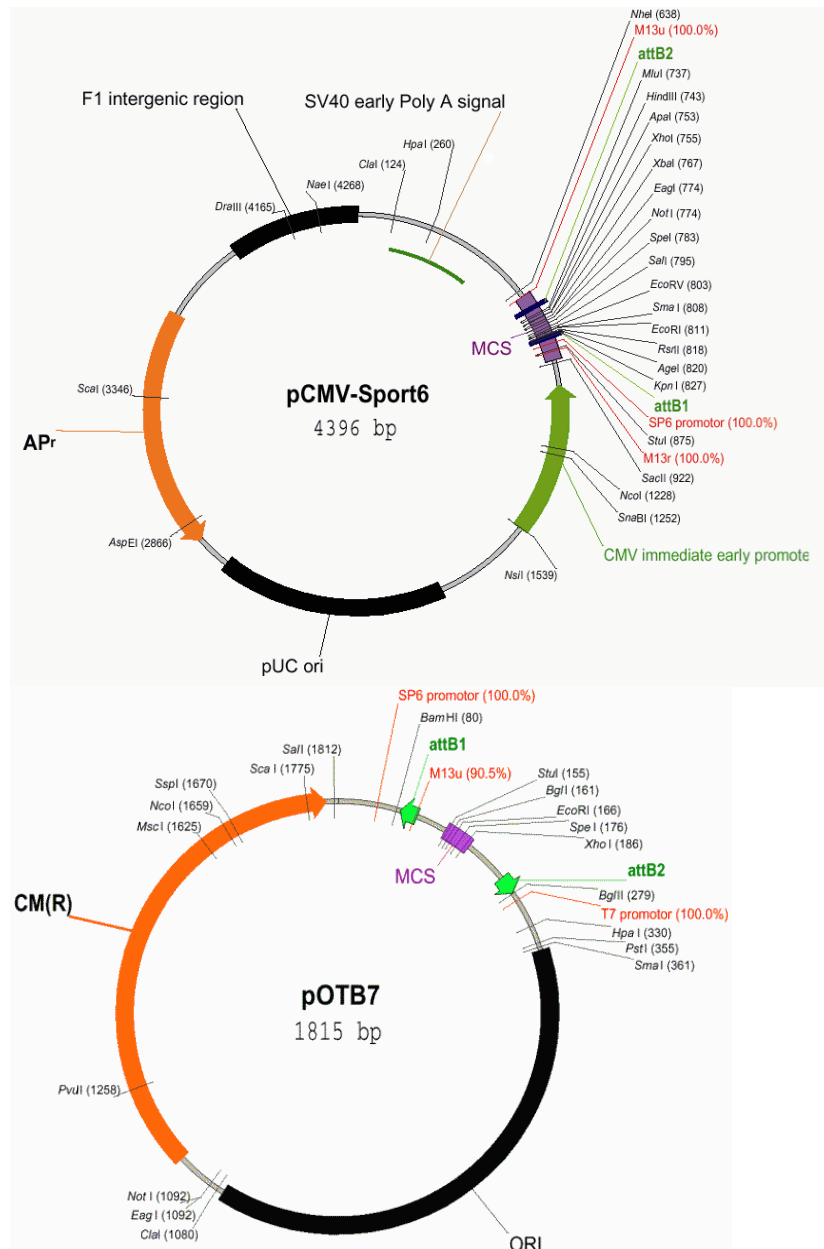


Figure 8. Expression vectors pCMV-Sport6 and pOTB7. Vectors containing the coding sequence of genes of interest were ordered at the German Resource Centre of Genome Research RZPD and delivered as vector containing *E. coli*'s in step agar.

E. coli transformed with a vector containing the gene of interest were picked from LB plates to inoculate 4 ml of LB Medium, supplemented with 4 µl of antibiotics (ampicillin 100 µg/µl, chloramphenicol 30 µl/µg, kanamycin 25 µl/µg) according to the vector resistance. Before harvesting, cells were incubated on a shaker (250 rpm, 37°C) for 20 hours.

Plasmid miniprep (DNA yield up to 20 µg) was done according to method “Genevieve” as well as miniprep with the QIAprep™ Spin Miniprep Kit. The latter is used to obtain high purity DNA for subsequent sequencing of positive clones verified by digestion and gel electrophoresis. DNA yield of miniprep

Method “Genevieve” starts with centrifugation of 1.5 ml suspension at 9.300 x g. Afterwards the cells were resuspended in 40 µl supernatant, 300 µl TENS was added and mixed by vortexing. 150 µl ice cold KAc (3M) was added subsequently and tubes were inverted, followed by spinning at 10,000 rpm for 2 min. Then the supernatant was placed into a new tube, 900µl ethanol (96%) added and stored for 30 min at -80 °C. After spinning (20 min, 9,500 x g, 4°C), the DNA pellet was washed with 70 % ethanol and centrifuged again for 2 min at 13,000 rpm. The ethanol was removed, the pellet air dried and finally dissolved in 50 µl DNase-free water.

Plasmid isolation using QIAprep™ Spin Miniprep Kit was initiated with centrifugation of 1.5 ml cell suspension at 9,300 x g. The resulting cell pellet was worked up according to protocol. Finally the isolated plasmid DNA was dissolved in 30 µl DNase-free water.

For **PCR amplification** of the coding sequence (cds) of the purchased clone a Gene Amp 9600 System from Perkin Elmer was used and the amplification was done according to a standard protocol

H ₂ O	32.75 µl
10 x Buffer	5.00 µl
MgCl ₂	3.00 µl (final concentration 1, 5 mM)
dNTPs	4.00 µl (final concentration 200 µM)
Rapid Load	3.00 µl
Taq Polymerase	0.25 µl (1, 25 Units)
Primer	0.50 µl (final concentration 1 µM)
DNA	1.00 µl

PCR Programm:

95 °C	10 min	
95 °C	1 min	} 40 cycles
58 °C	1 min	
72 °C	80 sec	
72 °C	10 min	
4 °C	forever	

The used primers include overhangs for restriction sites of the overexpression vector pIRES2-EGFP and were designed by OligoPerfectDesigner Tm (Invitrogen) and purchased from Invitrogen, www.invitrogen.com.

Gel electrophoresis was used to control the amplified vector insert on a 1 % TAE-agarosegel supplemented with 0.1 % ethidium bromide, running at 100 V for 20 to 30 min. For determination of the lengths of the DNA fragments, molecular weight markers (1 kb DNA-ladder, cat. no. N3232S and 100 bp DNA-ladder, cat. no. N3231S, both New England Bio Labs Inc., MA) were used (Fig. 8). After examination of the bands of interest by an UV transilluminator, the bands were cut out and the DNA was isolated by gel extraction.

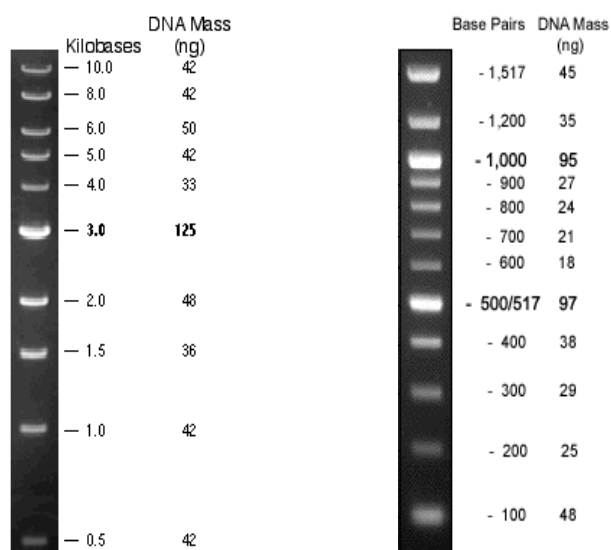


Figure 8. Molecular weight markers. 1 kb and 100 bp molecular weight markers were used to determine the length of the DNA fragments by gel electrophoresis.

Gel extraction was done with QIAquick™ Gel Extraction Kit (QIAGEN, PCR Purification Kit, cat. no. 28104) according to the protocol. Therefore, 3 volumes of Buffer QC (gel dissolving buffer) were added to the weighted cut out gel piece and incubated at 50 °C until the gel was completely dissolved. Afterwards the mixture was added on the QIAquick column, washed with buffer PE and eluted with 30 µl DNase free water.

For overexpression of the gene of interest, the vector pIRES2-EGFP (cat. no. 6029-1, Clontech Laboratories Inc., CA) was used (Fig.9). It contained an internal ribosome binding site (IRES) of the encephalomyocarditis virus (ECMV) between a multiple cloning site and the enhanced green fluorescent protein coding sequence. The cds of interest was cloned into the multiple cloning site. Thereby the candidate gene and the fluorescent protein were translated from one single bicistronic mRNA. This permitted an efficient selection of transiently transfected mammalian cells expressing the EGFP as well as the protein of interest simultaneously. Thus the rates of transcription and translation of the EGFP and the overexpressed protein were equal. Differences occurred only due to different stability of the expressed proteins. EGFP is a red shift variant of wild type GFP (a protein found in the jellyfish *Aequorea victoria*) that has been optimized for brighter fluorescence and stronger expression in mammalian cell lines.



Figure 9. pIRES2-EGFP expression vector. pIRES2-EGFP was used as expression vector for exogenous overexpression of the candidate gene.

Double digestion with appropriate restriction endonucleases (EcoRI, Cat.No. R0101S, SacII Cat. No. R0157S, BamHI, Cat.No. R0136S, New England Bio Labs Inc.) was used to generate sticky ends of the isolated gene fragments as well as of the expression vector. Adequate buffers (NEBuffer 4, Cat.No. B7004S, NEBuffer 3, Cat.No. B7003S, New England Bio Labs Inc.) were added and the reaction was carried out at 37°C or 2 to 20 hours.

DNA	5.0 µl
10 x Buffer	2.0 µl
100 x BSA	0.2 µl
Restriction enzyme	1.0 µl each (20 units / µl)
H ₂ O	10.8 µl

Before ligation, the overexpression vector was treated with 1µl CIP (calf intestinal alkaline phosphatase) for 1 h at 37 °C. CIP catalyzes the removal of 5' phosphate groups from DNA, and since fragments without 5'phosphat groups cannot self-ligate,

the amount of properly ligated products rises whereas vector background of improperly self-ligated constructs is reduced.

For **ligation** of the gene of interest into the overexpression vector pIRES2-EGFP, T4 DNA Ligase (Invitrogen, cat. no 15224017) as well as ligation buffer (5x T4 DNA Ligase Buffer, Invitrogen, cat. no. 46300-018) were used. The ligation was carried out for 1 h at room temperature according to the following reaction mix:

DNA insert	9 µl
5 x Ligation Buffer	3 µl
T4 DNA Ligase	1 µl 1 unit/µl
Vector	1 µl
H2O	1 µl

For **transformation** into ONE shot MAX Efficiency DH5αTM –T1R chemical competent cells (Invitrogen, cat. no. K4520-01) the cells (50 µl aliquot for each reaction) were thawed on ice and 5 µl of the ligation mix was pipetted directly into the competent cells, gently mixed by tapping and incubated on ice for 30 min, followed by heat shock at 42°C for 30 seconds.

Afterwards, 250 µl SOC medium (prewarmed to 37°C) were added and the mixture incubated for 60 min at 250 rpm and 37°C. The transformed cells were plated onto LB medium plates supplemented with kanamycin for selection of the transformed DH5αTM, and incubated overnight at 37 °C.

If direct ligation into pIRES2-EGFP was not successful, subcloning was done using TOPO TA Cloning ®Kit (Invitrogen, cat. no. K4520-01). 2 µl of the PCR product were directly ligated into 1 µl of TOPO® Vector and incubated for 10 to 30 minutes.

Glycerol stocks of positive transformed DH5αTM , carrying pIRES2-EGFP containing the gene of interest, were made by adding 300 µl of 87% glycerol to 700 µl bacterial suspensions (positive cultures) and stored at -80°C.

Capillary sequencing was done to verify the correct sequence of the cloned gene. Therefore, plasmid DNA was purified using the QIAprep Spin Miniprep Kit (QIAGEN, Cat. No. 27104) according to protocol. Sequencing was done with an ABI Prism 377 sequencing detection system (Applied Biosystems, CA.). First, cycle sequencing

reactions were carried out to generate ddNTP-labelled DNA fragments; which then could be detected by the ABI Prism.

Water (HPLC-grade)	5 μ l
Big Dye™ Reaction Mix (Applied Biosystems)	2 μ l
Sequencing primer (Invitrogen)	1 μ l
DNA	1 μ l

Cycle sequencing reaction program:

96 °C	1 min.		
96 °C	12 sec.	}	29 cycles
56 °C	7 sec.		
60 °C	2 min.		
4 °C	forever		

The labelled fragments were then isolated from remaining ddNTPs using DyeEX 2.0 Spin Kit (QIAGEN, cat. no. 63204) according to protocol. Finally the samples were prepared for sequencing by adding 20 μ l formamide.

Plasmid midipreparation results in DNA amounts up to 100 μ g and was used to obtain endotoxin free DNA for subsequent transfection steps. Therefore 50 ml of LB medium supplemented with 50 μ l kanamycin (25 μ l / μ g) were inoculated with 5 μ l of sequence verified bacterial stock. Before harvesting the cells were incubated on a shaker (250 rpm / 37°C) for 20 hours. Then the cell suspension was centrifuged (6000 x g / 4°C) and further handled according to protocol. Finally the endotoxin free DNA was dissolved in 100 μ l DNase free water.

DNA concentration was determined by measurement of the absorbance of the DNA sample at 260 nm using a U-2000 Spectrophotometer (Hitachi). Knowledge of the exact DNA concentration is relevant for subsequent experiments, since plasmid amount has to be adjusted to applied quantity of lipofectamin, a reagent essential for transfection. For the measurement 3 μ l of the DNA sample were diluted 1:200 in 600 μ l of DNase free water and DNA concentration was obtained by following formula

$$c [\mu\text{g/ml}] = \text{OD}_{260} \times D \times F$$

c ...concentration of initial sample
 OD₂₆₀ ...absorption at 260 nm
 D ...dilution factor
 F ...empirical factor (50 for dsDNA)

For **RNA isolation** cells were harvested and centrifuged (300 x g for 2 min). Afterwards cells were instantly resuspended in lysis buffer supplemented with 1 % β -mercaptoethanol. For homogenizing of the cell sample a QIAshredder® (QIAGEN) was used. Up to 700 μ l of lysate was loaded on a QIAshredder spin column that was placed in a 2 ml collection tube, and centrifuged at maximum speed for 2 minutes. RNA Isolation of the homogenized lysate was carried out using Rneasy® Mini Kit (QIAGEN). The sample was mixed with one volume of 80 % RNase-free ethanol and applied on an RNeasy column and centrifuged for 2 min at 13.000 x g. After a subsequent washing step the RNA was submitted to an on-column DNase digestion with an RNase-free DNase set (QIAGEN cat. no. 79254) to remove genomic DNA that could interfere with following real time PCR experiments. After further washing steps isolated RNA was eluted with 30 μ l of RNase-free water.

For further Real Time PCR Experiments, the previous isolated RNA was transcribed into cDNA. Therefore 1 μ g of isolated RNA was stocked up with DEPC-water to a volume of 10.5 μ l, 0.5 μ l of random hexamer primer as well as 1 μ l 10 mM dNTPs were added and incubated for 5 min at 65°C. 4 μ l single strand buffer, 2 μ l 0.1 M DTT and 1 μ l RNase were added whilst the sample was put on ice. After an incubation step of 2 minutes at 25° C 1 μ l Super Script II was added and the reverse transcription program using a thermal cycler was carried out as follows:

25 °C 10 min.
 42 °C 50 min.
 70 °C 15 min.

The generated cDNA samples were stored at –20° C for further use in High Throughput RT PCR.

Since integrity of the target sequence is one of the key factors influencing the sensitivity of PCR experiments, a quality control of the transcribed cDNA was performed. The

method of choice was a multiplex PCR assay, which permits a valuation of the extent of RNA degradation due to the simultaneous amplification of control genes that are expressed at different levels. The transcripts were derived from four different housekeeping genes, generating four bands of different size, (Bcr, Abl, β 2-MG and Pbgd), ranging from 128 bp to 377 bp. In high quality samples all four bands were visible whereas decline of quality due to degradation of the primary RNA samples or unsuccessfully reverse transcription decreasingly transcripts were amplified (Watzinger and Lion, 1998).

High throughput real time PCR was carried out using TaqMan Low Density Custom Arrays (Applied Biosystems) that enables to perform 384 real time PCR reactions simultaneous, with both primers and probes already spotted on the plates. The arrays were designed using the 64 well formats that enable to apply 64 different pre-made assays on a 384-well plate thereby forming two series of triplicates. The assays were selected from a set of pre-made assays available on www.appliedbiosystems.com. When for one target gene multiple assays were available, the assay located nearest to the 5' end of the target was chosen. This permits successful amplification of cDNA even in case of incomplete reverse transcription of mRNA.

To start the real time experiments the cDNA samples were diluted to a final volume of 430 μ l, mixed with 430 μ l of TaqMan PCR Mastermix and 100 μ l were applied directly into the loading ports of the TaqMan plates, resulting in four ports per cDNA sample and Low Density custom arrays. Centrifugation for two minutes at 330 g ensures an equal distribution of the applied mix into the designed wells and sealing of the plates inhibits diffusion between the reaction wells and prevents forming of bubbles. The following Real time PCR was carried out using a ABI Prism 7700 sequence detection system and the obtained data analyzed using the SDS 2.2 software. It was necessary to adjust threshold as baselines manually before the data were exported and further analyzed using Windows Excel program.

Analyzing was done using the $\Delta\Delta C_t$ method, where the change of transcription of the samples is compared to a reference group of housekeeping genes (Schmittgen and Livak, 2008). Since two arrays (DMA1 and DMA2) were used for the measurement of one sample, differences had to be corrected. Therefore C_t values of the sample were normalized to C_t values of the housekeeping gene GAPDH, which was then normalized

to the average Ct values acquired from *Nars* and *Tardbp*, two further housekeeping genes localized on DMA2. For the final results the difference between a calibrator (cDNA from cells transfected with empty pIRES2-EGFP) and the actual sample (cDNA from cells transfected with pIRES2-EGFP overexpressing a target gene) was built.

4.3. Cell Culture

Human immortalized umbilical vein endothelial cells (iHUECS), an hTERT immortalized endothelial cell line were used as a model system of diabetic microangiopathy in vitro (Bian et al., 2005).

iHUECS were grown in RPMI 1640 medium (GIBCO, Cat.No. 51800-035), supplemented with 10 % FBS (GIBCO, Cat.No. 10108-157) and 1 % penicilline/streptomycine (GIBCO, Cat.No.15140-122). The cultivation of these cells was done in an incubator supplied with 5 % CO₂ and 90 % relative humidity at 37°C.

The cells were passaged at 90 to 95 % confluence. Old, exhausted medium was removed, the cells shortly washed with 1 x PBS in order to remove serum residues that would inhibit following trypsin reaction. 1.5 ml 1 x trypsin/EDTA (GIBCO) was added and incubated for 2 – 3 minutes at 37 °C. Afterwards the reaction was stopped by adding complete medium. Centrifugation and suspension took place before the cells were distributed to new culture flasks (75 cm²) containing 14 ml complete medium.

For long time storage cells were frozen in liquid nitrogen. Therefore iHUECs were grown up to 90 % confluence before trypsin was added and the cells were harvested. After centrifugation the pellet was resuspended with a mixture of 1800 µl FBS and 200 µl DMSO (99.5 %), distributed into two 1.5 ml tubes and stored at -80 °C for 2 to 3 days. Afterwards the cells were put into liquid nitrogen for long time storage.

For thawing of nitrogen frozen iHUECs the cells were put into a water bath at 37 °C until they get a crushed-ice like consistence. Then 7 ml of complete medium were added, cells were resuspended and centrifuged and finally distributed in appropriate cell culture flasks. For complete removal of DMSO it was necessary to change the medium the next day.

4.3.1. Immunofluorescence staining

For immunofluorescence staining iHuecs were seeded on chamber slides (40,000 cells / 0,7cm²) and treated with 25 mM D-glucose to stimulate diabetic conditions. 25 mM L-glucose was added as osmotic control since this sugar can not be metabolized in the cell. After 72 h of glucose treatment at which D- and L-glucose (on the control slides) were added every 12th hour the cells were washed with PBS and fixed in 4%

paraformaldehyde (100 μ l/cm²) for 10 minutes. Afterwards the cells were washed with PBS and treated with 0.1 % Triton X -100 (100 μ l /cm²) dissolved in PBS in order to solubilize the plasma membrane. After washing with PBS, foetal calf serum (1:100 in PBS) was added to the cells for 30 minutes to block unspecific binding sites.

Cells were washed again with PBS prior of incubation with 30 μ l of the primary antibody (rabbit anti-RPL3 polyclonal antibody, 11005-1-AP, ProteinTech Group, Inc., 1 μ g/ ml) for 45 minutes. After subsequent washing steps with PBS the secondary antibody (Alexa Fluor® 594 goat anti rabbit IgG (H+L), 2 μ g/ ml, A-21044, Molecular Probes) was applied for 45 min, cells were washed again with PBS and DAPI (10 mg/ml) was added for 50 seconds. Finally, cells were washed again and covered with GelTol Mounting Medium (Thermo Electron Corporation, Waltham, MA) for analysing with fluorescence microscopy (Axiophot, Zeiss).

4.3.2. Flow cytometry

Flow cytometry was used as method of choice to select successful transfected iHUECs due to the fluorescence ability of the EGFP protein. Therefore cells were harvesting 48 h after transfection by trypsinization, followed by centrifugation for 4 min at 1800 rpm. The cell pellet was then resuspended in 1 ml of complete medium and finally 1 μ g/ml of 7-amino-actinomycin D (7-AAD, Fluka, Buchs SG, Switzerland, cat. no. 06648) was added.

Flow cytometric cell sorting was carried out by the Division of Rheumatology/Department of Internal Medicine III in cooperation with the Core Unit Cell Sorting, both from the Medical University of Vienna. For sorting a BD FACSAria™ flow cytometer was used and EGFP emission was detected via FL1 channel using a bandpass filter at 530 \pm 15nm. Sort criteria combined a generously wide scatterlight region excluding small particles (cell fragments and debris) with positivity for EGFP as well as negativity for 7-AAD. Furthermore, transfection efficiencies and EGFP half-life were determined using a BD FACSCalibur™ flow cytometer. The sorted EGFP-positive, 7-AAD negative cells were lysed in 350 μ l of RLT buffer supplemented with 1% β -mercaptoethanol and stored at -80°C until RNA isolation was executed. For isolation of sufficient RNA, the sorting had to yield at least 300,000 EGFP-positive cells.

4.3.3. Transfection

Since cellular membranes create barriers for large and highly charged DNA molecules to enter cellular compartments, several techniques have been developed to facilitate cellular transfection. These methods include calcium phosphate precipitation, electroporation, DNA-DEAE complexes, microinjection, virus-mediated transfection, introduction of DNA via particle bombardment and lipid mediated transfection. The method of choice was liposome mediated transfection, using Lipofectamin2000, a cationic lipid carrier that complexes with nucleotides and mediates transfection of iHUECs with plasmid DNA (Tanner et al., 1997; Kaiser and Toborek, 2001).

For transfection the cells were cultured in a 75 cm² flask and 30 µg of DNA, resuspended in 1875 µl Opti-MEM®, were mixed with 37.5 µl of lipofectamin2000, resuspended in 1875 µl Opti-MEM®, and incubated for 20 to 30 minutes. IHUECs that were grown to confluence of 90 to 95 % were washed with Opti-MEM® before the transfection mix was added. After incubation of 2 hours the transfection mix was removed, the cells were washed and complete medium was added before incubation for 40 to 45 hours was accomplished (5 % CO₂, 90 % relative humidity, 37 °C). Afterwards tryptonized cells as well as removed medium were centrifuged at 1800 rpm, pellets pooled and prepared for flow cytometric cell sorting.

4.4. Biochemistry

4.4.1. Western blotting

Western blotting was used to verify interactions given by network algorithm. Therefore iHUECs were grown up to 90 % confluence and transfected with pIRES2-EGFP, containing genes coding for proteins of interest. After 40 h of transfection, cells were harvested by trypsin addition and centrifugation at 1800 rpm. Afterwards the cell sample was solubilized in laemmli buffer supplemented with 0,02 % DTT, heated up to 96 ° C for 3 minutes and centrifuged (10.000 x g, 5 minutes). For measurement of the protein concentration of the samples, a protein assay in laemmli buffer was done (Karlsson et al., 1994).

Therefore the solubilized cell sample was diluted in laemmli buffer to a final concentration of less than 0,3 mg/ml, and 150 µl were applied to a microtiter plate. Finally 100 µl of TCA were added, resulting in protein precipitation, illustrated in a yellowish colour of the sample. After a short incubation time of 10 to 30 minutes the turbidity at 570 nm was measured using a microplate reader. Absolute protein concentrations were determined with a BSA standard curve (measured concentrations starting at 10 up to 500 µg / ml).

Resolving – and stacking gel (12 % SDS-Acrylamid) were prepared and loaded with 20 µg of solubilized and diluted protein samples. To verify transfer efficiency and for approximating the molecular weight of the blotted proteins, a prestained protein ladder (Cat. No. #SM0671, Fermentas Life Science), consisting of highly purified coloured proteins, ranging from 10 kDa to 170 kDa was used.

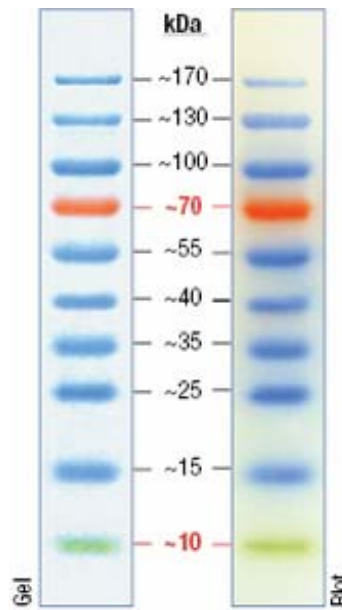


Figure 10. Protein ladder for western blotting. Ladder proteins are covalently coupled with a blue dye, except for two reference bands, which are prestained with green (10 kDa) and orange (72 kDa)

Electrophoreses (100 V, 90 minutes) and subsequently blotting onto a nitrocellulose membrane (17 V, overnight) made the proteins accessible to antibody detection and was performed prior to Ponceau S staining, that visualized transferred and separated proteins. Since nitrocellulose membrane was chosen due to its protein binding abilities, interactions between the membrane and the used antibody for protein detection had to be prevented. Consequently the membrane was washed and destained with TBS-T, followed by blocking for at least 20 minutes in 25 ml of 5 % non-fat dry milk in TBS-T to saturate membrane's binding sites, thus reducing background noise. After further washing steps the blotted membrane was incubated with a corresponding antibody against the protein of interest. The used primary antibody was diluted to the appropriate ratio in 4 ml 10 % non-fat dry milk in TBS-T and applied overnight at 4 °C. After rinsing the membrane (3 x 15 minutes) with TBS-T, incubation with the secondary antibody (HRP-antibody, anti-mouse or anti-rabbit, 1:4.000) was performed for one hour. After washing steps (3 x 15 minutes) the membrane was incubated with ECL plus™ Western Blotting Detection Reagent (Amersham Biosciences) for further detection and analyses using a Lumi-Imager F1™ (Roche Diagnostics).

4.4.2. Immunohistochemical staining

Immunohistochemical staining was carried out on paraffin sections of human diabetic tissue, using the Avidin/Biotin Complex method, where a biotinylated and covalently HRP (horseradish peroxidase) conjugated secondary antibody is used, which binds to this avidin/biotin complex. The enzyme catalyses a chromogenic reaction, in which diaminobenzidine is converted into a brownish, insoluble precipitate. Counterstaining with haematoxylin colours the nuclei blue to envision the structures of the sections. The slides were prewarmed at 55°C for 30 minutes before starting following rehydration steps:

Xylene 1	10 min
Xylene 2	10 min
Isopropanol 1	5 min
Isopropanol 2	5 min
96 % Ethanol	2 min
80 % Ethanol	2 min
70 % Ethanol	2 min
60 % Ethanol	2 min
H ₂ O	5 min

Afterwards the slides were incubated in citrate working solution at 100 °C for 20 minutes, followed by incubation in distilled water for 5 minutes and in 2 % H₂O₂ for 15 to 30 minutes. After washing steps in PBS the slides were blocked in 20 % BSA/PBS for 30 minutes before the first antibody was applied for 60 minutes. After subsequent washing steps in PBS, incubation for 30 minutes with the secondary, biotinylated antibody was carried out. After washing steps, the sections were incubated with Vectastain Elite ABC reagent for 30 minutes. In the next steps, DAB substrate solution was added for 2 to 10 minutes. For counterstaining with haematoxylin, the sections were again washed in distilled water for 5 minutes and stained with haematoxylin for 1 minute. The slides were washed with water for 10 minutes, dehydrated in 60% -, 70 % -, 80 % -, 96 % ethanol for 2 minutes each and in isopropanol and xylene for 5 minutes each. Finally the sections were embeded using Entellan® (Merck, Art. Nr. 1.07960).

5. Results

5.1 Gene selection

Network construction can be achieved by reverse engineering, a process of discovering the principles of a whole system by analysing its structure, function and operation. Perturbation experiments are carried out to calculate fold-changes in transcription level using TaqMan measurements. Subsequently, correlation coefficients can be determined, which describe the interactions between genes and so providing the basis for network architecture. Therefore, when starting practical work for this thesis, our first aim was to achieve fold-change data to start network calculation, assigning gene selection a crucial step in our work. As, however, technology restricted the number of genes, we had to select the genes contributing to the design of the low-density array following three strategies:

First, primary blood endothelial cells were isolated from skin samples of five diabetic and eight non-diabetic patients and compared due to their expression profiles by DNA chip experiments (N. Wick, personal communication). This strategy resulted in 559 genes (“ex vivo set”), showing differential regulation according to T-test and relative variance method (RVM). Out of this gene set two subsets (total of 74 genes, Appendix 2) were determined. Subset 1 passed conventional criteria like signal intensity or associated with parameters of clinical relevance like basal membrane thickness or serum creatinine, as well as identical chromosomal location of the chosen genes. Subset 2 was selected out of the 559 by means of a minimum spanning tree (a subgraph of a connected, undirected graph that connects all vertices and has the least of all weights). This method allowed a gene ranking due to their connectivity and betweenness. Further selection criteria were achieved through tertiary data analysis using STRING and iHOP databases to investigate known protein interactions. For the second gene set (“in vitro gene set”) cultured immortalized blood vascular endothelial cells (iBECs) were treated with D- or L-glucose to stimulate diabetic conditions and again subjected to chip experiment. Out of 1684 genes showing differential regulation according to T-test and RVM, 23 genes overlapped with the ex vivo set, and finally five genes were selected for the design of the array, since they were similar regulated in ex vivo as well as in vitro. The last gene set was achieved by carefully reviewing literature for genes relevant to

diabetes and diabetic microangiopathy and resulted in the “in libro set” that comprised 164 genes. Out of this literature search, 58 genes were included, completing the 125 genes that define the custom low density microarray (Fig.11). *Gapdh* was spotted on DMA1 and DMA2 both to normalize these plates, which then were normalized to the average Ct values acquired from *Nars* and *Tardbp*, two further housekeeping genes localized on DMA2.

After having finished the design of the LDA, the candidates for the cloning and subsequent transient expression process were selected (Krachler A., 2006). Note that these genes would finally be transiently overexpressed one at a time and their effect on transcription of all genes represented on LDA measured, including that of itself. However, due to cloning restrictions (i.e. fragments were too short or too long for cloning, *cds* was not available in expression vector or cloning process was not successful due to unknown reasons) expression data could not be generated from all of the 125 genes. To compensate for this, candidate gene selection was not limited to that present on the LDA but extended by educational decisions to additional genes derived from the *ex vivo* set.

From the latter, we specifically intended to achieve a better insight into fundamental cellular processes like translation in the context of diabetic microangiopathy. We felt that using the LDA as a platform for constructing a network we could also obtain information about the position of selected candidate RNA's in a diabetic network.

Therefore, we screened the possible candidates from the *ex vivo* gene set for translation-associated genes, and identified the five ribosomal proteins RPL13, RPL23a, RPL3, RPLP0 and RPS2. After careful review of literature reviewing we selected *Rpl3* over the other four genes, since *Rpl3* met our demands of a *bona fide* critical component of the translation, specifically contributing to ribosome stability and involvement in the most important process of peptide bond formation (Meskauskas et al., 2005).

After this semi-automated process of gene selection these were subjected to cloning process as described in material and methods and finally contributed to High Throughput RT PCR experiments. Representative for all selected genes, Figure 12 demonstrates distinct cloning steps like PCR amplification, subcloning into TOPO vector and cloning into pIRES2-EGFP, based on the results of *Rpl3*. Additionally, the designed primers, containing annealed extensions, are also illustrated. Successful experiments were detected by gel electrophoresis, resulting in bands according to *Rpl3* at 1211 kb.

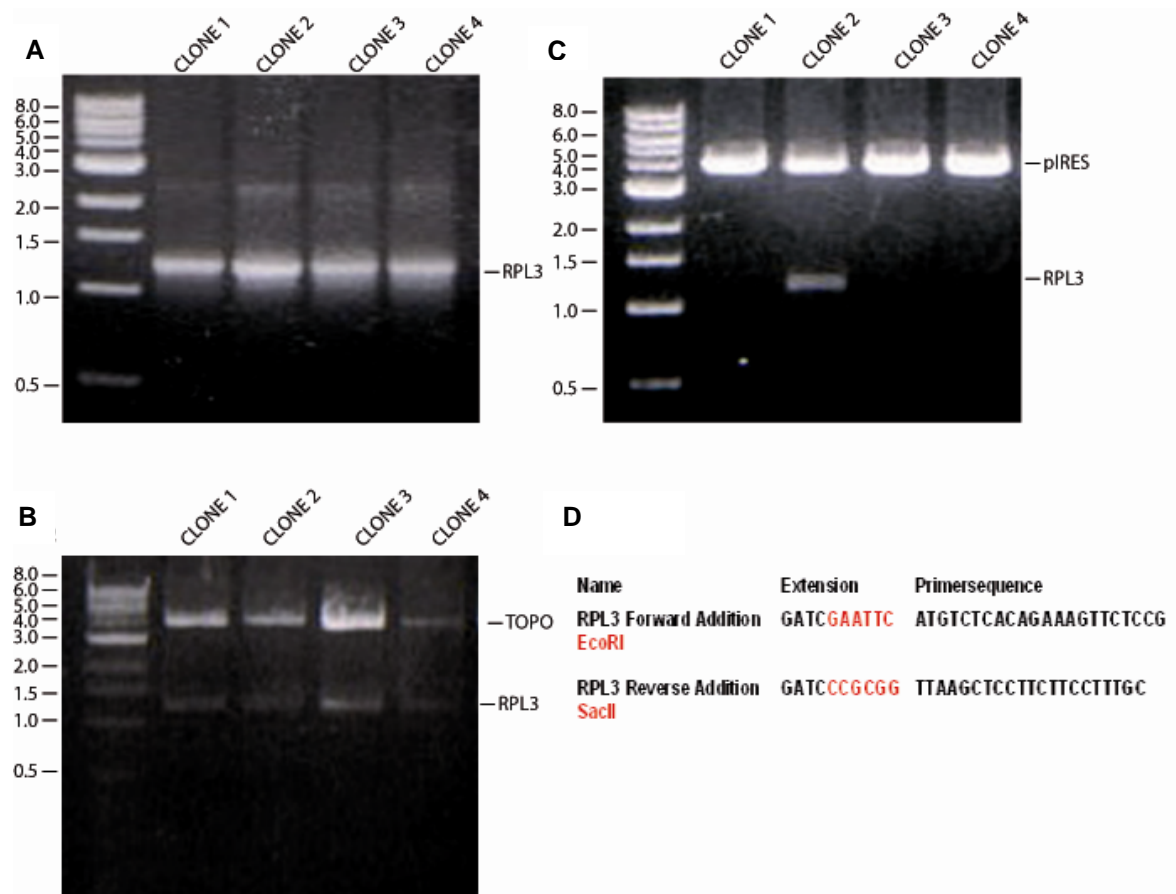


Figure 12. Overview of the cloning process of *Rpl3*. Distinct cloning steps like PCR amplification (A), subcloning into TOPO vector (B), and ligation into the expression vector pIRES2-EGFP (C) are illustrated. Primers were designed as illustrated (D). Gel electrophoresis resulted in bands according to *Rpl3* at 1211kb, to TOPO vector at 3.9 kb and to pIRES2-EGFP at 5.3 kb.

5.2. Endothelial RPL3 under diabetic conditions *in situ*

In order to assure that our selection was of clinical diagnostic significance, we assessed its presence in the sections of the very same diabetic patients that had been the original source for *ex vivo* gene expression analysis. Therefore, skin samples of diabetic and non-diabetic patients were tested for RPL3 protein distribution and semi-quantitation using immunohistochemistry was done (Fig. 13). In both settings, RPL3 was detected in the endothelium of dermal blood capillaries. The reactivity was cytoplasmic and present in all blood vascular endothelial cells. Critically, the staining intensity was different in capillaries of non-diabetic compared to diabetic patients. While there was only weak positivity under normal conditions, staining intensity of diabetic samples was very strong. Occasionally a granular cytoplasmic signal could be observed in diabetic vessels (not shown). These data confirmed the gene expression experiment from *ex vivo* BECs and motivated us to further investigate Rpl3 as a –at least on histopathological level– clinically trustful candidate protein in diabetic microangiopathy.

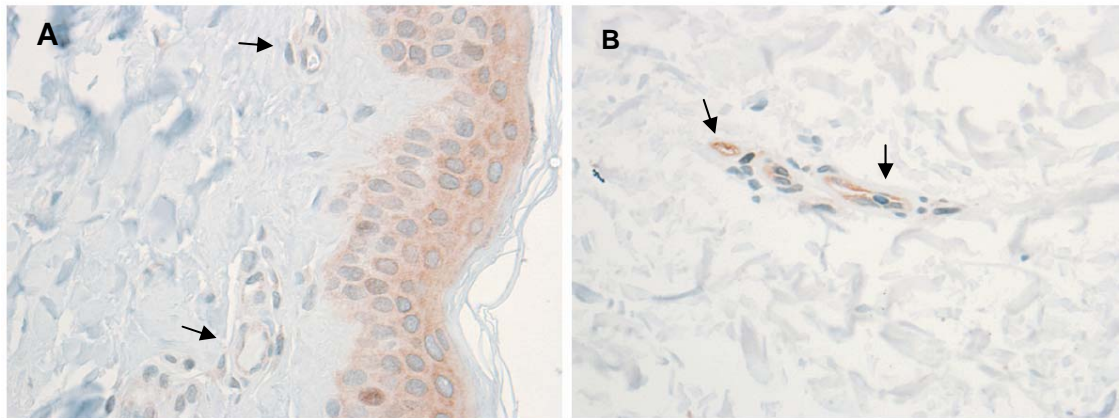


Figure 13. Immunohistochemical staining of RPL3 in non-diabetic and diabetic tissue. Skin samples from non-diabetic (A) and diabetic (B) patients were compared for RPL3 protein reactivity in the endothelial layer of dermal capillaries (arrows). Diabetic samples revealed a stronger reactivity. Magn.: 200x, epidermal reactivity in A is background signal.

5.3. Endothelial RPL3 under diabetic conditions *in vitro*

5.3.1. Endogenous RPL3 protein

Since *in vivo* experiments demonstrated no convincing insight regarding the effects of diabetic conditions on RPL3 protein expression, *in vitro* analyses were performed. We decided to characterize in more detail this protein morphologically, using immunofluorescence analysis. In a first setup the effect of diabetic conditions on endogenous RPL3 was examined. Therefore, iHUECs, immortalized cells mimicking the human endothelium, were treated with D-glucose. Osmotic control was achieved by treatment of parallel samples with L-glucose, a sugar that cannot be metabolized inside the cells. After 48 hours of induced diabetic conditions the stained protein accumulated in selected cells, where it enriched around the nucleus. In L-glucose treated cells a similar pattern was seen, but RPL3 seemed to be restricted to a small region around the nucleus. After 72 hours of diabetic treatment RPL3 aggregated in the whole cells whereas the majority of the L-glucose treated cells showed fluorescence staining still in a defined area around the nucleus. Nevertheless, a small part of these control cells demonstrated an aggregation pattern of the RPL3 protein as seen in diabetic cells. Since RPL3 was over expressed under diabetic conditions *in vivo* (as demonstrated in pre-existing data), this observation is a moderate suggestion for a increased RPL3 synthesis *in vitro* as well (Fig. 14).

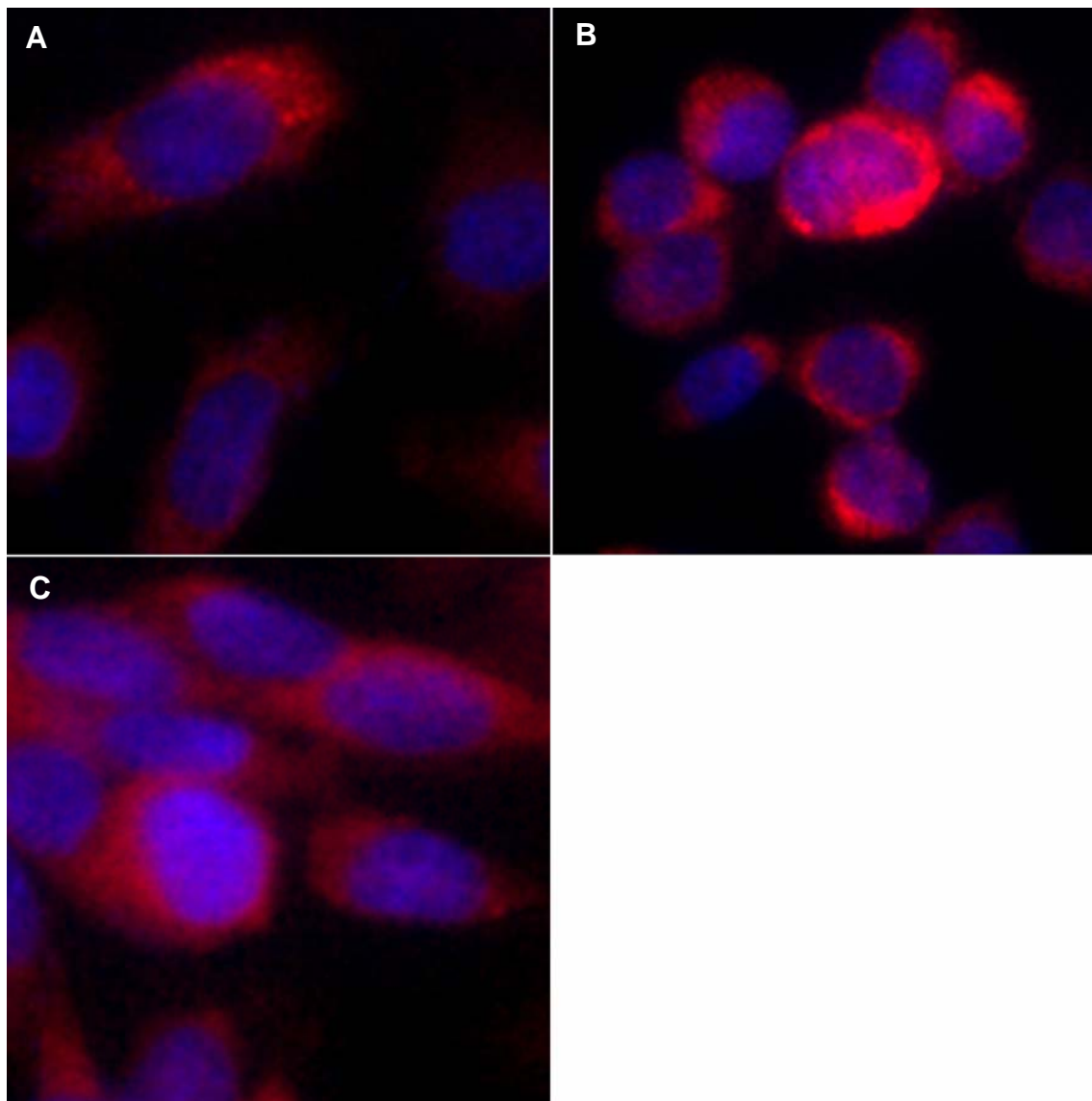


Figure 14. Immunofluorescence staining of endogenous RPL3 in iHuvecs. Cells were treated with D- and L-glucose and tested with an antibody against RPL3. D-glucose treatment for 48 hours displayed RPL3 enrichment around the nucleus and aggregated in the cytoplasm (A). Additional 24 h of diabetic conditions confirmed the previous detected aggregation (B), whereas control cells maintained a diffuse cytoplasmic distribution pattern (C).

5.3.2. Exogenous RPL3 protein

To ensure that all relevant effects regarding RPL3 under diabetic conditions were examined and to guarantee that important features were not ignored due to minimal concentration of the endogenous protein, the impact of enhanced glucose concentration on exogenous RPL3 was also investigated. After overexpression of protein and glucose treatment morphological changes were observed. Already after 48h of diabetic treatment we could observe an aggregation pattern of RPL3 as seen in endogenous cells just after 72h of glucose addition. Accumulation was observed in the whole cells and particularly in the areas around the nucleus. Furthermore, the most notable difference between exogenous and endogenous expression was an accumulation of RPL3 in some cells, thereby forming globular-shaped inclusions in the nuclei. These structures could only be detected after glucose treatment for at least 48 h hours, glucose treatment for additional 24 h showed no evident difference in the described aggregation pattern of RPL3.

In contrast, iHUVESs treated with L-glucose showed no comparable structures. RPL3 accumulation starts circular from the nucleus, completing the cytoplasm of the whole cells, resulting in a diffuse cytoplasmatic aggregation pattern. There was no detectable difference of this pattern after 24 h, 48 h and 72 h of L-glucose treatment. However, in some cells RPL3 was restricted to a small circular region around the nucleus. Summarizing, the pattern of aggregation in control cells showed high similarity to endogenous RPL3 expression under L-glucose enrichment (Fig. 15).

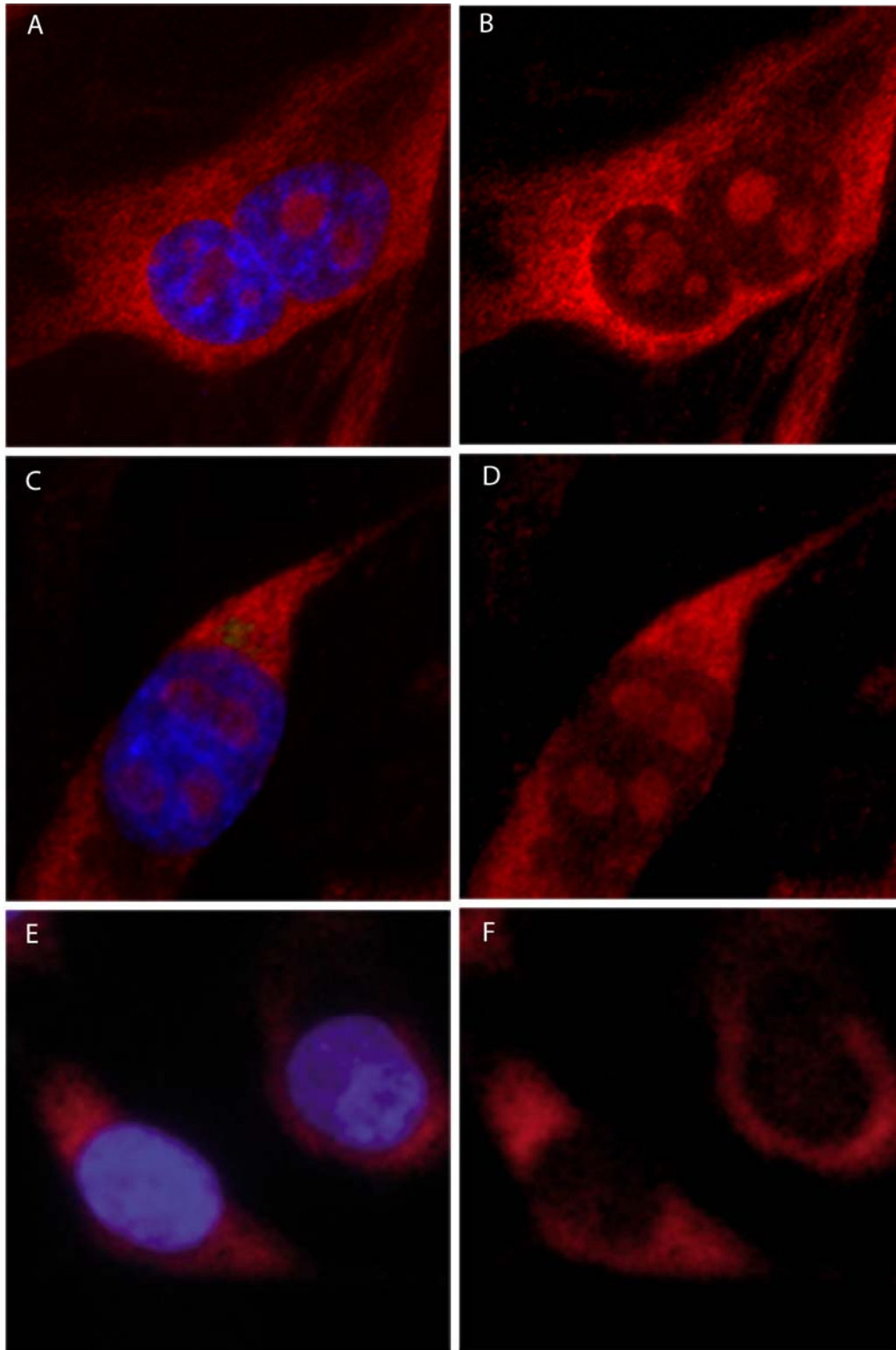


Figure 15. Immunofluorescence staining of iHuvacs expressing exogenous RPL3 after glucose treatment. Exogenous expressing iHUVACS were contributed to D-glucose treatment and stained with antibody against RPL3. After 48 hours globular shaped inclusions were detected (A, B, C, D). Control cells (E, F) displayed no similar structures.

5.4. Position of RPL3 in the genetic network

In order to identify yet unknown connections between candidate genes, the acquired fold-change data were used to gain additional information of the diverse expression patterns and their functional relations.

The final network was created by determining the fold change of all transiently expressed candidate genes and their effect on the expression of the residual gene set of the LDA. Although *Rpl3* itself was none of the genes comprising the low density array, it was still relevant to add its expression data to network calculation since as part of the *ex vivo* set, this protein displayed different expression patterns in diabetic and non diabetic primary blood endothelial cells, thereby allowing speculations about an important role of *Rpl3* in the pathogenesis of diabetic microangiopathy.

A special algorithm (Stokic et al., 2008) was applied to achieve on transcriptional level diverse profiles relative to the other 127 genes represented in the LDA. The *global expression* profile demonstrates the impact of a single candidate gene overexpression on the gene set of the LDA and the *global correlation* identifies similar expression patterns between these global expression profiles. The global expression profile of *Rpl3* was determined, demonstrating the impact of its transient expression on the gene set of the LDA. Although most of the perturbation experiment showed no relevant effect with fold change values ranging between 0.1 and 13.0, we still could detect 13 genes with different regulation due to *Rpl3* expression. The detected fold-changes ranged between $4 \cdot 10^{-4}$ and $1.85 \cdot 10^{16}$, with values less than -1 indicating downregulation and values greater than +1 upregulation (Fig. 16):

Rpl3 overexpression revealed a negative regulation on four genes: Complement component 1, s subcomponent (*C1s*), glyceraldehyde 3-phosphate dehydrogenase (*Gapdh*), platelet-derived growth factor alpha polypeptide (*Pdgfa*) and phosphoglycerate dehydrogenase (*Phgdh*), displaying the following fold change values: $1 \cdot 10^{-3}$ (*C1s*), $3.5 \cdot 10^{-3}$ (*Gapdh*), $4 \cdot 10^{-4}$ (*Pdgfa*) and $2.9 \cdot 10^{-2}$ (*Phgdh*).

Next we examined enhancing effects of *Rpl3* expression on the genes of the LDA set, thereby detecting five genes that were upregulated due to *Rpl3* overexpression: Chemokine (CXC motif) ligand 12 (*Cxcl12*), human fibroblast growth factor 1 (*Fgf1*), Ras homolog gene family, member J protein (*Rhoj*), Rap2 interacting protein (*Rpib9*)

and thrombomodulin (*Thbd*). These genes revealed, in alphabetical order, correlation values of 1.85×10^{16} , 22.74, 168.0, 169.0, 23.93.

As already mentioned, transient RPL3 expression did not have any significant effect on the remaining genes of the LDA set, since their detected fold-change values were limited to the span between 0.1 and 13.0 and according to our definition, upregulating and downregulating effects ranged higher or respectively lower than these values.

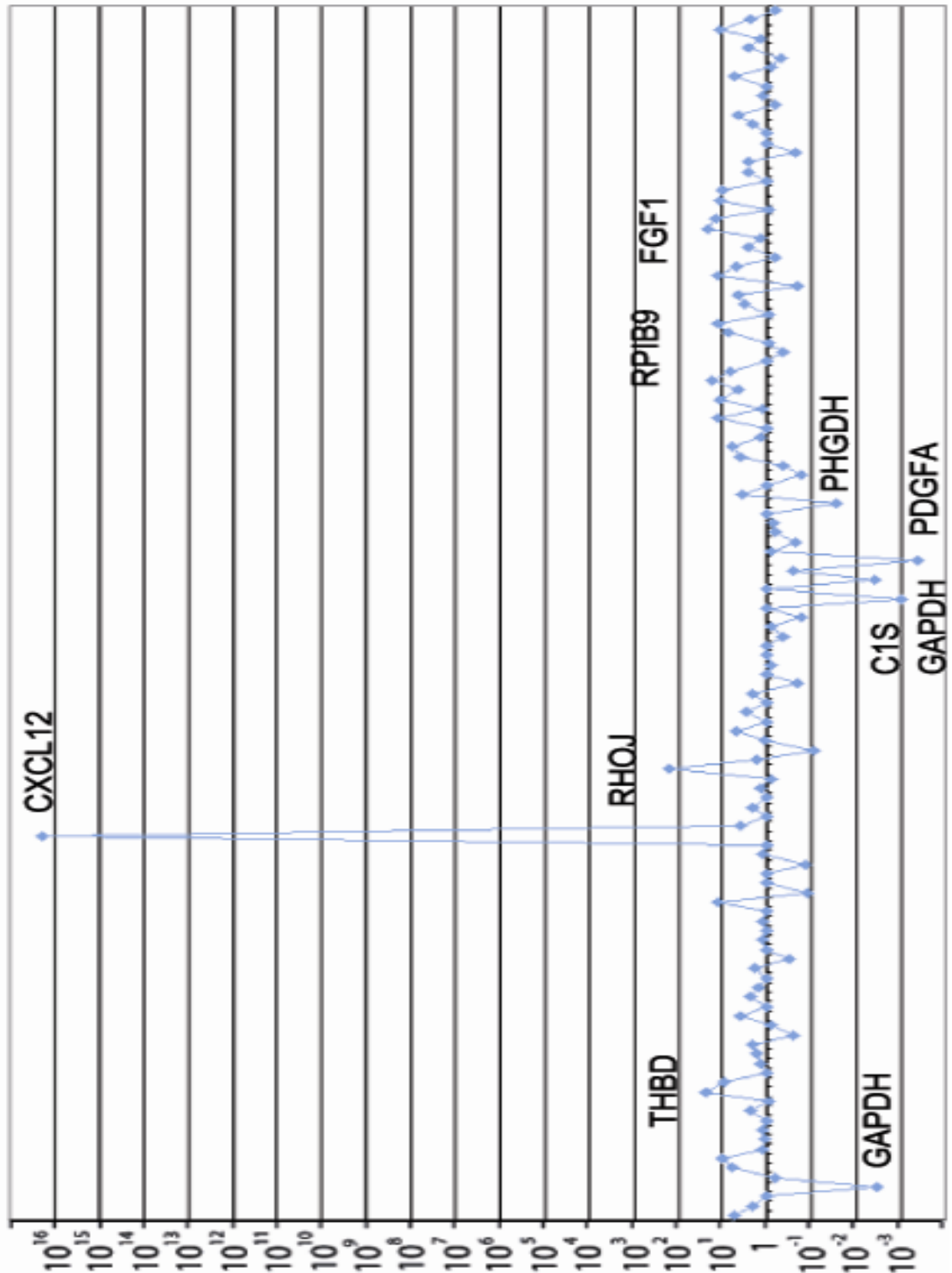


Figure 16. Global Expression Profile of RPL3. *C1s*, *Gapdh*, *Pdgfa* and *Phgda* were downregulated due to transient RPL3 expression while *Cxcl12*, *Fgf1*, *Rhoj*, *Rpib9* and *Thbd* revealed a positive regulation. The detected fold change values ranged between $4 \cdot 10^{-4}$ for *Pdgfa* and $1.85 \cdot 10^{16}$ for *Cxcl12*. The remaining genes of the LDA set did not respond to *Rpl3* overexpression, their fold change values ranged between 0.1 and 13.0.

Next the global correlation profile was determined, identifying overexpressed genes with the same effect on the LDA gene set as exogenous *Rpl3* (Table 1). Critically, *Btf3* showed a value of 0.84 relative to *Rpl3*, indicating a correlation of 84 %. This suggested a strong relationship between these two genes. The genes with correlation values next in size to *Btf3* were cholesterol-lowering factor (*Clf*) with 33 % and *Phgdh* with 31 %.

Table 1. The global correlation profil of RPL3.

Perturbation Experiment	Correlation in %	Perturbation Experiment	Correlation in %
AQP1	7	ICAM	10
ATP6V0D1	30	IFITM	11
BTF3	85	IMPA	18
CALM2	16	KLF6	6
CASP3	0	L-glucose treated iHUECs	9
CDYL12	11	NOS3	6
CFH	18	PHGDH	31
c-Jun	3	pIRES-EGFP empty	3
CLF	33	pIRES-EGFP empty	12
CSPG	5	pIRES-EGFP empty	29
CXCL12	27	pIRES-EGFP empty	22
CYR61	11	PKA	5
D-glucose treated iHUECs	27	PLD	10
ET1	8	PRG	23
FGF1	6	PRSS23	6
FZD4	14	RAMP3	5
GAPDH	9	RHOJ	26
GCA	6	RPL3	100
GDI2	6	Sample02	16
GNAS	23	SMAD2	5
GNAS2	7	SMAD3	7
GTPBP4	29	TGFb1	5
HOXA3	13	TGFb-R2	3
HOXA3_new	13	TOR3A	26
HOXA3-2nd run	9	UGDH	11

The correlation value entitles the degree of similarity between the expression patterns of the candidate genes.

To verify the indicated correlation between *Rpl3* and *Btf3*, we examined the expression profile of *Btf3*, thus identifying a relation between these two genes in the regulation of *Cxcl12*, *Rpib9* and *Gapdh* (Figure 17). *Cxcl12* and *Rpib9* revealed positive regulation upon transient BTF3 expression, with detected fold-changes of 3.9×10^{17} and 5565.0, whereas *Gapdh* was downregulated at a value of 3.7×10^{-3} . In contrast to these similar expression patterns of *Rpl3* and *Btf3*, *Pdgfa* showed a different regulation, revealing enhancing effects due to *Btf3* overexpression.

Table 2. Global expression profiles of BTF3 and RPL3.

Detected gene	Detected fold-change RPL3	Detected fold-change BTF3
ANGPT2	-	2747.0
C1S	1×10^{-3}	-
CXCL12	1.85×10^{16}	3.9×10^{17}
FGF1	22.74	-
GAPDH	3.5×10^{-3}	3.7×10^{-3}
GCA	-	1.8×10^{-2}
MMP9	-	11996
PDGFA	4×10^{-4}	1740
PHGDH	2.9×10^{-2}	-
RHOJ	169	-
RPIB9	17.93	5565
SOD1	-	444

The global expression profiles of *Rpl3* and *Btf3* revealed the detected fold-change values of the two genes. Note that only values over 13.0 for upregulation and under 0.1 for downregulation are listed.

Furthermore, the global expression profile of *Btf3* revealed four additional genes with notable regulation patterns, among which angiopoietin-2 (*Angpt2*), matrix metalloproteinase 9 (*Mmp9*) and superoxide dismutase 1 (*Sod1*) were upregulated, whereas grancalcin (*Gca*) showed downregulating effects due to transient *Btf3* expression.

Finally, we examined the correlation pattern of *Btf3*, thus identifying similar expression patterns of the candidate genes on the LDA set. Again, a correlation value of 0.85 with *Rpl3* was detected, thereby confirming our previous result. Taken together, this finding may suggest a strong “molecular” connection between the genes *Rpl3* and *Btf3*.

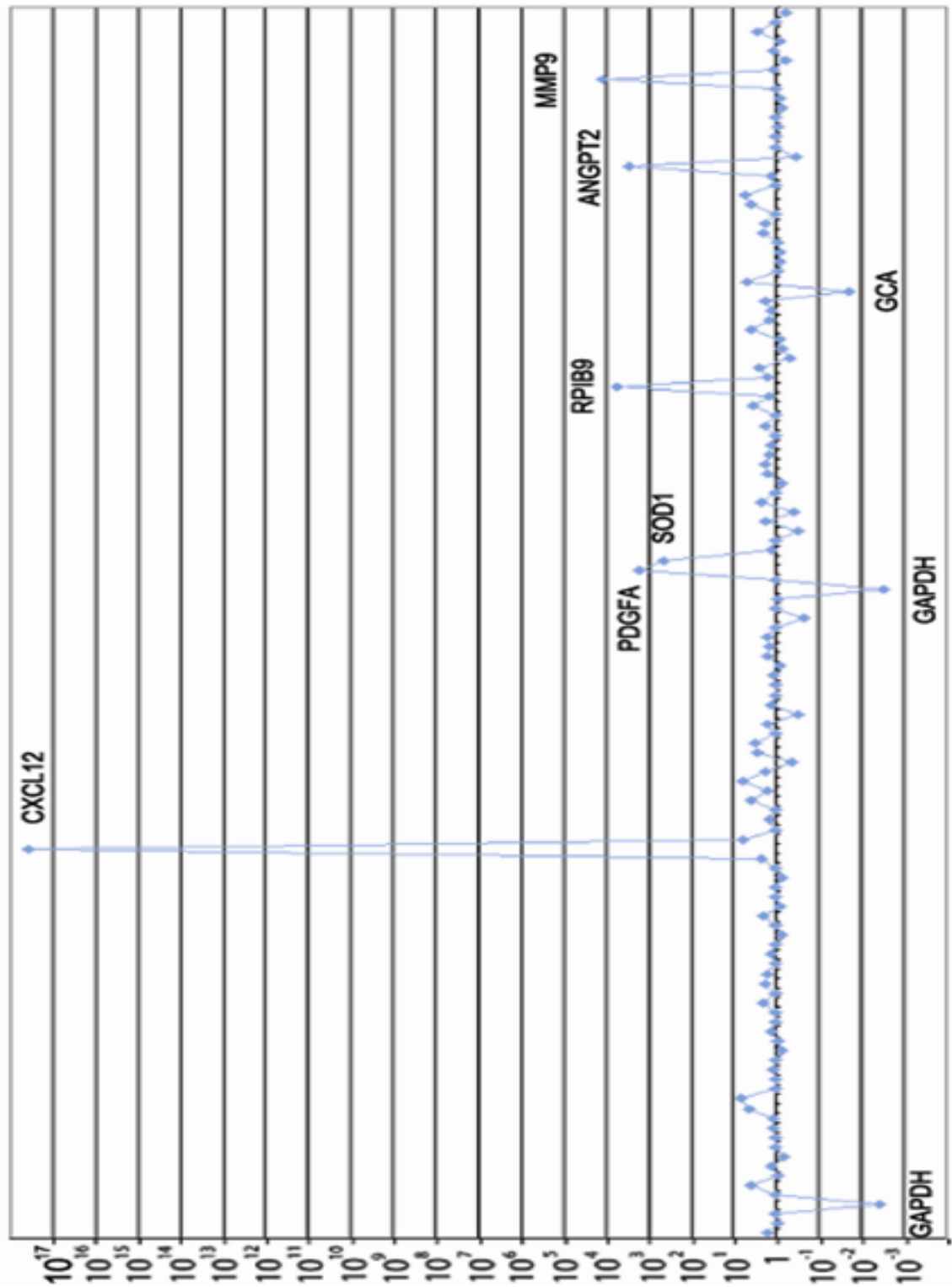


Figure 17. Global Expression Profile of BTF3. *Gapdh* and *Gca* were downregulated due to transient *Btf3* expression while *Cxcl12*, *Pdgfa*, *Sod*, *Rpib9*, *Angpt2* and *Mmp9* revealed a positive regulation with detected fold change values ranging between 3.7×10^{-3} and 3.9×10^{17} . The regulation patterns of *Cxcl12*, *Gapdh* and *Rpib9* resemble the expression profile of *Rpl3*, whereas *Pdgfa* reveals different regulation.

5.5. Verification of RPL3 interactions in a genetic network

The analysis of the expression patterns of *Rpl3* and *Btf3* revealed a similarity regarding their effects on the regulation of the LDA gene set. These results were confirmed by the high correlation values of 0.85, assuming a yet unknown connection between *Rpl3* and *Btf3*. Nevertheless, it was essential to verify these indicated interactions by separate methods. Since we assumed that RPL3 and BTF3 act together on protein level, Western blotting was chosen for further investigation. Thus, iHUECs expressing exogenous RPL3 and BTF3 were tested using antibodies specific for these proteins, and compared to cells transfected with empty pIRES2-EGFP expression vector. Besides, all three cell samples were also tested for CD31, a type I integral membrane glycoprotein, also known as platelet endothelial cell adhesion molecule 1 (PECAM1). Since CD31 is constitutively expressed on the surface of endothelial cells, it allows comparing of different cell samples due to their blotted protein concentration, thereby acting as marker protein for iHUECs.

The detection of BTF3 protein revealed expected results: Total BTF3 protein accumulated in cell samples that overexpressed BTF3 but was present at comparable and lower levels upon overexpression of RPL3 as well as control vector (data not shown).

On the contrary, when identifying RPL3 in iHUECs transiently expressing either RPL3 or BTF3, a high level of RPL3 was detected (Fig. 18). Specifically, both cell lysates displayed identical signal intensities, corresponding to RPL3's predicted molecular weight of 44 kDa, thereby demonstrating a sound accumulation of RPL3 protein in lysates of exogenous BTF3 expression. In control samples significantly less RPL3 protein was detected. The similar expression of the RPL3 protein both, in RPL3 and BTF3 overexpressing iHUECs, confirmed our previous results of a tight connection between these two proteins.

Summarizing, these findings allow the assumption of a unilateral pathway, in which BTF3 stimulates the expression of RPL3.

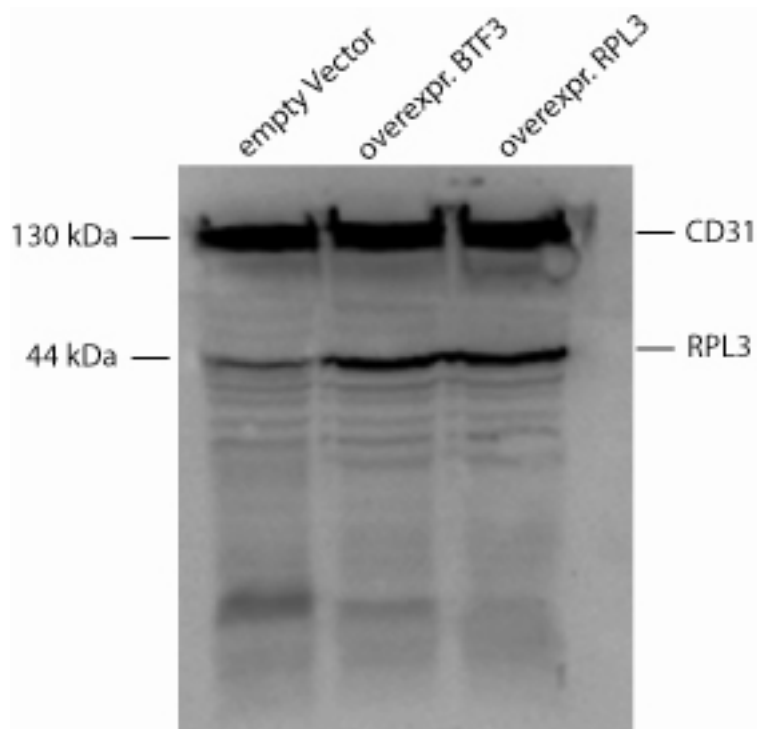


Figure 18. Western blot analyses of RPL3 and BTF3 overexpressing iHUECs. RPL3 detection in iHUECs expressing exogenous RPL3 and BTF3 results in equal signal intensities at 44 kDa, whereas control cells displayed a much weaker RPL3 expression, indicating an unilateral pathway with BTF3 enhancing the expression of RPL3.

5.6. The position of *BTF3* in the final gene network

The transcriptional network of diabetic microangiopathy was achieved with fold-change data of perturbation experiments and displayed the regulatory interactions of the participating genes. As described, candidate genes were subjected to a multi-step process, involving cloning into the expression vector pIRES2-EGFP, transformation into iHUEVCs, RNA isolation and reverse transcription into cDNA prior to quantitative real time PCR. Finally, Network identification was accomplished by multiple regression according to the following formula:

$$A = \ln (D+I)$$

Since the influence matrix D displayed the effect of perturbation experiments on the expression of the remaining genes, the network was designed by adding the regulatory interactions found between the transient expressed candidate genes, thereby revealing different regulation patterns. Functional links were determined between each of the genes, thus illustrating enhancing and inhibiting effects. Due to these regulatory interactions it was possible to establish the position of each gene in a network relevant to diabetic microangiopathy.

Since only genes with a correlation coefficient greater than the threshold were submitted to graph constructions, the definition of the applied threshold was significant for the calculation of the network and was set according to a previous carefully selected connectivity value. A threshold set too high results in small gene clusters and unconnected nodes, thereby concluding no functional connections of the involved genes. On the contrary, if threshold setting is too low, numerous false positive links are deduced from network topology. Based on this consideration we finally included only genes with correlation values above 1.334 for enhancing effects and below -1.130 for inhibiting effects.

Due to this stringency, the final network displayed 37 genes that were assumed to be relevant in the pathogenesis and the progression of diabetic microangiopathy (Figure 19). Out of these transiently expressed genes, caspase 3 (*Casp3*), calmodulin 2 (*Calm2*), *Clf*, *Cxcl12*, *Gapdh* and *Prss23* were detected to be key players of diabetic vascular diseases, since they displayed a vast number of regulatory interactions or network links, thus being identified as hubs of the network.

Rpl3 was not relevant for network design, since the detected correlation values did not exceed the defined threshold. However, regulatory interactions from *Btf3* to nine network participants were identified (Table 3).

Btf3 displayed enhancing effects on *Cxcl12*, chondroitin sulfate proteoglycan 2 (*Cspg2*) and *Rpib9*, whereas *Aqp1* (aquaporin 1), *Calm2*, *Fgf1*, complement factor H (*Cfh*) and phospholipase D (*Pld*) were downregulated upon exogenous *Btf3* (Table 3). Contrary, transient expressed *Casp3* revealed inhibitory effects, thereby downregulating the expression of *Btf3*. These detected functional links connected *Btf3* directly to four out of seven identified hubs, thus implying a significant role of *Btf3* in the network.

Table 3. Detected interactions between BTF3 and the 36 remaining genes of the network.

Effect of BTF3 to	Strength of detected interaction
AQP1	-3,65
CALM2	-2,13
FGF1	-1,97
CFH	-1,82
PLD	-1,75
ICAM	-1,74
SMAD2	-1,56
RPIB9	3,18
CSPG2	3,31
CXCL12	8,24
Effect to BTF3 from	Strength of detected interaction
CASP3	-1,55

Network interactions of *Btf3* to and from the 36 remaining genes. Note that only effects above threshold were listed.

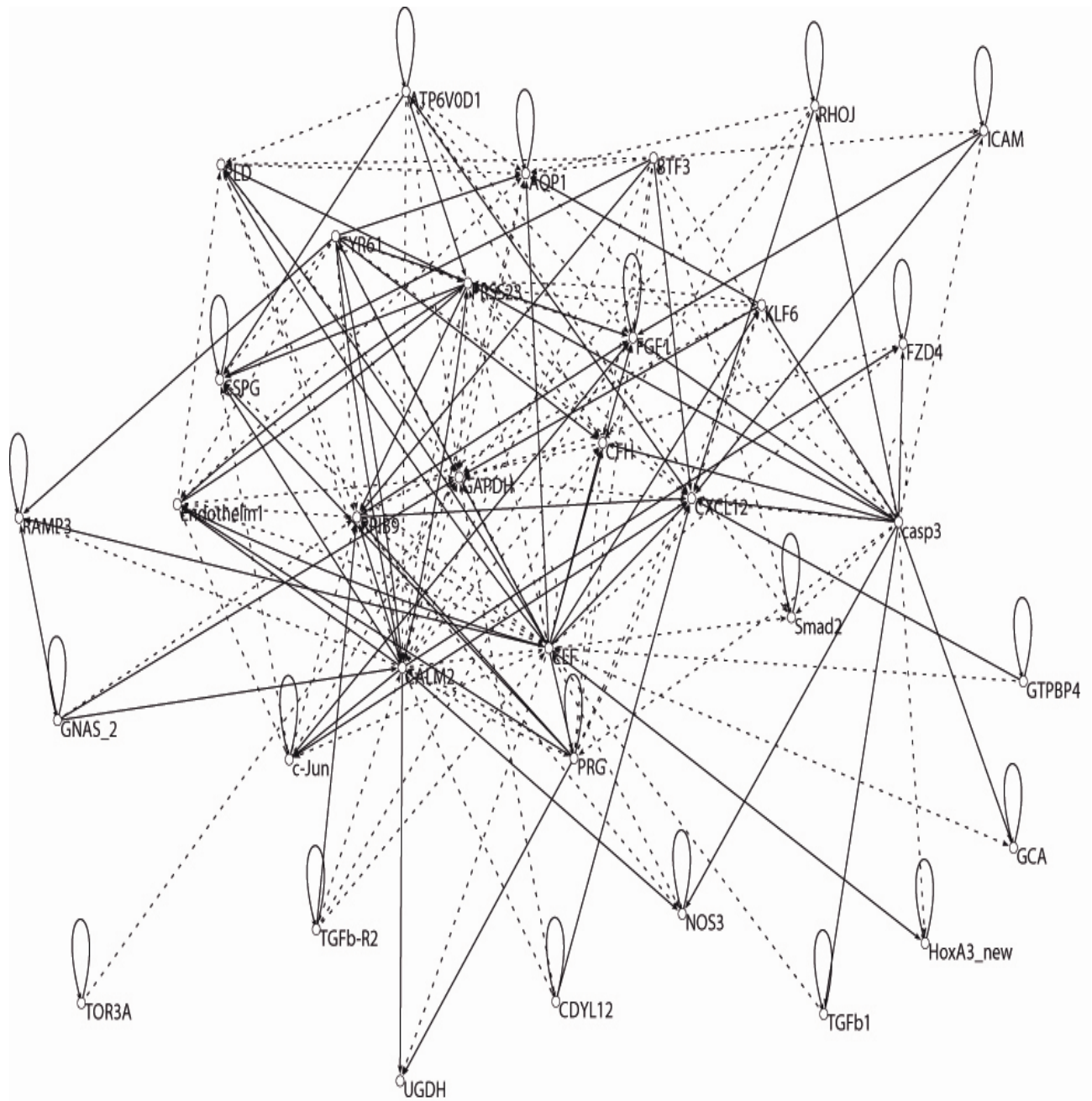


Figure 19. Final network of diabetic microangiopathy. The final network on diabetic microangiopathy displayed 37 genes, whereof *Casp3*, *Calm2*, *Clf*, *Cxcl12*, *Gapdh*, *Rpi9* and *Prss23* revealed a vast number of regulatory interactions. *Btf3* connects to four of these network hubs, in both upregulating and downregulating way, indicating the important role of this protein in diabetic microangiopathy. Note that enhancing effects were illustrated in unbroken, inhibiting effects in dotted lines.

6. Discussion

In this thesis we present the identification of a genetic network of human diabetic microangiopathy. Our ambition was to reveal definite target genes of this disease that prospectively could be subject to further investigation, thereby leading finally to drug development against this vascular disease. As described in this thesis, the target genes for the Low Density Array and for network construction respectively were selected out of three approaches. First, the *ex vivo* set was established from differential gene regulation in diabetic versus non-diabetic blood endothelial cells (BECs), whereas the *in vitro* set comprises immortalized BECs (iBECs) in cell culture mimicking diabetic condition by treatment with glucose. In the third approach an educated decision was performed by carefully reviewing literature on diabetic microangiopathy, resulting in the *in libro* set.

In order to construct the genetic network on diabetic microangiopathy, the selected candidate genes were subjected to working steps, involving the cloning into the expression vector pIRES2-EGFP, the transfection of iHUEVCs, subsequent RNA isolation of positively transfected cells, reverse transcription into cDNA and finally real time PCR.

The whole process resulted in a network consisting of 37 genes, their positions which were described due the functional and regulatory relations and illustrated by the number of given links between the network participants. The genes *Casp3*, *Calm2*, *Clf*, *Cxcl12*, *Gapdh*, *Rpib9* and *Prss23* were found in more central positions with vast numbers of interactions, thereby considered to act as hubs or key players. Although a large pool of target genes was available, only 37 of the originally present candidates were successfully subjected to the transcriptional network. The main reasons for this limitation were found in the time consuming-multi step process of transient target gene expression. Nevertheless, the small number of genes building the network gives rise to discussions about its relevance. Critically, it stays disputable, if these identified hubs are truly relevant in terms of understanding the whole process that underlies diabetic microangiopathy. It is highly unlikely that all diabetic complications are based on the action of one single gene. Instead, network hubs should be seen as indicative, since also genes in peripheral positions could be important for the complete comprehension of the

numerous factors involved in the occurrence and pathology of the discussed disease. Additionally, the ultimate target genes and their interactions could still be undetected due to the small number of participants.

Nevertheless, the network gives insight into the complex interactions of the disease in question and helps to identify possible key player of diabetic microvascular complications.

The workflow comprised the cloning of candidates into the expression vector pIRES2-EGFP, which permitted an efficient selection of transiently transfected cells expressing the enhanced green fluorescent protein EGFP as well as the protein of interest simultaneously. Unsuccessful ligation into pIRES2-EGFP in the first place required subcloning into the TOPO TA vector, thereby again prolonging the cloning process. The subsequent transfection step was accomplished in iHUECs, an hTERT immortalized endothelial cell line. iBECs would be the first choice for an *in vitro* system mimicking diabetic microangiopathy, but were changed to iHUECs due to low transfection rates. Former studies determined a total number of at least 250.000 positive transfected cells, since a smaller amount of iHUECs resulted in fewer material for succeeding total RNA isolation, thereby affecting the quality of cDNA as well as the validity of subsequent real-time experiments (Krachler A., 2006). Although transfection efficiency of iHUECs was much higher than of iBECs, successful transient gene expression often demanded repeated transfection and subsequent pooling of the GFP-expressing cells to acquire the minimal number of at least 250.000 cells, thereby again prolonging the process of transient gene expression. Nevertheless, we successfully finished this workflow with 45 overexpressed candidates, but this number was further limited due to threshold, which was set according to in advanced selected connectivity value. If setting was too high, only small gene clusters without further interactions between the genes would result from network calculation. Otherwise, if the threshold was set too low, the network would in fact conclude all the 45 transiently expressed genes. However, numerous false links would be deduced, thereby leaving the significance of such networks sceptical. Based on these considerations, only genes with correlation values in the range of -1.130 to 1.334 were subjected to the network, thus resulting in the total of our 37 participants.

As mentioned, the selected threshold criteria characterised network architecture by determining the number of participants. As a result, *Rpl3* was one out of eight

transiently expressed genes that was finally not represented on the network. Despite this fact, it was nevertheless important to add its fold-change data to network calculation, since its algorithm revealed a high similarity of *Rpl3* and *Btf3* concerning the effect of their transient expression on the gene set of the low density array. The high correlation of 85% between *Rpl3* and *Btf3* indicated a connection between these two genes, thereby linking *Rpl3* to the gene network. *Btf3* itself exposed interactions to four of the seven identified hubs, thus being highly interconnected to the network. Out of these, *Calm2* was downregulated, whereas *Cxcl12* and *Rpib9* were upregulated as an effect of transient *BTF3* expression.

Calm2 is one out of three genes coding for calmodulin, a calcium binding protein that is involved in numerous cellular processes like synthesis and degradation of cyclic nucleotides, the regulation of different transport system, in phosphorylation and dephosphorylation processes of proteins (Benaim and Villalobo, 2002).

The gene *Cxcl12* encodes the Chemokine (C-X-C motif) ligand 12, also referred as stromal cell-derived factor 1 (SDF-1) or pre-B cell growth stimulating factor (PBSF). CXCL12 triggers its functions primarily by binding to two main receptors, CXCR4 and CXCR7. The CXCL12/CXCR4 axis plays an important role in embryogenesis by directing the migration of haematopoietic stem/progenitor cells from foetal liver to bone marrow and in the formation of large blood vessels. In the adult body, CXCL12/CXCR4 binding is also involved in inflammatory processes and seems to be crucial for angiogenesis by recruiting endothelial progenitor cells from the bone marrow. Additionally, binding of CXCL12 to the CXCR7 receptor effects important processes as cell survival, cell adhesion and tumorigenesis (Kucia et al., 2003).

The *Rpib9* gene, also known as *Rpip9* (Rap2 interacting protein) or *Rundc3b* (RUN domain containing 3B) codes for the Rap2-binding protein 9. *Rpib9* is known to be activated in breast cancer and also correlates with metastatic lymph node invasion (Raquz et al., 2005).

Finally, *Btf3* itself revealed downregulating effect upon transient *Casp3* expression, the gene coding for caspase 3. Caspases are proteins of the cysteine-aspartic acid protease family and are involved in apoptotic pathways (Nuñez et al., 1998). *Casp3* is also associated with the apoptosis of the β islet in the pancreas, a process that is important for the development of type I diabetes (Liadis et al., 2005).

Although only *Casp3* and *Cxcl12* are known by former studies to be associated with diabetic microangiopathy, the genes *Calm2* and *Rpib9* are still relevant, since they are also targeted by a vast number of interactions and are highly connected to the other hubs as well as to more peripheral genes.

Still, these given network links have to be verified. Assuming that RPL3 and BTF3 act together on a protein level, western blot analysis was used to proof these indicated interactions. Thus, iHUECs that were transiently expressing RPL3 and BTF3 respectively were compared to cells transfected with empty pIRES2-EGFP, resulting in enhanced RPL3 expression in both cell samples. In order to avoid that eventual side-effect of the transfection process would distort western blot results or lead to false assumptions, control samples were transfected with empty pIRES2-EGFP. The immunoblotting result confirmed the indicated connection between both genes, thereby explaining the similarity of the effect of transiently expressed *Rpl3* and *Btf3* on the gene set of the LDA. Since only overexpressed BTF3 affected RPL3 expression and not *vice versa*, we assumed a unilateral pathway, in which BTF3 leads to an enhanced RPL3 expression.

Nevertheless, some technical problem had to be overcome in order to verify network links and to get reproducible results. A protein assay in Laemmli buffer (Karlsson et al, 1994) was performed to gain equal concentration of the applied cell extracts. However, this method proved to be unsuitable for our cell lines by causing incomparable protein concentration and consequently leading to false results. Therefore, protein concentrations of the used cell samples were additionally determined by BSA standard curve, resulting in comparable amounts of the blotted samples and thus in convincing results.

Additionally, the used iHUECs were a poor model for capillary endothelial cells. Initially, iBECS were intended as model system, since they were a more suitable system to mimic diabetic caused vascular complications. However, former experiments revealed transfection rates only between 0.1 % and 0.3 %. Therefore, iBECS were rejected for iHUECs, which allowed the use of Lipofectamine 2000, an effective transfection reagent, thus resulting in higher transfection efficiency (Krachler A, 2006).

Finally, transfection kinetics did also play an important role in getting reproducible network verifications. Former experiments (Krachler A, 2006) revealed a transfection curve peaking 22 hours after transfection, followed by a lower steady state level between 30 and 52 hours, in which stable expression of the candidate gene occurred.

For network construction, 48 hours after transfection were chosen for RNA measurement, thereby assuring that next to early genes also the effects of late responding genes were considered. For immunoblotting experiments we observed next to the approved time point of 48 hours also 24 and 36 hours after transfection. Nevertheless, after optimizing the referred working steps, only cell samples harvested 48 hours after transfection illustrated reproducible results, thereby verifying the assumed interaction between BTF3 and RPL3 and confirming the constructed network. Cell samples with time points of 24 and 36 hours did not reveal any interaction, giving way to the consideration that a threshold concentration of BTF3 protein was required to trigger RPL3 expression, or that the sensitivity of the technique did not expose this pathway.

Critically, for biochemical analyses the cell samples were not cultivated in hyperglycaemic serum, thereby raising the questions, if a diabetic glucose level confirmed or rejected the previous results. Nevertheless, immunoblotting was our method of choice for the verification of the detected network links. Given the fact that *Btf3* was part of the gene set comprising the Low Density Array, which was primary selected due to different regulation in diabetic compared to non-diabetic tissue, transient BTF3 expression in western blot analyses mimicked its enhanced expression as reported under diabetic conditions (N.Wick, personal communication). Finally, the enhanced RPL3 expression as illustrated in immunoblotting was based on transient expressed and thereby diabetic BTF3.

In summary, our results illustrated the upregulation of both genes, *Rpl3* and *Btf3*, under diabetic conditions. Given the fact that the designed network was based on regulatory interactions on the RNA level, further verifications of the observed network links would demand approaches on a protein level. These methods could include mass spectrometric screens, antibody arrays or even serological analyses.

Apart from its known function in ribosome assembly, recent findings indicated a more central role of RPL3 in translation by coordinating the functions of the sarcin/ricin loop (SRL) and the peptidyl transferase centre (PTC), thus taking part in translational elongation. Also BTF3 is known for acting in translation process in the proximity of the PTC by performing cotranslational targeting of polypeptides to the endoplasmic reticulum (ER). Given the fact that both proteins take part in translation associated processes, although fulfilling different functions, and are induced under diabetic conditions makes a common pathway in the presence of high glucose levels more likely.

In addition, the upregulation of RPL3 is consistent with known observations of higher translation rates as a consequence of high glucose levels. This goes in line with our observation of immunofluorescence analyses that revealed *bona fide* RPL3 containing aggregates.

Diabetic tissue analyses by immunohistochemistry confirmed the increase of RPL3 protein. Still, these findings are not significant in clinical-diagnostic terms, since IHC is as localization tool the method of choice for qualitative and not quantitative statements. However, these results could be considered as semi-quantitative according to the prominent RPL3 protein staining demonstrated in the tissue sections of diabetic patients. Additionally, the granular reactivity corresponds to the ribosomal pattern as already illustrated in *in vitro* immunofluorescence analyses.

Further confirmations of this enhanced RPL3 expression under the discussed conditions could include electron microscope analyses. Alternatively, subcellular fractionation resulting in high amounts of ribosome and upregulated RPL3 protein would allow a more direct verification of RPL3 on a protein level. Both techniques should be considered in follow up experiments.

To summarize our work, in this thesis we presented a genetic network comprising 37 genes. Within the network two new potential candidates relevant for diabetic micro-vascular complications, *Btf3* and *Rpl3* were identified. Although *Rpl3* itself was not represented on the LDA and thus not first choice for transient gene expression, the decision for this gene turned out useful eventually, since the correlation of *Rpl3* to *Btf3* and thus to four of the seven identified hubs or key players of the constructed network also links translation and ribosome function to diabetic microangiopathy. Of course, inferrel of functional information from this thesis is limited. For such a

conclusion, another level of inhibitory experiments, e.g. RNA interference, would have been necessary. However, the central role of ribosomal proteins would have made any experimental readout a difficult task as the differentiation of diabetic and non-diabetic effects would have been difficult. Probably, the method of choice is analysis of appropriate animal models. In light of this prospect, we feel that our insight into translation as a basic target for diabetic effects in endothelial cells is a step forward in understanding its functional relevance in this disease. Thus, in a wide context, this study might provide targets for future drug therapy against the onset of diabetic microangiopathy.

7. References

1. Agraftoti, I., et al., *Comparative analysis of the Saccharomyces cerevisiae and Caenorhabditis elegans protein interaction networks*. BMC Evol Biol, 2005. **5**(1): p. 23.
2. Allan, M.F., M.K. Nielsen, and D. Pomp, *Gene expression in hypothalamus and brown adipose tissue of mice divergently selected for heat loss*. Physiol Genomics, 2000. **3**(3): p. 149-56.
3. Allan, M.F., J.K. Potts, and D. Pomp, *Comparative mapping of RPL3, a gene overexpressed in multiple obesity models*. Anim Biotechnol, 2001. **12**(2): p. 167-71.
4. Ban, N., et al., *The complete atomic structure of the large ribosomal subunit at 2.4 Å resolution*. Science, 2000. **289**(5481): p. 905-20.
5. Barabasi, A.L. and Z.N. Oltvai, *Network biology: understanding the cell's functional organization*. Nat Rev Genet, 2004. **5**(2): p. 101-13.
6. Bartnik, M., A. Norhammar, and L. Ryden, *Hyperglycaemia and cardiovascular disease*. J Intern Med, 2007. **262**(2): p. 145-56.
7. Beatrix, B., H. Sakai, and M. Wiedmann, *The alpha and beta subunit of the nascent polypeptide-associated complex have distinct functions*. J Biol Chem, 2000. **275**(48): p. 37838-45.
8. Benaim, G. and A. Villalobo, *Phosphorylation of calmodulin. Functional implications*. Eur J Biochem, 2002. **269**(15): p. 3619-31.
9. Bian, C., et al., *Immortalization of human umbilical vein endothelial cells with telomerase reverse transcriptase and simian virus 40 large T antigen*. J Zhejiang Univ Sci B, 2005. **6**(7): p. 631-6.
10. Brodersen, D.E. and P. Nissen, *The social life of ribosomal proteins*. Febs J, 2005. **272**(9): p. 2098-108.
11. Brownlee, M., *Biochemistry and molecular cell biology of diabetic complications*. Nature, 2001. **414**(6865): p. 813-20.
12. Brownlee, M., *The pathobiology of diabetic complications: a unifying mechanism*. Diabetes, 2005. **54**(6): p. 1615-25.
13. Chan, H.Y., et al., *Identification and characterization of the gene for Drosophila L3 ribosomal protein*. Gene, 1998. **212**(1): p. 119-25.
14. de Silva, E. and M.P. Stumpf, *Complex networks and simple models in biology*. J R Soc Interface, 2005. **2**(5): p. 419-30.

15. De Vriese, A.S., et al., *Endothelial dysfunction in diabetes*. Br J Pharmacol, 2000. **130**(5): p. 963-74.
16. D'Haeseleer, P., S. Liang, and R. Somogyi, *Genetic network inference: from co-expression clustering to reverse engineering*. Bioinformatics, 2000. **16**(8): p. 707-26.
17. Doi, T., et al., *Receptor-specific increase in extracellular matrix production in mouse mesangial cells by advanced glycosylation end products is mediated via platelet-derived growth factor*. Proc Natl Acad Sci U S A, 1992. **89**(7): p. 2873-7.
18. Du, X.L., et al., *Hyperglycemia-induced mitochondrial superoxide overproduction activates the hexosamine pathway and induces plasminogen activator inhibitor-1 expression by increasing Sp1 glycosylation*. Proc Natl Acad Sci U S A, 2000. **97**(22): p. 12222-6.
19. Duga, S., et al., *The intron-containing L3 ribosomal protein gene (RPL3): sequence analysis and identification of U43 and of two novel intronic small nucleolar RNAs*. Biochim Biophys Acta, 2000. **1490**(3): p. 225-36.
20. Erlacher, M.D., et al., *Chemical engineering of the peptidyl transferase center reveals an important role of the 2'-hydroxyl group of A2451*. Nucleic Acids Res, 2005. **33**(5): p. 1618-27.
21. Evangelisti, A.M. and A. Wagner, *Molecular evolution in the yeast transcriptional regulation network*. J Exp Zool B Mol Dev Evol, 2004. **302**(4): p. 392-411.
22. Freire, M.A., *Translation initiation factor (iso) 4E interacts with BTF3, the beta subunit of the nascent polypeptide-associated complex*. Gene, 2005. **345**(2): p. 271-7.
23. Gardner, T.S., et al., *Inferring genetic networks and identifying compound mode of action via expression profiling*. Science, 2003. **301**(5629): p. 102-5.
24. Giardino, I., D. Edelstein, and M. Brownlee, *Nonenzymatic glycosylation in vitro and in bovine endothelial cells alters basic fibroblast growth factor activity. A model for intracellular glycosylation in diabetes*. J Clin Invest, 1994. **94**(1): p. 110-7.
25. Gugliucci, A., *Glycation as the glucose link to diabetic complications*. J Am Osteopath Assoc, 2000. **100**(10): p. 621-34.
26. Hansen, J.L., et al., *Progress toward an understanding of the structure and enzymatic mechanism of the large ribosomal subunit*. Cold Spring Harb Symp Quant Biol, 2001. **66**: p. 33-42.
27. Holcik, M. and N. Sonenberg, *Translational control in stress and apoptosis*. Nat Rev Mol Cell Biol, 2005. **6**(4): p. 318-27.

28. Huang, S., *Back to the biology in systems biology: what can we learn from biomolecular networks?* Brief Funct Genomic Proteomic, 2004. **2**(4): p. 279-97.
29. Irvin, J.D. and F.M. Uckun, *Pokeweed antiviral protein: ribosome inactivation and therapeutic applications.* Pharmacol Ther, 1992. **55**(3): p. 279-302.
30. Jansson, P.A., *Endothelial dysfunction in insulin resistance and type 2 diabetes.* J Intern Med, 2007. **262**(2): p. 173-83.
31. Jeong, H., et al., *The large-scale organization of metabolic networks.* Nature, 2000. **407**(6804): p. 651-4.
32. Kaiser, S. and M. Toborek, *Liposome-mediated high-efficiency transfection of human endothelial cells.* J Vasc Res, 2001. **38**(2): p. 133-43.
33. Kanno, M., C. Chalut, and J.M. Egly, *Genomic structure of the putative BTF3 transcription factor.* Gene, 1992. **117**(2): p. 219-28.
34. Karlsson, J.O., et al., *A method for protein assay in Laemmli buffer.* Anal Biochem, 1994. **219**(1): p. 144-6.
35. Kenmochi, N., et al., *A map of 75 human ribosomal protein genes.* Genome Res, 1998. **8**(5): p. 509-23.
36. Klann, E. and T.E. Dever, *Biochemical mechanisms for translational regulation in synaptic plasticity.* Nat Rev Neurosci, 2004. **5**(12): p. 931-42.
37. Klein, D.J., P.B. Moore, and T.A. Steitz, *The roles of ribosomal proteins in the structure assembly, and evolution of the large ribosomal subunit.* J Mol Biol, 2004. **340**(1): p. 141-77.
38. Kobayashi, Y., et al., *Identification of Saccharomyces cerevisiae ribosomal protein L3 as a target of curvularol, a G1-specific inhibitor of mammalian cells.* Biosci Biotechnol Biochem, 2006. **70**(10): p. 2451-9.
39. Korostelev, A. and H.F. Noller, *The ribosome in focus: new structures bring new insights.* Trends Biochem Sci, 2007. **32**(9): p. 434-41.
40. Korshunov, S.S., V.P. Skulachev, and A.A. Starkov, *High protonic potential actuates a mechanism of production of reactive oxygen species in mitochondria.* FEBS Lett, 1997. **416**(1): p. 15-8.
41. Kowluru, R.A. and P.S. Chan, *Oxidative stress and diabetic retinopathy.* Exp Diabetes Res, 2007. **2007**: p. 43603.
42. Koya, D. and G.L. King, *Protein kinase C activation and the development of diabetic complications.* Diabetes, 1998. **47**(6): p. 859-66.
43. Krachler A, *Transcriptional regulatory networks in human diabetic microangiopathy.* 2006

44. Kuboki, K., et al., *Regulation of endothelial constitutive nitric oxide synthase gene expression in endothelial cells and in vivo : a specific vascular action of insulin*. Circulation, 2000. **101**(6): p. 676-81.
45. Kucia, M., et al., *CXCR4-SDF-1 signalling, locomotion, chemotaxis and adhesion*. J Mol Histol, 2004. **35**(3): p. 233-45.
46. Lafontaine, D.L. and D. Tollervy, *The function and synthesis of ribosomes*. Nat Rev Mol Cell Biol, 2001. **2**(7): p. 514-20.
47. Lee, A.Y. and S.S. Chung, *Contributions of polyol pathway to oxidative stress in diabetic cataract*. Faseb J, 1999. **13**(1): p. 23-30.
48. Liadis, N., et al., *Caspase-3-dependent beta-cell apoptosis in the initiation of autoimmune diabetes mellitus*. Mol Cell Biol, 2005. **25**(9): p. 3620-9.
49. Liebich, I., et al., *Two genes encoding ribosomal protein L3 of Schizosaccharomyces pombe and their proximal promoter regions*. Gene, 1994. **142**(1): p. 119-22.
50. Liljas, A., *Deepening ribosomal insights*. ACS Chem Biol, 2006. **1**(9): p. 567-9.
51. Lindsay, R.S. and P.H. Bennett, *Type 2 diabetes, the thrifty phenotype - an overview*. Br Med Bull, 2001. **60**: p. 21-32.
52. Ma, H. and A.P. Zeng, *Reconstruction of metabolic networks from genome data and analysis of their global structure for various organisms*. Bioinformatics, 2003. **19**(2): p. 270-7.
53. Ma, H.W. and A.P. Zeng, *The connectivity structure, giant strong component and centrality of metabolic networks*. Bioinformatics, 2003. **19**(11): p. 1423-30.
54. Maslov, S. and K. Sneppen, *Specificity and stability in topology of protein networks*. Science, 2002. **296**(5569): p. 910-3.
55. Meskauskas, A. and J.D. Dinman, *Ribosomal protein L3: gatekeeper to the A site*. Mol Cell, 2007. **25**(6): p. 877-88.
56. Meskauskas, A. and J.D. Dinman, *Ribosomal protein L3 functions as a 'rocker switch' to aid in coordinating of large subunit-associated functions in eukaryotes and Archaea*. Nucleic Acids Res, 2008. **36**(19): p. 6175-86.
57. Meskauskas, A., A.N. Petrov, and J.D. Dinman, *Identification of functionally important amino acids of ribosomal protein L3 by saturation mutagenesis*. Mol Cell Biol, 2005. **25**(24): p. 10863-74.
58. Newman, M.E.J., *The structure and function of complex networks*. SIAM review, 2003. **45**(2): p. 167 - 256.
59. Nishikawa, T., et al., *Normalizing mitochondrial superoxide production blocks three pathways of hyperglycaemic damage*. Nature, 2000. **404**(6779): p. 787-90.

60. Nowotny, V. and K.H. Nierhaus, *Initiator proteins for the assembly of the 50S subunit from Escherichia coli ribosomes*. Proc Natl Acad Sci U S A, 1982. **79**(23): p. 7238-42.
61. Nunez, G., et al., *Caspases: the proteases of the apoptotic pathway*. Oncogene, 1998. **17**(25): p. 3237-45.
62. Peltz, S.W., et al., *Ribosomal protein L3 mutants alter translational fidelity and promote rapid loss of the yeast killer virus*. Mol Cell Biol, 1999. **19**(1): p. 384-91.
63. Petrov, A., A. Meskauskas, and J.D. Dinman, *Ribosomal protein L3: influence on ribosome structure and function*. RNA Biol, 2004. **1**(1): p. 59-65.
64. Polacek, N. and A.S. Mankin, *The ribosomal peptidyl transferase center: structure, function, evolution, inhibition*. Crit Rev Biochem Mol Biol, 2005. **40**(5): p. 285-311.
65. Popescu, S.C. and N.E. Tumer, *Silencing of ribosomal protein L3 genes in N. tabacum reveals coordinate expression and significant alterations in plant growth, development and ribosome biogenesis*. Plant J, 2004. **39**(1): p. 29-44.
66. Raguz, S., et al., *Expression of RPIP9 (Rap2 interacting protein 9) is activated in breast carcinoma and correlates with a poor prognosis*. Int J Cancer, 2005. **117**(6): p. 934-41.
67. Rask-Madsen, C. and G.L. King, *Mechanisms of Disease: endothelial dysfunction in insulin resistance and diabetes*. Nat Clin Pract Endocrinol Metab, 2007. **3**(1): p. 46-56.
68. Ronen, M., et al., *Assigning numbers to the arrows: parameterizing a gene regulation network by using accurate expression kinetics*. Proc Natl Acad Sci U S A, 2002. **99**(16): p. 10555-60.
69. Rosado, I.V., D. Kressler, and J. de la Cruz, *Functional analysis of Saccharomyces cerevisiae ribosomal protein Rpl3p in ribosome synthesis*. Nucleic Acids Res, 2007. **35**(12): p. 4203-13.
70. Rospert, S., Y. Dubaquier, and M. Gautschi, *Nascent-polypeptide-associated complex*. Cell Mol Life Sci, 2002. **59**(10): p. 1632-9.
71. Sanbonmatsu, K.Y., S. Joseph, and C.S. Tung, *Simulating movement of tRNA into the ribosome during decoding*. Proc Natl Acad Sci U S A, 2005. **102**(44): p. 15854-9.
72. Schmittgen, T.D. and K.J. Livak, *Analyzing real-time PCR data by the comparative C(T) method*. Nat Protoc, 2008. **3**(6): p. 1101-8.
73. Selmer, M., et al., *Structure of the 70S ribosome complexed with mRNA and tRNA*. Science, 2006. **313**(5795): p. 1935-42.

74. Shinohara, M., et al., *Overexpression of glyoxalase-I in bovine endothelial cells inhibits intracellular advanced glycation endproduct formation and prevents hyperglycemia-induced increases in macromolecular endocytosis*. J Clin Invest, 1998. **101**(5): p. 1142-7.
75. Skolnik, E.Y., et al., *Human and rat mesangial cell receptors for glucose-modified proteins: potential role in kidney tissue remodelling and diabetic nephropathy*. J Exp Med, 1991. **174**(4): p. 931-9.
76. Spillmann, S., F. Dohme, and K.H. Nierhaus, *Assembly in vitro of the 50 S subunit from Escherichia coli ribosomes: proteins essential for the first heat-dependent conformational change*. J Mol Biol, 1977. **115**(3): p. 513-23.
77. Spirin, A.S., *The ribosome as an RNA-based molecular machine*. RNA Biol, 2004. **1**(1): p. 3-9.
78. Steitz, T.A., *A structural understanding of the dynamic ribosome machine*. Nat Rev Mol Cell Biol, 2008. **9**(3): p. 242-53.
79. Stokic, D., R. Hanel, and S. Thurner, *Inflation of the edge of chaos in a simple model of gene interaction networks*. Phys Rev E Stat Nonlin Soft Matter Phys, 2008. **77**(6 Pt 1): p. 061917.
80. Tanner, F.C., et al., *Transfection of human endothelial cells*. Cardiovasc Res, 1997. **35**(3): p. 522-8.
81. Thorp, M.L., *Diabetic nephropathy: common questions*. Am Fam Physician, 2005. **72**(1): p. 96-9.
82. Uetz, P., et al., *A comprehensive analysis of protein-protein interactions in Saccharomyces cerevisiae*. Nature, 2000. **403**(6770): p. 623-7.
83. Vila-Sanjurjo, A., et al., *X-ray crystal structures of the WT and a hyper-accurate ribosome from Escherichia coli*. Proc Natl Acad Sci U S A, 2003. **100**(15): p. 8682-7.
84. Wagner, A. and D.A. Fell, *The small world inside large metabolic networks*. Proc Biol Sci, 2001. **268**(1478): p. 1803-10.
85. Watkins, P.J., *ABC of Diabetes*. 2003: BMJnPublishing Group Ltd, BMA House.
86. Watts, D.J. and S.H. Strogatz, *Collective dynamics of 'small-world' networks*. Nature, 1998. **393**(6684): p. 440-2.
87. Watzinger, F. and T. Lion, *Multiplex PCR for quality control of template RNA/cDNA in RT-PCR assays*. Leukemia, 1998. **12**(12): p. 1984-6; discussion 1987-93.

88. Wei, G.H., D.P. Liu, and C.C. Liang, *Charting gene regulatory networks: strategies, challenges and perspectives*. Biochem J, 2004. **381**(Pt 1): p. 1-12.
89. Wells, L. and G.W. Hart, *O-GlcNAc turns twenty: functional implications for post-translational modification of nuclear and cytosolic proteins with a sugar*. FEBS Lett, 2003. **546**(1): p. 154-8.
90. Wickner, W., *The nascent-polypeptide-associated complex: having a "NAC" for fidelity in translocation*. Proc Natl Acad Sci U S A, 1995. **92**(21): p. 9433-4.
91. Wiedmann, B., et al., *A protein complex required for signal-sequence-specific sorting and translocation*. Nature, 1994. **370**(6489): p. 434-40.
92. World Health Organization, D.o.N.D.S., Geneva, *Definition, Diagnosis and Classification of Diabetes Mellitus and its Complications*. 1999.
93. Xia, P., et al., *Characterization of the mechanism for the chronic activation of diacylglycerol-protein kinase C pathway in diabetes and hypergalactosemia*. Diabetes, 1994. **43**(9): p. 1122-9.
94. Yerneni, K.K., et al., *Hyperglycemia-induced activation of nuclear transcription factor kappaB in vascular smooth muscle cells*. Diabetes, 1999. **48**(4): p. 855-64.
95. Zheng, X.M., et al., *Sequencing and expression of complementary DNA for the general transcription factor BTF3*. Nature, 1990. **344**(6266): p. 556-9.
96. Zheng, X.M., et al., *A general transcription factor forms a stable complex with RNA polymerase B (II)*. Cell, 1987. **50**(3): p. 361-8.

8. Appendix

Table 4. Networkinteractions

Interaction from	Interaction to	Strenght of Interaction	Interaction from	Interaction to	Strenght of Interaction
AQP1	AQP1	2,722051	ATP6V0D1	CSPG	2,07361
AQP1	ATP6V0D1	-0,007463	ATP6V0D1	CXCL12	5,265143
AQP1	BTF3	0,134059	ATP6V0D1	CYR61	0,81192
AQP1	CALM2	0,025582	ATP6V0D1	Endothelin 1	0,790161
AQP1	CASP3	0,369031	ATP6V0D1	FGF1	-1,242175
AQP1	CDYL12	0,031851	ATP6V0D1	FZD4	0,629283
AQP1	CFH	-0,30251	ATP6V0D1	GAPDH	-3,279249
AQP1	c-Jun	0,293258	ATP6V0D1	GCA	-0,619129
AQP1	CLF	0,283436	ATP6V0D1	GDI2	0,089239
AQP1	CSPG	1,141788	ATP6V0D1	GNAS2	-0,414404
AQP1	CXCL12	-0,548603	ATP6V0D1	GTPBP4	-0,100111
AQP1	CYR61	0,270721	ATP6V0D1	HOXA3	0,122829
AQP1	Endothelin1	0,16569	ATP6V0D1	ICAM	0,89925
AQP1	FGF1	-0,505472	ATP6V0D1	KLF6	0,117326
AQP1	FZD4	0,092528	ATP6V0D1	NOS3	0,893727
AQP1	GAPDH	0,100185	ATP6V0D1	PHGDH	-0,808789
AQP1	GCA	0,081266	ATP6V0D1	PLD	-1,496417
AQP1	GDI2	-0,023122	ATP6V0D1	PRG	-0,589468
AQP1	GNAS2	-0,002362	ATP6V0D1	PRSS23	1,535841
AQP1	GTPBP4	-0,011851	ATP6V0D1	RAMP3	-0,429829
AQP1	HOXA3	0,068006	ATP6V0D1	RHOJ	0,806569
AQP1	ICAM	0,301902	ATP6V0D1	RPIB9	-0,119441
AQP1	KLF6	0,134175	ATP6V0D1	Smad2	-1,246196
AQP1	NOS3	0,064439	ATP6V0D1	SMAD3	0,441503
AQP1	PHGDH	-0,053721	ATP6V0D1	TGFb1	0,164494
AQP1	PLD	-0,189371	ATP6V0D1	TGFb-R2	-0,273231
AQP1	PRG	0,12705	ATP6V0D1	TOR3A	-0,43736
AQP1	PRSS23	0,147562	ATP6V0D1	UGDH	0,917983
AQP1	RAMP3	-0,201398	BTF3	AQP1	-3,652131
AQP1	RHOJ	-0,000233	BTF3	ATP6V0D1	0,414528
AQP1	RPIB9	0,159107	BTF3	BTF3	1,229077
AQP1	SMAD2	0,219555	BTF3	CALM2	-2,130973
AQP1	SMAD3	0,253928	BTF3	CASP3	-0,545044
AQP1	TGFb1	-0,005141	BTF3	CDYL12	-0,301147
AQP1	TGFb-R2	0,102489	BTF3	CFH	-1,81942
AQP1	TOR3A	-0,075687	BTF3	c-Jun	0,704005
AQP1	UGDH	0,19852	BTF3	CLF	-0,933266
ATP6V0D1	AQP1	-3,08974	BTF3	CSPG	3,306348
ATP6V0D1	ATP6V0D1	2,325257	BTF3	CXCL12	8,242679
ATP6V0D1	BTF3	-0,376401	BTF3	CYR61	1,073831
ATP6V0D1	CALM2	-1,974402	BTF3	Endothelin1	0,813671
ATP6V0D1	CASP3	-0,085988	BTF3	FGF1	-1,968983
ATP6V0D1	CDYL12	-0,676129	BTF3	FZD4	0,657172
ATP6V0D1	CFH	-2,044165	BTF3	GAPDH	-0,619802
ATP6V0D1	c-Jun	0,988746	BTF3	GCA	-0,479607
ATP6V0D1	CLF	-0,920006	BTF3	GDI2	0,280371

Interaction from	Interaction to	Strenght of Interaction	Interaction from	Interaction to	Strenght of Interaction
BTF3	GNAS2	-0,450612	CALM2	SMAD2	-1,782508
BTF3	GTPBP4	-0,144592	CALM2	SMAD3	0,970076
BTF3	HOXA3	-0,226815	CALM2	TGFb1	1,074866
BTF3	ICAM	-1,74477	CALM2	TGFb-R2	0,365716
BTF3	KLF6	0,144336	CALM2	TOR3A	-0,578279
BTF3	NOS3	0,909243	CALM2	UGDH	2,927373
BTF3	PHGDH	-0,591673	CASP3	AQP1	-2,656819
BTF3	PLD	-1,748211	CASP3	ATP6V0D1	1,140607
BTF3	PRG	-0,863597	CASP3	BTF3	-1,546986
BTF3	PRSS23	1,095389	CASP3	CALM2	0,888856
BTF3	RAMP3	-0,603226	CASP3	CASP3	-3,999093
BTF3	RHOJ	0,665645	CASP3	CDYL12	-0,604778
BTF3	RPIB9	3,182712	CASP3	CFH	3,117886
BTF3	SMAD2	-1,555074	CASP3	c-Jun	0,185592
BTF3	SMAD3	-0,225375	CASP3	CLF	0,798349
BTF3	TGFb1	-0,478121	CASP3	CSPG	0,953982
BTF3	TGFb-R2	-0,707906	CASP3	CXCL12	3,062254
BTF3	TOR3A	-0,146376	CASP3	CYR61	1,290601
BTF3	UGDH	0,904876	CASP3	Endothelin1	-0,113279
CALM2	AQP1	-3,046736	CASP3	FGF1	2,179099
CALM2	ATP6V0D1	0,239007	CASP3	FZD4	2,062084
CALM2	BTF3	-1,077063	CASP3	GAPDH	-1,386159
CALM2	CALM2	-3,732761	CASP3	GCA	1,576945
CALM2	CASP3	-0,153562	CASP3	GDI2	0,478653
CALM2	CDYL12	0,018216	CASP3	GNAS2	-0,11571
CALM2	CFH	-1,92955	CASP3	GTPBP4	0,542718
CALM2	c-Jun	2,078061	CASP3	HOXA3	-3,037106
CALM2	CLF	0,616158	CASP3	ICAM	-7,712362
CALM2	CSPG	2,96628	CASP3	KLF6	1,4507
CALM2	CXCL12	0,807208	CASP3	NOS3	2,708902
CALM2	CYR61	3,233838	CASP3	PHGDH	-1,457463
CALM2	Endothelin1	3,835349	CASP3	PLD	-0,267839
CALM2	FGF1	-3,181601	CASP3	PRG	-5,738937
CALM2	FZD4	1,619776	CASP3	PRSS23	2,727602
CALM2	GAPDH	-4,815197	CASP3	RAMP3	-0,776737
CALM2	GCA	0,996761	CASP3	RHOJ	2,60178
CALM2	GDI2	-0,565448	CASP3	RPIB9	0,744745
CALM2	GNAS2	-0,789899	CASP3	SMAD2	-6,414143
CALM2	GTPBP4	-0,161493	CASP3	SMAD3	-2,728214
CALM2	HOXA3	-0,977092	CASP3	TGFb1	1,402141
CALM2	ICAM	-1,051629	CASP3	TGFb-R2	0,125311
CALM2	KLF6	-1,06752	CASP3	TOR3A	0,062116
CALM2	NOS3	2,3354	CASP3	UGDH	0,97002
CALM2	PHGDH	-1,105632	CDYL12	AQP1	-1,017664
CALM2	PLD	-4,478745	CDYL12	ATP6V0D1	0,117312
CALM2	PRG	-1,799347	CDYL12	BTF3	-0,610371
CALM2	PRSS23	3,02272	CDYL12	CALM2	-1,443827
CALM2	RAMP3	-2,231726	CDYL12	CASP3	0,170126
CALM2	RHOJ	1,081526	CDYL12	CDYL12	1,897598
CALM2	RPIB9	4,66573	CDYL12	CFH	0,032497

Interaction from	Interaction to	Strenght of Interaction	Interaction from	Interaction to	Strenght of Interaction
CDYL12	c-Jun	0,303417	CFH	GNAS2	-0,244501
CDYL12	CLF	-0,757179	CFH	GTPBP4	-0,035682
CDYL12	CSPG	0,250842	CFH	HOXA3	0,571996
CDYL12	CXCL12	1,487483	CFH	ICAM	0,021479
CDYL12	CYR61	0,175548	CFH	KLF6	-0,009063
CDYL12	Endothelin1	0,300286	CFH	NOS3	0,242949
CDYL12	FGF1	0,157463	CFH	PHGDH	-0,488553
CDYL12	FZD4	0,261701	CFH	PLD	0,074743
CDYL12	GAPDH	-1,482582	CFH	PRG	0,272365
CDYL12	GCA	-0,429901	CFH	PRSS23	0,780167
CDYL12	GDI2	0,093695	CFH	RAMP3	-0,000653
CDYL12	GNAS2	-0,184377	CFH	RHOJ	0,426008
CDYL12	GTPBP4	-0,125345	CFH	RPIB9	0,424983
CDYL12	HOXA3	0,268072	CFH	SMAD2	-0,085103
CDYL12	ICAM	-0,232719	CFH	SMAD3	0,28332
CDYL12	KLF6	0,319906	CFH	TGFb1	0,201212
CDYL12	NOS3	0,53664	CFH	TGFb-R2	0,150135
CDYL12	PHGDH	-0,64088	CFH	TOR3A	-0,069621
CDYL12	PLD	-0,599745	CFH	UGDH	0,429609
CDYL12	PRG	0,322572	c-Jun	AQP1	-0,064146
CDYL12	PRSS23	0,626512	c-Jun	ATP6V0D1	0,032591
CDYL12	RAMP3	-0,051987	c-Jun	BTF3	-0,381775
CDYL12	RHOJ	0,449222	c-Jun	CALM2	0,607867
CDYL12	RPIB9	0,397418	c-Jun	CASP3	0,202097
CDYL12	SMAD2	-0,480506	c-Jun	CDYL12	-0,245587
CDYL12	SMAD3	0,401069	c-Jun	CFH	0,566377
CDYL12	TGFb1	0,246506	c-Jun	c-Jun	2,125499
CDYL12	TGFb-R2	-0,070223	c-Jun	CLF	-0,120851
CDYL12	TOR3A	-0,125409	c-Jun	CSPG	-1,254964
CDYL12	UGDH	0,448834	c-Jun	CXCL12	1,532972
CFH	AQP1	-0,929077	c-Jun	CYR61	-0,444088
CFH	ATP6V0D1	0,065912	c-Jun	Endothelin1	-1,14776
CFH	BTF3	-0,309593	c-Jun	FGF1	1,54171
CFH	CALM2	-0,960891	c-Jun	FZD4	-0,128566
CFH	CASP3	0,341853	c-Jun	GAPDH	-1,179839
CFH	CDYL12	0,062279	c-Jun	GCA	-0,581458
CFH	CFH	0,345406	c-Jun	GDI2	0,172997
CFH	c-Jun	0,384285	c-Jun	GNAS2	0,255923
CFH	CLF	-0,718437	c-Jun	GTPBP4	-0,016115
CFH	CSPG	0,601111	c-Jun	HOXA3	0,109867
CFH	CXCL12	0,578945	c-Jun	ICAM	0,136716
CFH	CYR61	0,164056	c-Jun	KLF6	0,933512
CFH	Endothelin1	0,552145	c-Jun	NOS3	-0,001442
CFH	FGF1	-0,447435	c-Jun	PHGDH	-0,321302
CFH	FZD4	0,238589	c-Jun	PLD	0,504646
CFH	GAPDH	-2,719102	c-Jun	PRG	1,136098
CFH	GCA	-0,652579	c-Jun	PRSS23	0,140679
CFH	GDI2	0,205872	c-Jun	RAMP3	0,214328

Interaction from	Interaction to	Strenght of Interaction	Interaction from	Interaction to	Strenght of Interaction
c-Jun	RPIB9	-2,183915	CSPG	CASP3	0,046823
c-Jun	SMAD2	-0,007251	CSPG	CDYL12	-0,030937
c-Jun	SMAD3	0,485082	CSPG	CFH	0,048031
c-Jun	TGFb1	0,11057	CSPG	c-Jun	0,007172
c-Jun	TGFb-R2	-0,048419	CSPG	CLF	-0,144475
c-Jun	TOR3A	-0,127674	CSPG	CSPG	3,731625
c-Jun	UGDH	-0,55193	CSPG	CXCL12	0,234863
CLF	AQP1	1,92925	CSPG	CYR61	0,017712
CLF	ATP6V0D1	0,131621	CSPG	Endothelin1	0,0181
CLF	BTF3	-0,368529	CSPG	FGF1	0,37619
CLF	CALM2	0,452025	CSPG	FZD4	-0,003139
CLF	CASP3	0,506538	CSPG	GAPDH	-0,514425
CLF	CDYL12	-0,328737	CSPG	GCA	-0,138902
CLF	CFH	1,979011	CSPG	GDI2	0,041696
CLF	c-Jun	-2,3076	CSPG	GNAS2	-0,019624
CLF	CLF	-3,081079	CSPG	GTPBP4	-0,020641
CLF	CSPG	-2,344377	CSPG	HOXA3	0,071653
CLF	CXCL12	2,419278	CSPG	ICAM	0,013586
CLF	CYR61	-3,263373	CSPG	KLF6	-0,036301
CLF	Endothelin1	-2,678154	CSPG	NOS3	0,003981
CLF	FGF1	3,782886	CSPG	PHGDH	-0,095599
CLF	FZD4	-1,654806	CSPG	PLD	0,023137
CLF	GAPDH	2,696649	CSPG	PRG	0,064071
CLF	GCA	-2,242516	CSPG	PRSS23	0,116173
CLF	GDI2	1,145122	CSPG	RAMP3	-0,000426
CLF	GNAS2	0,45734	CSPG	RHOJ	0,048541
CLF	GTPBP4	0,004236	CSPG	RPIB9	-0,021518
CLF	HOXA3	3,861057	CSPG	SMAD2	-0,004167
CLF	ICAM	0,571748	CSPG	SMAD3	0,057168
CLF	KLF6	1,576523	CSPG	TGFb1	0,004105
CLF	NOS3	-1,962628	CSPG	TGFb-R2	-0,013688
CLF	PHGDH	-0,065913	CSPG	TOR3A	-0,005917
CLF	PLD	4,656133	CSPG	UGDH	0,022083
CLF	PRG	3,395434	CXCL12	AQP1	0,979658
CLF	PRSS23	-2,629604	CXCL12	ATP6V0D1	-0,102499
CLF	RAMP3	2,458638	CXCL12	BTF3	0,040212
CLF	RHOJ	-0,332018	CXCL12	CALM2	0,352665
CLF	RPIB9	-1,715203	CXCL12	CASP3	0,169904
CLF	SMAD2	1,019112	CXCL12	CDYL12	0,254639
CLF	SMAD3	-0,894491	CXCL12	CFH	-0,019394
CLF	TGFb1	-0,968707	CXCL12	c-Jun	0,044251
CLF	TGFb-R2	-0,633826	CXCL12	CLF	0,470731
CLF	TOR3A	0,720497	CXCL12	CSPG	-0,433789
CLF	UGDH	-2,052853	CXCL12	CXCL12	1,068447
CSPG	AQP1	-0,127365	CXCL12	CYR61	0,123507
CSPG	ATP6V0D1	-0,002376	CXCL12	Endothelin1	0,28751
CSPG	BTF3	-0,074958	CXCL12	FGF1	-0,132652

Interaction from	Interaction to	Strenght of Interaction	Interaction from	Interaction to	Strenght of Interaction
CXCL12	FZD4	0,049283	CYR61	PLD	0,799185
CXCL12	GAPDH	-0,193411	CYR61	PRG	0,620565
CXCL12	GCA	0,2288	CYR61	PRSS23	-1,150767
CXCL12	GDI2	-0,106753	CYR61	RAMP3	2,999542
CXCL12	GNAS2	0,025759	CYR61	RHOJ	-0,386008
CXCL12	GTPBP4	0,029552	CYR61	RPIB9	-2,333872
CXCL12	HOXA3	0,041873	CYR61	SMAD2	1,122306
CXCL12	ICAM	0,473598	CYR61	SMAD3	-0,156653
CXCL12	KLF6	-0,239119	CYR61	TGFb1	0,39706
CXCL12	NOS3	-0,02826	CYR61	TGFb-R2	0,488599
CXCL12	PHGDH	0,189017	CYR61	TOR3A	0,067978
CXCL12	PLD	0,072361	CYR61	UGDH	-0,938486
CXCL12	PRG	-0,030393	Endothelin1	AQP1	-1,423115
CXCL12	PRSS23	-0,067909	Endothelin1	ATP6V0D1	0,06901
CXCL12	RAMP3	-0,107473	Endothelin1	BTF3	-0,234424
CXCL12	RHOJ	-0,101821	Endothelin1	CALM2	0,738925
CXCL12	RPIB9	0,532244	Endothelin1	CASP3	0,180086
CXCL12	SMAD2	0,416041	Endothelin1	CDYL12	-0,154949
CXCL12	SMAD3	0,066343	Endothelin1	CFH	-0,09834
CXCL12	TGFb1	0,151731	Endothelin1	c-Jun	1,243444
CXCL12	TGFb-R2	0,322165	Endothelin1	CLF	2,024652
CXCL12	TOR3A	0,052434	Endothelin1	CSPG	-0,210143
CXCL12	UGDH	0,073585	Endothelin1	CXCL12	0,391085
CYR61	AQP1	1,733734	Endothelin1	CYR61	1,118653
CYR61	ATP6V0D1	-0,276139	Endothelin1	Endothelin1	0,44604
CYR61	BTF3	0,91894	Endothelin1	FGF1	0,074869
CYR61	CALM2	1,517557	Endothelin1	FZD4	0,861509
CYR61	CASP3	0,196327	Endothelin1	GAPDH	-1,313102
CYR61	CDYL12	0,083023	Endothelin1	GCA	0,636822
CYR61	CFH	2,369235	Endothelin1	GDI2	-0,345289
CYR61	c-Jun	-0,699378	Endothelin1	GNAS2	-0,036484
CYR61	CLF	1,035112	Endothelin1	GTPBP4	-0,031419
CYR61	CSPG	-2,217062	Endothelin1	HOXA3	-1,073105
CYR61	CXCL12	-2,091655	Endothelin1	ICAM	0,005312
CYR61	CYR61	-0,005309	Endothelin1	KLF6	0,367888
CYR61	Endothelin1	-1,162037	Endothelin1	NOS3	1,072445
CYR61	FGF1	1,954061	Endothelin1	PHGDH	-0,320208
CYR61	FZD4	-0,658798	Endothelin1	PLD	-1,523676
CYR61	GAPDH	2,192965	Endothelin1	PRG	-0,803353
CYR61	GCA	-0,204767	Endothelin1	PRSS23	1,94045
CYR61	GDI2	-0,216719	Endothelin1	RAMP3	-0,880815
CYR61	GNAS2	0,48172	Endothelin1	RHOJ	0,586128
CYR61	GTPBP4	-0,015793	Endothelin1	RPIB9	-2,168576
CYR61	HOXA3	-0,064949	Endothelin1	SMAD2	-0,251569
CYR61	ICAM	1,315667	Endothelin1	SMAD3	1,230222
CYR61	KLF6	0,34182	Endothelin1	TGFb1	0,450065
CYR61	NOS3	-0,525726	Endothelin1	TGFb-R2	0,117336
CYR61	PHGDH	0,753908	Endothelin1	TOR3A	-0,303502

Interaction from	Interaction to	Strenght of Interaction	Interaction from	Interaction to	Strenght of Interaction
Endothelin1	UGDH	0,298661	FZD4	CXCL12	1,262295
FGF1	AQP1	0,090385	FZD4	CYR61	-0,05394
FGF1	ATP6V0D1	0,069161	FZD4	Endothelin1	0,295482
FGF1	BTF3	-0,052939	FZD4	FGF1	-0,106148
FGF1	CALM2	0,012379	FZD4	FZD4	2,128543
FGF1	CASP3	0,159011	FZD4	GAPDH	-1,96532
FGF1	CDYL12	0,196979	FZD4	GCA	-0,936292
FGF1	CFH	0,004089	FZD4	GDI2	0,315538
FGF1	c-Jun	-0,006599	FZD4	GNAS2	-0,199054
FGF1	CLF	-0,241329	FZD4	GTPBP4	-0,057107
FGF1	CSPG	-0,324237	FZD4	HOXA3	0,545993
FGF1	CXCL12	0,047263	FZD4	ICAM	-0,10025
FGF1	CYR61	0,085685	FZD4	KLF6	0,175129
FGF1	Endothelin1	0,006814	FZD4	NOS3	0,086504
FGF1	FGF1	2,515363	FZD4	PHGDH	-0,503613
FGF1	FZD4	0,085373	FZD4	PLD	0,277162
FGF1	GAPDH	-0,00809	FZD4	PRG	0,579215
FGF1	GCA	-0,105136	FZD4	PRSS23	0,465435
FGF1	GDI2	0,126447	FZD4	RAMP3	0,150172
FGF1	GNAS2	0,036397	FZD4	RHOJ	0,322986
FGF1	GTPBP4	0,003615	FZD4	RPIB9	0,537328
FGF1	HOXA3	0,239667	FZD4	SMAD2	-0,139913
FGF1	ICAM	0,046307	FZD4	SMAD3	0,283262
FGF1	KLF6	0,23843	FZD4	TGFb1	-0,178481
FGF1	NOS3	0,055732	FZD4	TGFb-R2	-0,231483
FGF1	PHGDH	-0,058264	FZD4	TOR3A	-0,05375
FGF1	PLD	0,293499	FZD4	UGDH	0,236679
FGF1	PRG	0,255403	GAPDH	AQP1	-1,285852
FGF1	PRSS23	-0,119329	GAPDH	ATP6V0D1	0,062921
FGF1	RAMP3	-0,06658	GAPDH	BTF3	-0,290265
FGF1	RHOJ	0,08113	GAPDH	CALM2	-0,721993
FGF1	RPIB9	0,091172	GAPDH	CASP3	0,592818
FGF1	SMAD2	0,107148	GAPDH	CDYL12	-0,018925
FGF1	SMAD3	0,143185	GAPDH	CFH	-0,336479
FGF1	TGFb1	0,035926	GAPDH	c-Jun	0,79265
FGF1	TGFb-R2	-0,014054	GAPDH	CLF	-0,322811
FGF1	TOR3A	0,054268	GAPDH	CSPG	0,400566
FGF1	UGDH	-0,010446	GAPDH	CXCL12	0,62672
FZD4	AQP1	-0,853477	GAPDH	CYR61	0,494133
FZD4	ATP6V0D1	0,069382	GAPDH	Endothelin1	0,506889
FZD4	BTF3	-0,456124	GAPDH	FGF1	-0,330092
FZD4	CALM2	-0,994436	GAPDH	FZD4	0,308799
FZD4	CASP3	0,423494	GAPDH	GAPDH	0,050888
FZD4	CDYL12	-0,104829	GAPDH	GCA	0,12856
FZD4	CFH	-0,826351	GAPDH	GDI2	-0,003754
FZD4	c-Jun	0,159408	GAPDH	GNAS2	-0,136431
FZD4	CLF	-1,100342	GAPDH	GTPBP4	0,027262
FZD4	CSPG	0,546913	GAPDH	HOXA3	0,385663

Interaction from	Interaction to	Strenght of Interaction	Interaction from	Interaction to	Strenght of Interaction
GAPDH	ICAM	0,419292	GCA	SMAD3	0,117338
GAPDH	KLF6	0,202552	GCA	TGFb1	0,00773
GAPDH	NOS3	0,326284	GCA	TGFb-R2	-0,093554
GAPDH	PHGDH	-0,321702	GCA	TOR3A	-0,002917
GAPDH	PLD	-0,604335	GCA	UGDH	0,040334
GAPDH	PRG	0,224281	GDI2	AQP1	-0,522203
GAPDH	PRSS23	0,968161	GDI2	ATP6V0D1	0,030233
GAPDH	RAMP3	-0,317611	GDI2	BTF3	-0,098632
GAPDH	RHOJ	0,248126	GDI2	CALM2	0,234539
GAPDH	RPIB9	-0,045898	GDI2	CASP3	0,19451
GAPDH	SMAD2	-0,007294	GDI2	CDYL12	-0,043086
GAPDH	SMAD3	0,777137	GDI2	CFH	-0,105751
GAPDH	TGFb1	0,117956	GDI2	c-Jun	0,446012
GAPDH	TGFb-R2	0,057832	GDI2	CLF	0,684758
GAPDH	TOR3A	-0,220995	GDI2	CSPG	-0,118149
GAPDH	UGDH	0,428592	GDI2	CXCL12	0,211289
GCA	AQP1	-0,198923	GDI2	CYR61	0,409766
GCA	ATP6V0D1	0,057357	GDI2	Endothelin1	0,048475
GCA	BTF3	-0,284124	GDI2	FGF1	0,059297
GCA	CALM2	-0,514125	GDI2	FZD4	0,298291
GCA	CASP3	0,10447	GDI2	GAPDH	-0,484308
GCA	CDYL12	-0,105097	GDI2	GCA	0,210284
GCA	CFH	0,06698	GDI2	GDI2	1,886837
GCA	c-Jun	-0,077142	GDI2	GNAS2	0,027886
GCA	CLF	-0,892572	GDI2	GTPBP4	-0,011329
GCA	CSPG	-0,153859	GDI2	HOXA3	-0,293912
GCA	CXCL12	0,836269	GDI2	ICAM	0,040684
GCA	CYR61	-0,060192	GDI2	KLF6	0,166866
GCA	Endothelin1	0,016283	GDI2	NOS3	0,782998
GCA	FGF1	0,475266	GDI2	PHGDH	-0,114569
GCA	FZD4	0,040527	GDI2	PLD	-0,619083
GCA	GAPDH	-0,534175	GDI2	PRG	-0,139531
GCA	GCA	1,996602	GDI2	PRSS23	0,7428
GCA	GDI2	0,242542	GDI2	RAMP3	-0,336962
GCA	GNAS2	-0,037891	GDI2	RHOJ	0,221758
GCA	GTPBP4	-0,010385	GDI2	RPIB9	-0,841091
GCA	HOXA3	0,457223	GDI2	SMAD2	0,00147
GCA	ICAM	-0,128633	GDI2	SMAD3	0,509539
GCA	KLF6	0,331737	GDI2	TGFb1	0,180345
GCA	NOS3	0,077197	GDI2	TGFb-R2	0,047316
GCA	PHGDH	-0,367007	GDI2	TOR3A	-0,102458
GCA	PLD	0,337256	GDI2	UGDH	0,112341
GCA	PRG	0,373063	GNAS2	AQP1	0,631276
GCA	PRSS23	0,125945	GNAS2	ATP6V0D1	-0,043007
GCA	RAMP3	0,096418	GNAS2	BTF3	0,186395
GCA	RHOJ	0,259841	GNAS2	CALM2	1,438364
GCA	RPIB9	0,286851	GNAS2	CASP3	-0,082553
GCA	SMAD2	-0,118574	GNAS2	CDYL12	-0,153049

Interaction from	Interaction to	Strenght of Interaction	Interaction from	Interaction to	Strenght of Interaction
GNAS2	CFH	1,257652	GTPBP4	GDI2	0,389734
GNAS2	c-Jun	-0,341702	GTPBP4	GNAS2	-0,012982
GNAS2	CLF	0,836314	GTPBP4	GTPBP4	1,89768
GNAS2	CSPG	0,077801	GTPBP4	HOXA3	0,644008
GNAS2	CXCL12	-0,076881	GTPBP4	ICAM	-0,158091
GNAS2	CYR61	-0,74119	GTPBP4	KLF6	0,565255
GNAS2	Endothelin1	-1,031415	GTPBP4	NOS3	-0,270796
GNAS2	FGF1	1,052674	GTPBP4	PHGDH	-0,499135
GNAS2	FZD4	-0,104385	GTPBP4	PLD	0,964364
GNAS2	GAPDH	1,987186	GTPBP4	PRG	1,068494
GNAS2	GCA	-0,335394	GTPBP4	PRSS23	-0,234567
GNAS2	GDI2	-0,127158	GTPBP4	RAMP3	0,41166
GNAS2	GNAS2	2,187287	GTPBP4	RHOJ	0,242985
GNAS2	GTPBP4	0,040727	GTPBP4	RPIB9	0,267293
GNAS2	HOXA3	-0,329482	GTPBP4	SMAD2	-0,041879
GNAS2	ICAM	0,39632	GTPBP4	SMAD3	-0,032841
GNAS2	KLF6	0,592359	GTPBP4	TGFb1	-0,392196
GNAS2	NOS3	-0,421791	GTPBP4	TGFb-R2	-0,185649
GNAS2	PHGDH	0,127728	GTPBP4	TOR3A	0,191929
GNAS2	PLD	0,501432	GTPBP4	UGDH	-0,025925
GNAS2	PRG	0,335174	HOXA3	AQP1	-0,4941
GNAS2	PRSS23	-0,436322	HOXA3	ATP6V0D1	0,061754
GNAS2	RAMP3	2,226801	HOXA3	BTF3	-0,14705
GNAS2	RHOJ	-0,012764	HOXA3	CALM2	-0,003165
GNAS2	RPIB9	-2,293562	HOXA3	CASP3	0,129217
GNAS2	SMAD2	0,334785	HOXA3	CDYL12	-0,109686
GNAS2	SMAD3	0,122901	HOXA3	CFH	0,052311
GNAS2	TGFb1	0,231002	HOXA3	c-Jun	0,347007
GNAS2	TGFb-R2	0,071475	HOXA3	CLF	0,238254
GNAS2	TOR3A	-0,214781	HOXA3	CSPG	-0,120706
GNAS2	UGDH	-0,593696	HOXA3	CXCL12	0,299946
GTPBP4	AQP1	-0,019944	HOXA3	CYR61	0,277071
GTPBP4	ATP6V0D1	0,177547	HOXA3	Endothelin1	0,069464
GTPBP4	BTF3	-0,511736	HOXA3	FGF1	0,203323
GTPBP4	CALM2	-0,780322	HOXA3	FZD4	0,239946
GTPBP4	CASP3	0,214397	HOXA3	GAPDH	-0,721046
GTPBP4	CDYL12	-0,257282	HOXA3	GCA	0,066035
GTPBP4	CFH	0,357408	HOXA3	GDI2	-0,039585
GTPBP4	c-Jun	-0,433004	HOXA3	GNAS2	-0,008812
GTPBP4	CLF	-1,480965	HOXA3	GTPBP4	-0,042365
GTPBP4	CSPG	-0,249621	HOXA3	HOXA3	2,284825
GTPBP4	CXCL12	1,457217	HOXA3	ICAM	-0,057733
GTPBP4	CYR61	-0,46138	HOXA3	KLF6	0,232501
GTPBP4	Endothelin1	-0,202608	HOXA3	NOS3	0,3172
GTPBP4	FGF1	1,067299	HOXA3	PHGDH	-0,255345
GTPBP4	FZD4	-0,262349	HOXA3	PLD	-0,411843
GTPBP4	GAPDH	-0,162759	HOXA3	PRG	-0,015214
GTPBP4	GCA	-0,702158	HOXA3	PRSS23	0,526719

Interaction from	Interaction to	Strenght of Interaction	Interaction from	Interaction to	Strenght of Interaction
HOXA3	RAMP3	-0,206556	KLF6	BTF3	0,813969
HOXA3	RHOJ	0,284675	KLF6	CALM2	1,30467
HOXA3	RPIB9	-0,458962	KLF6	CASP3	0,459868
HOXA3	SMAD2	-0,116524	KLF6	CDYL12	0,259899
HOXA3	SMAD3	0,426192	KLF6	CFH	1,022732
HOXA3	TGFb1	0,116499	KLF6	c-Jun	-0,479879
HOXA3	TGFb-R2	0,0281	KLF6	CLF	0,492448
HOXA3	TOR3A	-0,122777	KLF6	CSPG	1,286562
HOXA3	UGDH	0,166775	KLF6	CXCL12	-1,892251
ICAM	AQP1	-0,055842	KLF6	CYR61	-0,761481
ICAM	ATP6V0D1	0,160282	KLF6	Endothelin1	-0,913173
ICAM	BTF3	-0,42817	KLF6	FGF1	0,126154
ICAM	CALM2	-0,098076	KLF6	FZD4	-0,367284
ICAM	CASP3	0,155861	KLF6	GAPDH	2,549512
ICAM	CDYL12	-0,241314	KLF6	GCA	0,156962
ICAM	CFH	0,620361	KLF6	GDI2	-0,120326
ICAM	c-Jun	-0,499641	KLF6	GNAS2	0,258047
ICAM	CLF	-0,898077	KLF6	GTPBP4	-0,0846
ICAM	CSPG	-0,677438	KLF6	HOXA3	0,469992
ICAM	CXCL12	1,345553	KLF6	ICAM	1,068114
ICAM	CYR61	-0,493526	KLF6	KLF6	1,226434
ICAM	Endothelin1	-0,63608	KLF6	NOS3	-0,532306
ICAM	FGF1	1,334682	KLF6	PHGDH	0,166961
ICAM	FZD4	-0,15303	KLF6	PLD	1,211519
ICAM	GAPDH	-0,017039	KLF6	PRG	0,926734
ICAM	GCA	-0,59269	KLF6	PRSS23	-1,269263
ICAM	GDI2	0,372268	KLF6	RAMP3	0,488305
ICAM	GNAS2	0,086516	KLF6	RHOJ	-0,331237
ICAM	GTPBP4	0,002773	KLF6	RPIB9	-1,329022
ICAM	HOXA3	0,337033	KLF6	SMAD2	1,0852
ICAM	ICAM	1,642936	KLF6	SMAD3	0,057792
ICAM	KLF6	0,653758	KLF6	TGFb1	0,033117
ICAM	NOS3	-0,052836	KLF6	TGFb-R2	0,427413
ICAM	PHGDH	-0,537722	KLF6	TOR3A	0,172837
ICAM	PLD	0,987355	KLF6	UGDH	-0,72825
ICAM	PRG	0,999998	NOS3	AQP1	0,194468
ICAM	PRSS23	-0,12977	NOS3	ATP6V0D1	0,025143
ICAM	RAMP3	0,381481	NOS3	BTF3	-0,237475
ICAM	RHOJ	0,311002	NOS3	CALM2	0,178299
ICAM	RPIB9	-0,735808	NOS3	CASP3	0,134759
ICAM	SMAD2	0,020781	NOS3	CDYL12	-0,208658
ICAM	SMAD3	0,135896	NOS3	CFH	0,34896
ICAM	TGFb1	-0,099432	NOS3	c-Jun	0,152776
ICAM	TGFb-R2	-0,192266	NOS3	CLF	0,041936
ICAM	TOR3A	0,198179	NOS3	CSPG	-0,688913
ICAM	UGDH	-0,339851	NOS3	CXCL12	0,962163
KLF6	AQP1	1,664461	NOS3	CYR61	-0,14822
KLF6	ATP6V0D1	-0,164714	NOS3	Endothelin1	-0,357291

Interaction from	Interaction to	Strenght of Interaction	Interaction from	Interaction to	Strenght of Interaction
NOS3	FGF1	0,792039	PHGDH	PHGDH	1,853456
NOS3	FZD4	0,169745	PHGDH	PLD	0,992965
NOS3	GAPDH	-0,562523	PHGDH	PRG	0,739949
NOS3	GCA	-0,213649	PHGDH	PRSS23	-0,283235
NOS3	GDI2	0,067631	PHGDH	RAMP3	0,383569
NOS3	GNAS2	0,046218	PHGDH	RHOJ	0,257652
NOS3	GTPBP4	-0,092357	PHGDH	RPIB9	-0,383497
NOS3	HOXA3	-0,011407	PHGDH	SMAD2	-0,02565
NOS3	ICAM	0,077071	PHGDH	SMAD3	-0,011334
NOS3	KLF6	0,293661	PHGDH	TGFb1	-0,260175
NOS3	NOS3	2,098091	PHGDH	TGFb-R2	-0,25053
NOS3	PHGDH	-0,261336	PHGDH	TOR3A	0,245874
NOS3	PLD	0,060515	PHGDH	UGDH	-0,242587
NOS3	PRG	0,204702	PLD	AQP1	-1,304656
NOS3	PRSS23	0,48024	PLD	ATP6V0D1	0,07524
NOS3	RAMP3	0,110214	PLD	BTF3	-0,252284
NOS3	RHOJ	0,212726	PLD	CALM2	1,249145
NOS3	RPIB9	-1,233677	PLD	CASP3	0,134269
NOS3	SMAD2	-0,049944	PLD	CDYL12	-0,338918
NOS3	SMAD3	0,431952	PLD	CFH	0,559681
NOS3	TGFb1	0,11867	PLD	c-Jun	0,965911
NOS3	TGFb-R2	-0,06661	PLD	CLF	1,604756
NOS3	TOR3A	-0,054059	PLD	CSPG	-0,720347
NOS3	UGDH	-0,210265	PLD	CXCL12	0,594866
PHGDH	AQP1	0,192622	PLD	CYR61	0,784333
PHGDH	ATP6V0D1	0,160081	PLD	Endothelin1	-0,523273
PHGDH	BTF3	-0,234119	PLD	FGF1	0,863824
PHGDH	CALM2	0,168511	PLD	FZD4	0,67139
PHGDH	CASP3	-0,036258	PLD	GAPDH	-1,376722
PHGDH	CDYL12	-0,18084	PLD	GCA	0,504969
PHGDH	CFH	0,530371	PLD	GDI2	-0,307012
PHGDH	c-Jun	-0,421911	PLD	GNAS2	0,107368
PHGDH	CLF	-0,946539	PLD	GTPBP4	-0,111398
PHGDH	CSPG	-0,641865	PLD	HOXA3	-0,969137
PHGDH	CXCL12	0,691945	PLD	ICAM	-0,115976
PHGDH	CYR61	-0,497396	PLD	KLF6	0,646984
PHGDH	Endothelin1	-0,426788	PLD	NOS3	0,887649
PHGDH	FGF1	1,327598	PLD	PHGDH	-0,530245
PHGDH	FZD4	-0,17661	PLD	PLD	-0,709276
PHGDH	GAPDH	-0,012926	PLD	PRG	-0,397471
PHGDH	GCA	-0,455638	PLD	PRSS23	1,642682
PHGDH	GDI2	0,317786	PLD	RAMP3	-0,686776
PHGDH	GNAS2	0,098245	PLD	RHOJ	0,644232
PHGDH	GTPBP4	0,085801	PLD	RPIB9	-2,768838
PHGDH	HOXA3	0,36762	PLD	SMAD2	-0,277574
PHGDH	ICAM	-0,27431	PLD	SMAD3	1,219833
PHGDH	KLF6	0,611256	PLD	TGFb1	0,427115
PHGDH	NOS3	-0,205624	PLD	TGFb-R2	0,163462

Interaction from	Interaction to	Strenght of Interaction	Interaction from	Interaction to	Strenght of Interaction
PLD	TOR3A	-0,303559	PRSS23	CSPG	1,817921
PLD	UGDH	0,156602	PRSS23	CXCL12	-3,413204
PRG	AQP1	0,879461	PRSS23	CYR61	1,253514
PRG	ATP6V0D1	0,139465	PRSS23	Endothelin1	2,842801
PRG	BTF3	0,422625	PRSS23	FGF1	-2,538473
PRG	CALM2	-1,656693	PRSS23	FZD4	0,018764
PRG	CASP3	0,060645	PRSS23	GAPDH	-1,317217
PRG	CDYL12	0,581995	PRSS23	GCA	0,232562
PRG	CFH	-1,450461	PRSS23	GDI2	0,236799
PRG	c-Jun	-0,220247	PRSS23	GNAS2	-0,291544
PRG	CLF	-0,298701	PRSS23	GTPBP4	0,070735
PRG	CSPG	1,721634	PRSS23	HOXA3	0,740413
PRG	CXCL12	-2,66132	PRSS23	ICAM	-0,039704
PRG	CYR61	1,282092	PRSS23	KLF6	-1,375956
PRG	Endothelin1	2,617896	PRSS23	NOS3	-0,139539
PRG	FGF1	-2,585011	PRSS23	PHGDH	0,365794
PRG	FZD4	0,333999	PRSS23	PLD	-0,680746
PRG	GAPDH	0,152326	PRSS23	PRG	-0,311732
PRG	GCA	0,880418	PRSS23	PRSS23	0,847285
PRG	GDI2	-0,065074	PRSS23	RAMP3	-0,880577
PRG	GNAS2	-0,324713	PRSS23	RHOJ	-0,258409
PRG	GTPBP4	0,143221	PRSS23	RPIB9	7,857261
PRG	HOXA3	0,242248	PRSS23	SMAD2	0,161709
PRG	ICAM	-0,167208	PRSS23	SMAD3	-0,935454
PRG	KLF6	-1,637824	PRSS23	TGFb1	-0,414377
PRG	NOS3	0,288936	PRSS23	TGFb-R2	0,050703
PRG	PHGDH	0,672652	PRSS23	TOR3A	0,423672
PRG	PLD	-0,980209	PRSS23	UGDH	1,333416
PRG	PRG	1,456033	RAMP3	AQP1	-0,260592
PRG	PRSS23	-0,270675	RAMP3	ATP6V0D1	0,019166
PRG	RAMP3	-0,82963	RAMP3	BTF3	-0,150158
PRG	RHOJ	-0,228541	RAMP3	CALM2	-0,354093
PRG	RPIB9	6,210309	RAMP3	CASP3	0,125197
PRG	SMAD2	0,209534	RAMP3	CDYL12	-0,057261
PRG	SMAD3	-0,562137	RAMP3	CFH	-0,289608
PRG	TGFb1	-0,153684	RAMP3	c-Jun	0,066469
PRG	TGFb-R2	0,103448	RAMP3	CLF	-0,273036
PRG	TOR3A	0,298233	RAMP3	CSPG	0,201877
PRG	UGDH	1,348567	RAMP3	CXCL12	0,373445
PRSS23	AQP1	1,008426	RAMP3	CYR61	0,006419
PRSS23	ATP6V0D1	0,053409	RAMP3	Endothelin1	0,0293
PRSS23	BTF3	0,613626	RAMP3	FGF1	-0,036553
PRSS23	CALM2	-2,163368	RAMP3	FZD4	0,054218
PRSS23	CASP3	0,076568	RAMP3	GAPDH	-0,697487
PRSS23	CDYL12	0,672295	RAMP3	GCA	-0,095663
PRSS23	CFH	-1,425859	RAMP3	GDI2	0,095051
PRSS23	c-Jun	0,075995	RAMP3	GNAS2	-0,068126
PRSS23	CLF	-1,05331	RAMP3	GTPBP4	-0,03857

Interaction from	Interaction to	Strenght of Interaction	Interaction from	Interaction to	Strenght of Interaction
RAMP3	HOXA3	0,183082	RHOJ	SMAD2	-0,33421
RAMP3	ICAM	-0,073403	RHOJ	SMAD3	0,313565
RAMP3	KLF6	-0,010189	RHOJ	TGFb1	-0,08597
RAMP3	NOS3	0,025804	RHOJ	TGFb-R2	-0,229026
RAMP3	PHGDH	-0,180068	RHOJ	TOR3A	-0,088269
RAMP3	PLD	0,064598	RHOJ	UGDH	0,316683
RAMP3	PRG	0,151859	RPIB9	AQP1	-0,930272
RAMP3	PRSS23	0,121545	RPIB9	ATP6V0D1	0,110544
RAMP3	RAMP3	3,575295	RPIB9	BTF3	-0,682635
RAMP3	RHOJ	0,11189	RPIB9	CALM2	0,162924
RAMP3	RPIB9	0,160901	RPIB9	CASP3	0,292656
RAMP3	SMAD2	-0,072731	RPIB9	CDYL12	-0,466737
RAMP3	SMAD3	0,115017	RPIB9	CFH	1,010395
RAMP3	TGFb1	-0,067827	RPIB9	c-Jun	-0,083738
RAMP3	TGFb-R2	-0,063445	RPIB9	CLF	-0,412118
RAMP3	TOR3A	0,011063	RPIB9	CSPG	-0,916101
RAMP3	UGDH	0,077934	RPIB9	CXCL12	2,479657
RHOJ	AQP1	-1,280362	RPIB9	CYR61	-0,509635
RHOJ	ATP6V0D1	0,091783	RPIB9	Endothelin1	-1,131415
RHOJ	BTF3	-0,663887	RPIB9	FGF1	1,620557
RHOJ	CALM2	-0,887787	RPIB9	FZD4	0,055868
RHOJ	CASP3	0,268817	RPIB9	GAPDH	-0,777969
RHOJ	CDYL12	-0,182935	RPIB9	GCA	-0,654921
RHOJ	CFH	-1,151993	RPIB9	GDI2	0,178603
RHOJ	c-Jun	0,295836	RPIB9	GNAS2	0,090822
RHOJ	CLF	-0,96468	RPIB9	GTPBP4	-0,061006
RHOJ	CSPG	0,776246	RPIB9	HOXA3	0,219708
RHOJ	CXCL12	1,921979	RPIB9	ICAM	-0,121627
RHOJ	CYR61	0,131644	RPIB9	KLF6	0,974219
RHOJ	Endothelin1	0,197263	RPIB9	NOS3	0,249131
RHOJ	FGF1	-0,292086	RPIB9	PHGDH	-0,74399
RHOJ	FZD4	0,26688	RPIB9	PLD	0,50319
RHOJ	GAPDH	-1,982485	RPIB9	PRG	0,863141
RHOJ	GCA	-0,682826	RPIB9	PRSS23	0,180337
RHOJ	GDI2	0,277609	RPIB9	RAMP3	0,362849
RHOJ	GNAS2	-0,21972	RPIB9	RHOJ	0,554255
RHOJ	GTPBP4	-0,070687	RPIB9	RPIB9	-0,947515
RHOJ	HOXA3	0,486262	RPIB9	SMAD2	-0,133732
RHOJ	ICAM	-0,249554	RPIB9	SMAD3	0,769392
RHOJ	KLF6	0,227239	RPIB9	TGFb1	0,247692
RHOJ	NOS3	0,386474	RPIB9	TGFb-R2	-0,054799
RHOJ	PHGDH	-0,509805	RPIB9	TOR3A	-0,234201
RHOJ	PLD	-0,122358	RPIB9	UGDH	-0,476633
RHOJ	PRG	0,342943	SMAD2	AQP1	-0,171812
RHOJ	PRSS23	0,683442	SMAD2	ATP6V0D1	0,010975
RHOJ	RAMP3	0,018729	SMAD2	BTF3	-0,265004
RHOJ	RHOJ	2,49185	SMAD2	CALM2	-0,183287
RHOJ	RPIB9	0,380013	SMAD2	CASP3	0,174729

Interaction from	Interaction to	Strenght of Interaction	Interaction from	Interaction to	Strenght of Interaction
SMAD2	CDYL12	-0,140778	SMAD3	GCA	-0,259429
SMAD2	CFH	0,44157	SMAD3	GDI2	0,048709
SMAD2	c-Jun	-0,106852	SMAD3	GNAS2	-0,097178
SMAD2	CLF	-0,494962	SMAD3	GTPBP4	-0,072951
SMAD2	CSPG	-0,477231	SMAD3	HOXA3	0,324979
SMAD2	CXCL12	0,985341	SMAD3	ICAM	0,218015
SMAD2	CYR61	-0,378648	SMAD3	KLF6	0,417051
SMAD2	Endothelin1	-0,476078	SMAD3	NOS3	0,121789
SMAD2	FGF1	0,856169	SMAD3	PHGDH	-0,261475
SMAD2	FZD4	-0,080911	SMAD3	PLD	-0,205723
SMAD2	GAPDH	-0,083507	SMAD3	PRG	0,46935
SMAD2	GCA	-0,393349	SMAD3	PRSS23	0,238448
SMAD2	GDI2	0,174495	SMAD3	RAMP3	0,154578
SMAD2	GNAS2	0,08878	SMAD3	RHOJ	0,143075
SMAD2	GTPBP4	-0,046543	SMAD3	RPIB9	-0,302382
SMAD2	HOXA3	0,417238	SMAD3	SMAD2	-0,019514
SMAD2	ICAM	0,034694	SMAD3	SMAD3	2,33675
SMAD2	KLF6	0,44373	SMAD3	TGFb1	0,076864
SMAD2	NOS3	0,049899	SMAD3	TGFb-R2	-0,104073
SMAD2	PHGDH	-0,320187	SMAD3	TOR3A	-0,085956
SMAD2	PLD	0,437831	SMAD3	UGDH	0,052293
SMAD2	PRG	0,712885	TGFb1	AQP1	-0,04787
SMAD2	PRSS23	-0,090107	TGFb1	ATP6V0D1	0,109299
SMAD2	RAMP3	0,255614	TGFb1	BTF3	-0,371438
SMAD2	RHOJ	0,258073	TGFb1	CALM2	-0,633426
SMAD2	RPIB9	-0,457652	TGFb1	CASP3	0,026022
SMAD2	SMAD2	1,966927	TGFb1	CDYL12	-0,099515
SMAD2	SMAD3	0,220741	TGFb1	CFH	0,137997
SMAD2	TGFb1	0,03644	TGFb1	c-Jun	-0,361341
SMAD2	TGFb-R2	-0,010061	TGFb1	CLF	-1,433114
SMAD2	TOR3A	0,07211	TGFb1	CSPG	1,12179
SMAD2	UGDH	-0,247075	TGFb1	CXCL12	1,041784
SMAD3	AQP1	-0,470039	TGFb1	CYR61	-0,272378
SMAD3	ATP6V0D1	0,035381	TGFb1	Endothelin1	-0,18914
SMAD3	BTF3	-0,290751	TGFb1	FGF1	0,321726
SMAD3	CALM2	-0,51931	TGFb1	FZD4	-0,032205
SMAD3	CASP3	0,417966	TGFb1	GAPDH	0,153084
SMAD3	CDYL12	-0,09506	TGFb1	GCA	-0,54898
SMAD3	CFH	-0,13046	TGFb1	GDI2	0,388874
SMAD3	c-Jun	0,248093	TGFb1	GNAS2	-0,032829
SMAD3	CLF	-0,436647	TGFb1	GTPBP4	-0,005989
SMAD3	CSPG	1,235187	TGFb1	HOXA3	0,735693
SMAD3	CXCL12	0,865239	TGFb1	ICAM	-0,32212
SMAD3	CYR61	-0,122251	TGFb1	KLF6	0,67219
SMAD3	Endothelin1	-0,045374	TGFb1	NOS3	0,028084
SMAD3	FGF1	-0,125278	TGFb1	PHGDH	-0,407542
SMAD3	FZD4	0,115177	TGFb1	PLD	0,651457
SMAD3	GAPDH	0,120993	TGFb1	PRG	0,588396

Interaction from	Interaction to	Strenght of Interaction	Interaction from	Interaction to	Strenght of Interaction
TGFb1	PRSS23	-0,298462	TOR3A	ATP6V0D1	0,068918
TGFb1	RAMP3	0,265818	TOR3A	BTF3	-0,413956
TGFb1	RHOJ	0,316043	TOR3A	CALM2	-1,060599
TGFb1	RPIB9	0,701872	TOR3A	CASP3	0,289129
TGFb1	SMAD2	-0,205828	TOR3A	CDYL12	-0,099789
TGFb1	SMAD3	-0,037211	TOR3A	CFH	-0,813397
TGFb1	TGFb1	1,633198	TOR3A	c-Jun	0,194724
TGFb1	TGFb-R2	-0,154977	TOR3A	CLF	-1,00681
TGFb1	TOR3A	0,101178	TOR3A	CSPG	0,609698
TGFb1	UGDH	-0,038122	TOR3A	CXCL12	1,026558
TGFb-R2	AQP1	-0,650353	TOR3A	CYR61	0,082552
TGFb-R2	ATP6V0D1	0,151817	TOR3A	Endothelin1	0,463403
TGFb-R2	BTF3	-0,504576	TOR3A	FGF1	-0,223439
TGFb-R2	CALM2	-1,424873	TOR3A	FZD4	0,142345
TGFb-R2	CASP3	0,078106	TOR3A	GAPDH	-1,895986
TGFb-R2	CDYL12	0,059089	TOR3A	GCA	-0,736713
TGFb-R2	CFH	-2,136859	TOR3A	GDI2	0,275635
TGFb-R2	c-Jun	0,101163	TOR3A	GNAS2	-0,222805
TGFb-R2	CLF	-1,336576	TOR3A	GTPBP4	-0,04841
TGFb-R2	CSPG	1,016944	TOR3A	HOXA3	0,612508
TGFb-R2	CXCL12	0,954057	TOR3A	ICAM	-0,16147
TGFb-R2	CYR61	0,230689	TOR3A	KLF6	0,157412
TGFb-R2	Endothelin1	0,715016	TOR3A	NOS3	0,18301
TGFb-R2	FGF1	-0,477687	TOR3A	PHGDH	-0,483153
TGFb-R2	FZD4	0,332204	TOR3A	PLD	0,12787
TGFb-R2	GAPDH	-0,819272	TOR3A	PRG	0,37954
TGFb-R2	GCA	-0,593891	TOR3A	PRSS23	0,410234
TGFb-R2	GDI2	0,392268	TOR3A	RAMP3	0,056591
TGFb-R2	GNAS2	-0,223673	TOR3A	RHOJ	0,496005
TGFb-R2	GTPBP4	-0,046167	TOR3A	RPIB9	0,872244
TGFb-R2	HOXA3	0,742079	TOR3A	SMAD2	-0,190656
TGFb-R2	ICAM	-0,463773	TOR3A	SMAD3	0,213453
TGFb-R2	KLF6	0,250044	TOR3A	TGFb1	-0,136906
TGFb-R2	NOS3	0,402942	TOR3A	TGFb-R2	-0,165327
TGFb-R2	PHGDH	-0,271544	TOR3A	TOR3A	1,904106
TGFb-R2	PLD	0,121529	TOR3A	UGDH	0,344782
TGFb-R2	PRG	0,124962	UGDH	AQP1	0,284509
TGFb-R2	PRSS23	0,355099	UGDH	ATP6V0D1	0,02521
TGFb-R2	RAMP3	-0,042349	UGDH	BTF3	0,065391
TGFb-R2	RHOJ	0,547531	UGDH	CALM2	0,367226
TGFb-R2	RPIB9	1,903911	UGDH	CASP3	0,245382
TGFb-R2	SMAD2	-0,349989	UGDH	CDYL12	0,307307
TGFb-R2	SMAD3	0,024022	UGDH	CFH	0,388493
TGFb-R2	TGFb1	-0,978712	UGDH	c-Jun	-0,006185
TGFb-R2	TGFb-R2	2,036906	UGDH	CLF	0,148204
TGFb-R2	TOR3A	0,058657	UGDH	CSPG	-0,752372
TGFb-R2	UGDH	0,496391	UGDH	CXCL12	-0,119975
TOR3A	AQP1	-0,847746	UGDH	CYR61	-0,148293

Interaction from	Interaction to	Strenght of Interaction	Interaction from	Interaction to	Strenght of Interaction
UGDH	Endothelin1	-0,239631	UGDH	PLD	0,312842
UGDH	FGF1	0,781267	UGDH	PRG	0,359132
UGDH	FZD4	0,072966	UGDH	PRSS23	-0,04542
UGDH	GAPDH	0,207119	UGDH	RAMP3	0,064014
UGDH	GCA	-0,042267	UGDH	RHOJ	0,110438
UGDH	GDI2	0,080081	UGDH	RPIB9	-0,756906
UGDH	GNAS2	0,117645	UGDH	SMAD2	0,298387
UGDH	GTPBP4	-0,004599	UGDH	SMAD3	0,344669
UGDH	HOXA3	0,106492	UGDH	TGFb1	0,144615
UGDH	ICAM	0,320821	UGDH	TGFb-R2	0,015939
UGDH	KLF6	0,21904	UGDH	TOR3A	0,076896
UGDH	NOS3	-0,32921	UGDH	UGDH	1,310948
UGDH	PHGDH	-0,07038			

Table 5. List of genes comprising the *ex vivo* set after secondary and tertiary data analysis.

ANX2	GAPDH	PKN2
AQP1	GCL	PPAP2A
ATP6V0D1	GDI2	PPP1CB
ABL2	GL004	PRG1
ANP32E	GNAS	PRSS23
ARF4	GNB2L1	RAD6
BMX	HERC4	RHOJ
C1S	HOXA3/5	RPIB9
C7	HNRPA3	RHOJ
CD99	HSPG2	RPIB9
CDH1	IFTM2	RPL3
CDYL2	IFTM3	RPL10
CFH	ITM1	RPL13a
CSPG2	KLF6	SDF1
CTBP2	LBR	SEC23A
CTTNBP2NL	LEPR	SFRS12
CXCR4	LMCD1	SH3D5
CYR61	LZTFL1	SH3PXD2B
DAZAP1	MAP4	SIAT7C
EBF	NEGR1	TAF2F
EPAG9	NESP55	TBCA
EPHA4	OASL	TH1L
FBN1	OATPB	TOR3A
FN1	OSBPL1A	UGDH
FZD4	OSBPL10	VEGF

9. Abbreviations

AGE	Advanced glycation end products
ANGPT2	Angiopoietin-2
AQP1	Aquaporin 1
ATP6V0D1	D1 subunit of the transmembrane VO domain of ATPase
ATPase	Adenosine triphosphatase
BECs	Blood vessel endothelial cells
BTF3	Basic transcription factor 3
C1S	Complement component 1, s subcomponent
CALM2	Calmodulin 2
CASP3	Caspase 3
CDS	Coding sequence
CFH	Complement factor H
CIP	Calf intestinal alkaline phosphatase
CLF	Cholesterol lowering factor
CSPG2	Chondroitin sulfate proteoglycan 2
Ct	Cycle threshold
CXCL12	Chemokine (CXC motif) ligand 12
CXCR4	Chemokine (C-X-C motif) receptor 4
CXCR7	Chemokine (C-X-C motif) receptor 7
CYR61	Cysteine-rich angiogenic inducer 61
DAG	Diacylglycerol
DM	Diabetes mellitus
DMA	Diabetic microangiopathy
ECMV	encephalomyocarditis virus
EGFP	Enhanced green fluorescent protein
eNOS	Endothelial nitric oxide synthase
ER	Endoplasmatic Reticulum
ET-1	Endothelin 1
FGF1	Human fibroblast growth factor 1
FZD4	Frizzled homolog 4
GAPDH	Glyceraldehyde-3-phosphate dehydrogenase
GCA	Grancalcin
GDI2	GDP-dissociation inhibitor 2
GFP	Green fluorescent protein
GNAS2	Guanine nucleotide binding protein 2
GTPBP4	GTP binding protein 4
HOXA3	Homeobox A3
hTERT	Human telomerase reverse transcriptase
ICAM1	Intercellular adhesion molecule 1
iHUECs	Immortalized human umbilical vein endothelial cells
IRES	Internal ribosomal entry site
KLF6	Kruppel-like transcription factor 6
LDA	Low density array
MMP9	Matrix metalloproteinase 9
NAC	nascent-polypeptide-associated complex
NF- κ B	Nuclear factor-kappa B
NIR	network identification by multiple regression
NOS3	Nitric oxide synthase 3
PABP	Poly(A)-binding protein
PAI-1	Plasminogen activator inhibitor-1

PARP	Poly (ADP-ribose) polymerase
PBS	Phosphate buffered saline
PBSF	Pre-B cell growth stimulating factor
PCR	Polymerase chain reaction
PDGFA	Platelet-derived growth factor alpha polypeptide
PECAM1	Platelet endothelial cell adhesion molecule
PHGDH	Phosphoglycerate dehydrogenase
PKC	Protein kinase C
PLD	Phospholipase D
PRSS23	Protease serine 23
PTC	Peptidyl Transferase Center
RAMP3	Receptor (G protein-coupled) activity modifying protein 3
RHOJ	Ras homolog gene family, member J protein
ROS	Reactive oxygen species
RPIB9	Rap2 interacting protein
RPL3	Ribosomal protein of the large subunit 3
Rundc3	RUN domain containing 3B
RVM	Relative variance method
RZPD	German Resource Center for Genome Research
SDF-1	stromal cell-derived factor 1
SDS	sodium dodecyl sulfate or sequence detection software
SMAD2	Smad family member 2
SMAD3	Smad family member 3
SOD1	superoxide dismutase 1
SRL	Sarcin Ricin Loop
TGF-b	Transforming growth factor-beta
THBD	Thrombomodulin
TOR3A	Torsin 3A
UGDH	Uridine diphosphate -glucose dehydrogenase
VEGF	Vascular endothelial growth factor

CURRICULUM VITAE

Persönliche Daten

Hannelore Lechtermann
Spargelfeldstraße 127/143
1220 Wien

29.12.1976, Wien

Studium und Ausbildung

10/1995 – 12/2009	Universität Wien, Institut für Mikrobiologie und Genetik, Campus Vienna Biocenter, Wien Studium der Mikrobiologie, Schwerpunkt Immunbiologie
10/2006 – 05/2008	Institut für Ultrastrukturpathologie und Zellbiologie, Arbeitsgruppe Wick et al., AKH und Medizinisch Universität Wien Diplomarbeit
09/1987 – 06/1995	Realgymnasium Wien 22, Naturwissenschaftlicher Zweig

Berufliche Tätigkeiten

01/2009 – 12/2009	SMZO Donauespital, Institut für Mund-, Kiefer- und Gesichtschirurgie, Wien Aufbau und Wartung einer aktuellen Studiendatenbank
10/2004 – 12/2008	Competence Call Center AG, Wien Senior Team Support Projektmanagement einer Fluglärmbeschwerdehotline der Flughafen Wien AG, Qualitätsmanagement
11/2002 – 09/2003	KMA Knowledge Management Associates GmbH, Wien Assistenz der Geschäftsführung Projektmanagement diverser Marketing und PR-Initiativen
03/2001 – 10/2002	ENCOM Energy Communication Management Teamleitung Projektmanagement, Schulungs-und Qualitätsmanagement

